Pre-normative REsearch for Safe use of Liquid Hydrogen (PRESLHY)

Project Deliverable

Handbook of hydrogen safety: Chapter on LH2 safety

Deliverable Number:	6.1
Work Package:	6
Version:	4.0
Author(s), Institution(s):	K. Verfondern, HySafe D. Cirrone, V. Molkov, D. Makarov, UU S. Coldrick, HSE, Z. Ren, J. Wen, UWAR, C. Proust, INERIS, A. Friedrich, PS T. Jordan, M. Kuznetsov, KIT
Submission Date:	28 May 2021
Due Date:	31 March 2021
Report Classification:	Public

This project has received funding from the Fuel Cells and Hydrogen 2 Joint Undertaking under the European Union's Horizon 2020 research and innovation programme under grant agreement No 779613.

History		
Nr.	Date	Changes/Author
0.0 – MS26	14.12.2018	Compilation of Milestone 26 “ToC of handbook of hydrogen safety: chapter on LH2 safety” / K. Verfondern (HySafe), D. Cirrone, V. Molkov, D. Makarov (UU)
1.0	13.02.2021	Compilation of first draft / K. Verfondern (HySafe)
1.0b	12.03.2021	Addition of contributions by UU / D. Cirrone (UU)
2.0	23.03.2021	Second draft / K. Verfondern (HySafe)
2.0a	26.03.2021	Addition of contributions by HSE / S. Coldrick (HSE)
2.0b	28.03.2021	Addition of contributions by UU, UWAR, INERIS / D. Cirrone (UU), J. Wen (UWAR), C. Proust (INERIS)
2.0c	29.03.2021	Addition of contributions by PS, UU, KIT / A. Friedrich (PS), D. Cirrone (UU), T. Jordan (KIT)
3.0	30.03.2021	Final draft / K. Verfondern (HySafe)
4.0a	21.05.2021	Addition of contributions by M. Kuznetsov (KIT)
4.0	28.05.2021	Final draft / K. Verfondern (HySafe)

Approvals			
Version	Name	Organisation	Date
4.0	T. Jordan	KIT	28.05.2021

Acknowledgements

This project has received funding from the Fuel Cells and Hydrogen 2 Joint Undertaking under the European Union’s Horizon 2020 research and innovation programme under grant agreement No 779613. The HSE work programme acknowledges funding from its sponsors Shell, Lloyd’s Register Foundation and Equinor and instrumentation provided by NREL and Dräger.

Disclaimer

Keywords

FAIR data management, pre-normative research, experimental data, accessibility, re-use, long-term data storage, research data repository, liquid hydrogen, accidental behavior, release, ignition, combustion

Publishable Short Summary

The interest in hydrogen as a clean fuel and energy carrier of the future has grown in many countries and initiated comprehensive research, development, and demonstration activities with the main objective of the transition from a fossil towards a CO_2 emission lean energy structure as the ultimate goal.

Hydrogen represents an energy carrier with high energy content and a clean, environmentally benign source of energy to the end-user. The volume-related energy content of gaseous hydrogen, however, is comparatively small. For various applications of hydrogen where volume is an essential issue, it is necessary to liquefy the hydrogen for the sake of volume reduction. But there are also other situations where the liquid state represents a reasonable and economic solution for storage and distribution of large amounts of hydrogen depending on the end-user's requirements. Furthermore liquid hydrogen has the advantage of extreme cleanliness making it appropriate in many industrial applications. Major drawback is the enormous energy input required to liquefy the hydrogen gas, which has a significant impact on the economy of handling LH_2.

The hazards associated with the presence and operation of LH_2 containing systems are subject of safety and risk assessments. Essential part of such accident sequence analyses is the simulation of the physical phenomena which occur in connection with the inadvertent release of LH_2 into the environment by computation models. The behavior of cryogenic pool propagation and vaporization on either a liquid or a solid ground as well as potential pool burning is principally well understood. Furthermore state-of-the-art computer models have been developed and validated against respective experimental data. There are, however, still open questions which require further efforts to extent the still poor experimental data basis.

The experimental and theoretical investigation of the characteristics of liquid hydrogen, its favorable and unfavorable properties, as well as the lessons learnt from accidents have led to a set of codes, standards, regulations, and guidelines, which resulted in a high level of safety achieved today. This applies to both LH_2 production and the methods of mobile or stationary LH_2 storage and transportation/distribution, and its application in both science and industries.

Abbreviations

BLEVE	Boiling Liquid Expansion Vapor Cloud Explosion
BOS	Background-Oriented Schlieren
DLR	Deutsches Zentrum für Luft- und Raumfahrt
DNB	Departure of Nucleate Boiling
GH_2	Gaseous Hydrogen
HHV	Higher Heating Value
KHI	Kawasaki Heavy Industries
KSC	Kennedy Space Center, Florida
LEL	Lower Explosion Limit
LFL	Lower Flammability Limit
LH_2	Liquid Hydrogen
LHSC	Liquid Hydrogen Storage System
LHV	Lower Heating Value
MIE	Minimum Ignition Energy
MLI	Multi layer insulation
NPSH	Net Positive Suction Head
PPP	Pressure Peaking Phenomenon
RPT	Rapid phase transition
SLH_2	Slush Hydrogen
SNL	Sandia National Laboratory
UFL	Upper Flammability Limit

Table of Contents

1 Properties

1.1 Physical Characteristics

Hydrogen is the lightest and most abundant element in the universe. At standard temperature and pressure conditions, hydrogen is a colorless, odorless, tasteless, non-toxic, non-acid, non-metallic diatomic gas, which is in principle physiologically not dangerous. The energy density of hydrogen is very high; 1 kg of hydrogen contains approximately 2.5 times more energy than 1 kg of natural gas. One of the most important characteristics is its low density which makes it necessary for any practical applications to either compress the hydrogen or liquefy it.

Hydrogen can be considered an ideal gas over a wide range of (not too low) temperatures and (not too high, up to 10 MPa) pressures. At some point, however, like any other substance that is sufficiently cooled or compressed, hydrogen will act like a real gas. This behavior when departing from an ideal gas can be described, e.g. by the Redlich-Kwong-Soave equation [Soave 1972]:

$$p = \frac{RT}{V_m - b} - \frac{a\alpha}{V_m\left(V_m + b\right)}$$

with $a = 0.42747\frac{R^2 T_c^2}{p_c}$ and $b = 0.08664\frac{RT_c}{p_c}$

and for hydrogen: $\alpha = \alpha\left(T_r\right) = 1.202\exp\left\{-0.30288\,T_r\right\}$ with $T_r = \frac{T}{T_c}$

where p – pressure, Pa; T – temperature, K; V_m – molar volume, m^3/mol; R – universal gas constant, = 8.3145 J/(mol·K); T_r – reduced temperature; T_c – critical temperature, = 33.25 K; p_c – critical pressure, = 1.297 MPa.

At standard pressure the boiling temperature (20.3 K) liquid hydrogen has a density of 70.8 kg/m^3 which is high compared to the gaseous form (Fig. 1-1), thus allowing for a substantial volume reduction by a factor of 845 versus the gaseous state at ambient conditions. Therefore, hydrogen in the form of a liquid is typically used for storage/transportation purposes if volume is an issue. This density, however, is low compared to water. Its specific gravity is 0.07 meaning that, in case of an LH_2 spill onto water, more than 90% would be moving above the water surface. As Fig. 1-1 indicates, there is also a cryo-range which yields even higher densities than the liquid state if at sufficiently high pressures and sufficiently low temperatures.

Hydrogen gas is highly diffusive and highly buoyant. It is lighter than air above a temperature of 22 K, i.e. over (almost) the whole temperature range of its gaseous state at atmospheric pressure. Due to its high diffusivity, it rapidly mixes with the ambient air upon release. The diffusion velocity is proportional to the diffusion coefficient and varies with temperature according to T^n with n in the range of 1.72–1.8. Because of its small molecular weight and its low viscosity, hydrogen can cause a problem with respect to the propensity of the gas to leak. Diffusion in small amounts is even possible through intact materials, in particular organic materials. Leakage rates are by a factor of 50 higher compared to water and by a factor of 10 compared to nitrogen. Unlike invisible “normal” gaseous leakages, the release of liquid hydrogen (LH_2) or gaseous hydrogen at cryogenic temperature will usually produce a visible water vapor fog. The addition of an odorant

or colorant would ease the detection of small leaks; however, this is not feasible in most situations due to freezing-out of the substances added at those cryogenic temperatures.

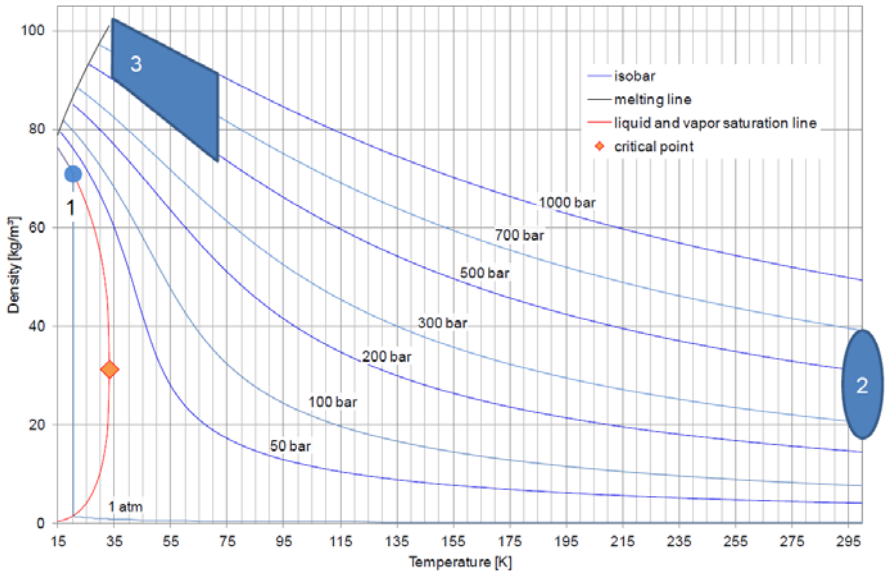

1 - liquid @ ~20 K; 2 - pressurised gas @ ~300 K; 3 - cryogenic compressed gas

Figure 1-1. Density of hydrogen in the low temperature range as a function of pressure [Klier 2012].

When handling LH_2 in confined areas, a hazard is given by the fact that due to the volume increase by a factor of 845, when LH_2 is heated up from its boiling point (20.369 K) to ambient conditions, the composition of the local atmosphere may change drastically. In an enclosed space completely filled with LH_2, final pressure after warm-up to 300 K may rise to a theoretical estimate of 172 MPa which certainly overpressurizes systems to bursting [Edeskuty 1996].

A further temperature decrease below the boiling point eventually results in the generation of solid hydrogen. Mixtures of coexisting liquid and solid hydrogen or slush hydrogen (SLH_2) offer the advantages of a higher density by up to 16%, a higher heat capacity by up to 18%, and a prolongation of the storage time of the cryogen as the solid melts and absorbs heat. Therefore it is of particular interest to use slush as a rocket fuel in space missions. Due to the fact that the hydrogen vapor pressure is strongly reduced with decreasing temperatures, from 98 kPa (which is about atmospheric pressure) at 20 K down to 13 kPa at 13 K, SLH_2 systems must be designed to safely operate below atmospheric pressure. At a pressure below ambient pressure the storage system has to be protected against air ingress, which represented a hazard.

At the triple point of hydrogen with the temperature of 13.8 K and a pressure of 7.2 kPa, at which all three phases can exist in equilibrium (Fig. 1-2). The boiling point increases with pressure to the critical point which is given by T_c = 33.15 K, p_c = 1.296 MPa with a critical density of γ_c = 31.4 kg/m³. A pressure increase beyond the critical point has no further influence.

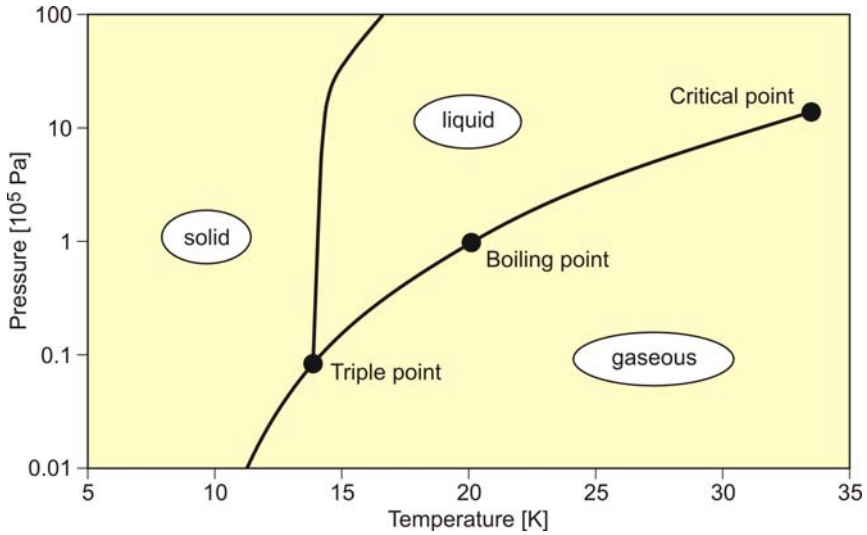

Figure 1-2. Phase diagram of hydrogen.

There is no liquid phase of hydrogen existing above its critical temperature. If a fluid is heated and maintained above its critical temperature, it becomes impossible to liquefy it with pressure. When pressure is applied, a single phase "supercritical fluid" forms which is characterized by T_c and p_c. "Supercritical" generally refers to conditions above the critical temperature and close to the critical pressure. It has characteristics similar to a gas and a liquid without changing its chemical structure. It is gas-like in that it is compressible and easily diffuses through materials; it is liquid-like in that it has a comparable density and may dissolve materials. And there are some transition states in between characterized by strong structural fluctuations causing the unusual behavior of fluids near the critical point covering all scales from microscopic to macroscopic.

Due to the strong dependence on temperature and pressure in the supercritical state, the thermophysical properties of cryogenic hydrogen vary strongly especially in the near-critical region. By proper control of pressure and temperature, one can access a significant range of physico-chemical properties, i.e. density, viscosity, diffusivity, without passing through a phase boundary. The specific heat capacity has a maximum at the so-called pseudo-critical temperature. Also, the isothermal compressibility is particularly large just above the critical temperature; at the critical point, it tends to infinity. For a highly compressible fluid, a small temperature gradient implies a large density gradient. It exhibits higher flow rates as compared with liquids. An important factor may be that the fluid might undergo a turbulent-to-laminar transition due to the dependence of viscosity on temperature. Heat transfer coefficients are unpredictable in the transition regime, and are much lower in the laminar regime.

Hydrogen coexists in two isomeric forms, ortho and para hydrogen. A small energetic difference is given, if the spins of the two protons of a hydrogen molecule are either aligned parallel (ortho) or anti-parallel (para). The existence of the two forms was proven experimentally in 1929 by Bonhoeffer and Harteck using charcoal as catalyst for the separation. The partition is dependent on the temperature (Fig. 1-3). Normal hydrogen at room temperature is a mixture of 75% ortho and 25% para hydrogen. In the lower temperature range < 80 K, para hydrogen is the more stable form. At 20 K, in thermal equilibrium, the concentrations are 99.825% para and 0.175% ortho. The rate of conversion between ortho and para states is with 0.0114 h^{-1} slow in the gas phase. The non-catalyzed transition takes place over a longer period (about 3–4 days), until a new

equilibrium state is reached. However, magnetic materials and also small oxygen concentrations are able to accelerate ortho-para conversion raising the rate by several orders of magnitude to the order of hours. $Fe(OH)_3$ is used in many technical applications as a very good catalyst for the conversion.

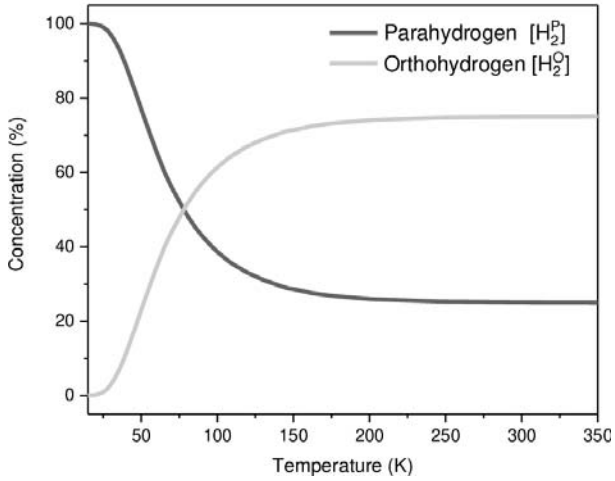

Figure 1-3. Equilibrium concentration of ortho- and para-hydrogen vs. temperature [Karlsson 2017].

The conversion from ortho to para is an exothermal reaction with a conversion energy of 270 kJ/kg at room temperature which increases with decreasing temperature. At temperatures below 77 K, it is almost constant at 523 kJ/kg. The liberated heat of ortho-para conversion is larger than the latent heat of vaporization/condensation (446 kJ/kg at the same temperature), which means that normal liquid hydrogen is able to vaporize completely even in a perfectly insulated vessel. It therefore represents a safety issue requiring a design of the LH_2 containing systems to be able to remove the heat of ortho-para conversion in a safe manner.

For internal cooling of gases adiabatic ideal throttling process may be applied. This so-called Joule-Thomson effect arises from the forces between the gas molecules. It is "internal work" against or in the direction of the van der Waals forces acting among the molecules. This means that the temperature of a real gas decreases below the inversion temperature ($T < T_I$) or increases above this temperature ($T > T_I$) upon expansion (depressurization) at constant enthalpy.

The Joule-Thomson effect is quantified with the Joule-Thomson coefficient, describing the temperature change by changing pressure at constant enthalpy

$$\mu_{TJ} = \left(\frac{dT}{dp}\right)_H$$

It is negative, if the temperature is decreasing, and positive for an increasing temperature. It is zero for an ideal gas or at the inversion temperature. So, all locations where there is no temperature change are forming the so-called inversion curve shown for hydrogen as a real gas, see Fig. 1-4. Unlike most other gases, the inversion temperature of H_2 gas is with 193 K at atmospheric pressure much lower than ambient temperature. A safety concern is that the sudden depressurization of a GH_2 storage vessel may lead to an ignition because of the negative Joule-Thomson coefficient of hydrogen at standard temperature. The actual temperature increase, however, is only 6 K, if a sudden pressure drop from 20 MPa to ambient pressure takes place. The chance of a spontaneous ignition just by that effect

is small. An explosion is more likely to occur because of electrostatic charging of dust particles during the depressurization or auto-ignition, shock diffusion ignition, or other mechanisms such as spark discharges from isolated conductors, brush discharges, corona discharges [Astbury 2005].

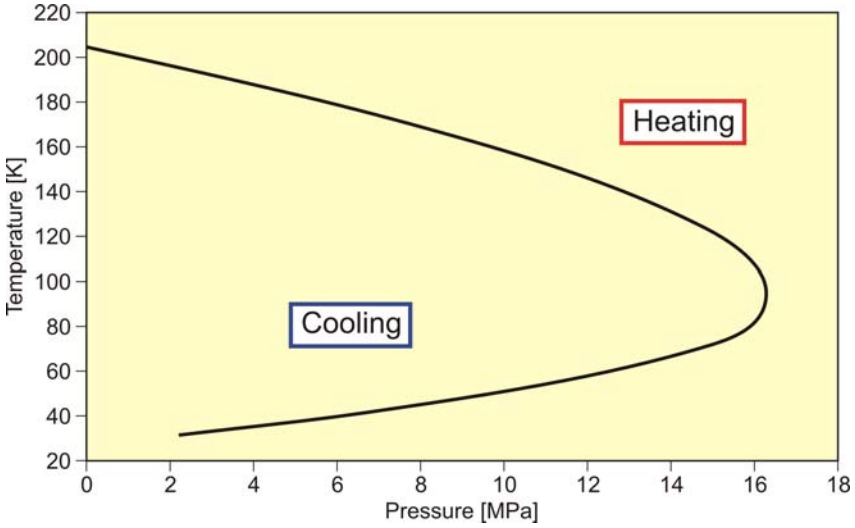

Figure 1-4. Inversion temperature of hydrogen.

1.2 Chemical Characteristics

Hydrogen is able to react chemically with most other elements. In connection with oxygen, hydrogen is highly flammable over a wide range of concentrations. It burns in a non-luminous hot flame to water vapor liberating the chemically bound energy as heat (gross heat of combustion: 286 kJ/mol). A stoichiometric hydrogen-air mixture contains 29.5 vol% of hydrogen. The flammability range is of 4–75 vol% of concentration in air, up to 95 vol% in oxygen, and widens with increasing temperatures. The lower flammability limit (LFL) as the minimum amount of fuel that supports combustion, is usually the more important limit for low-rate releases, since it will be reached first in a continuous leakage. The influence of the temperature is expressed in the modified Burgess-Wheeler equation for the LFL, which is for hydrogen (at ambient pressure) [Zabetakis 1967]:

$$c_{LFL} = c_{LFL}(300\,K) - \frac{3.14}{\Delta H_c}(T - 300) = 4.0 - 0.013\,(T - 300)\ \ (vol\%)$$

where ΔH_c – net heat of combustion, = 242 kJ/mol; T – temperature, K.

For just vaporized hydrogen at the boiling point, the LFL is 7.7%. The respective equation for the upper flammability limit (UFL) is [Eichert 1992]:

$$c_{UFL} = 74.0 + 0.026\,(T - 300)\ \ (vol\%)$$

valid for the temperature range $150 \leq T \leq 300$, with T in K.

A more recent experimental study [Kuznetsov 2013] concludes a slightly modified linear relationship between flammability limits and temperature recommending the following equations:

$$c_{LFL} = 4.64 - 0.0067\,T \quad (vol\%)$$

in the temperature range -150°C ≤ T ≤ 400, with T in °C, and

$$c_{UFL} = 73.8 + 0.033\,T \quad (vol\%)$$

in the temperature range -60°C ≤ T ≤ 400, with T in °C.

All above LFL and UFL correlations are depicted in Fig. 1-5.

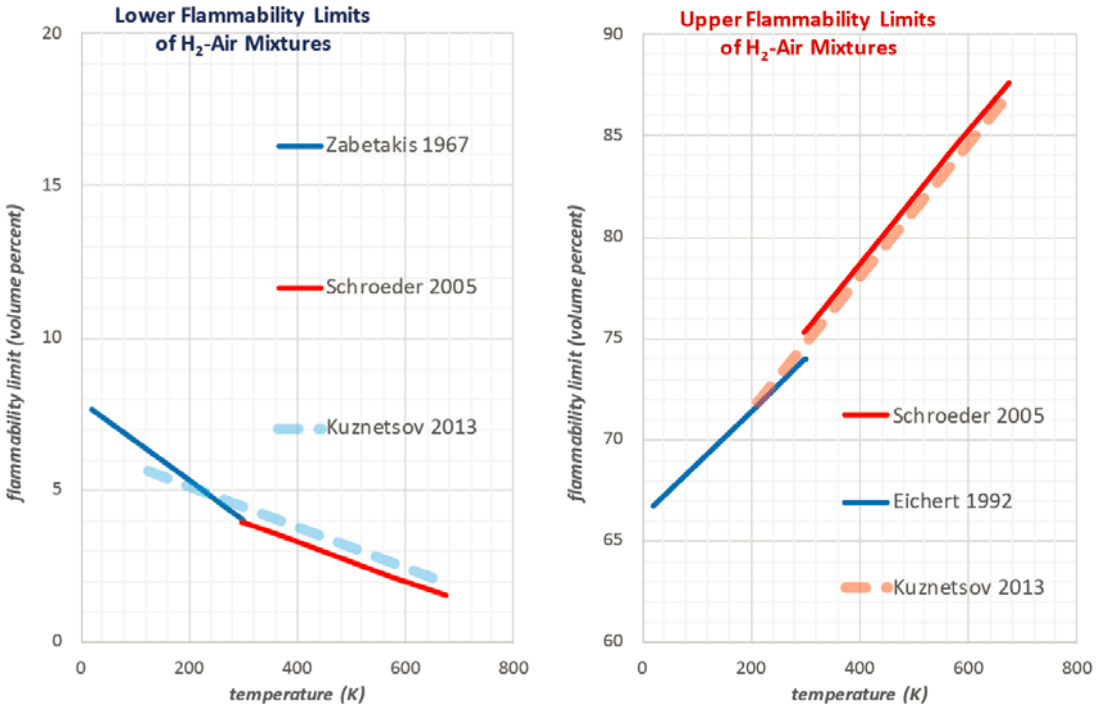

Figure 1-5. Flammability limits in hydrogen-air mixtures, LFL (left) and UFL (right).

The auto-ignition temperature of 858 K is relatively high, but can be lowered by catalytic surfaces. The minimum ignition energy at stoichiometric mixture is with 0.02 mJ very low, much lower than for hydrocarbon-air mixtures. A weak spark or the electrostatic discharge by a human body, which is in the range of 10 mJ, would suffice for an ignition; this is, however, no different from other burnable gases. The minimum ignition energy is even further decreasing with increasing temperature, pressure, or oxygen contents. Measurements at cryogenic temperatures have been provided recently [Proust, 2020].

The thermal radiation emitted from hydrogen combustion in narrow infra-red bands essentially originates from the water vapor within the hydrogen flame. The emissivity factor of water vapor, however, is comparatively low (ε < 0.1). Therefore, despite its potentially high flame temperature (adiabatic temperature of 2318 K in air), the radiation hazard from a hydrogen flame is small compared to other fuels. It also results in the non-visibility of hydrogen flames even in a dark room (unless impurities in the air are present), and therefore a hydrogen fire is difficult to recognize and localize. This is a major problem with regard to the detection of hydrogen fire accidents. In contrast, other gases containing carbon generate – in addition to water vapor and carbon dioxide – also soot within the flame. Soot is an efficient infrared emitter, leading to a strong thermal radiation and visible flames.

The laminar burning velocity in a flammable gas mixture, defined as the speed with which a smooth plane combustion wave advances into a stationary flammable mixture, is a pertinent property of the gas depending on temperature, pressure, and concentration. The burning velocity of hydrogen in air at stoichiometric ambient conditions is 2.37 m/s reaching a maximum of 3.46 m/s at a concentration of 42.5%. Compared to other hydrocarbon fuel-air mixtures (e.g. methane: 0.43 m/s), it is the highest for hydrogen because of its fast chemical kinetics and high diffusivity.

The flame front velocity is defined as the product of laminar burning velocity and expansion ratio for constant pressure leading to a value up to ~24 m/s for hydrogen. Most realistic flames are turbulent. The turbulent burning velocity is significantly higher and reaches the order of several hundreds of m/s resulting from small-scale turbulence and flame instabilities which increase both energy transfer and flame surface.

This comparatively high burning velocity results in a greater chance for a transition from deflagration to detonation (DDT). The detonability range is usually given as 18–59 vol% of hydrogen concentration, however, the range was found to be depending on the system size. In the Russian detonation test facility RUT, the largest of its kind, a lower detonability limit of as low as 12.5 vol% has been observed [Breitung 1995]. The detonation velocity reaches values in the range of 2000 m/s. The detonability limits for the DRIVER facility at Kurchatov Institute were also extended to 14–62.3 vol.% of hydrogen [Dorofeev 2000], much wider than compared with commonly used limits 18.3-59 vol%-H_2 [NASA 1997a].

For open LH_2 pools, it needs to be considered that cold hydrogen gas is less volatile compared to ambient gas and thus more prone to the formation of a flammable mixture with air. Furthermore LH_2 in direct contact with the ambient air quickly contaminates itself due to condensation and solidification of air constituents. Solid particles may lead to plugging of pressure relief valves, vents or filters. In addition, due to the different boiling points of nitrogen (77.3 K) and oxygen (90.2 K), the oxygen condenses first upon cooling down or vaporizes last upon warming up, both situations always connected with an oxygen-enriched condensate forming shock-explosive mixtures. Also liquid or solid oxygen in combination with another combustible material, even if solid and thus not “flammable”, may form highly explosive mixtures with drastically decreased ignition energies. Examples are LH_2 plus solid air having an O_2 fraction of > 40%, or liquid oxygen spilled onto asphalt [Zabetakis 1967].

1.3 Impact of Cryogenic Hydrogen on Materials

The stress which a structural material is able to withstand is determined by its ductility (Fig. 1-6). A material is elastic if, after being elongated under stress, it returns to its original shape and volume as soon as the stress is removed. At a certain strain, it departs from linearity, i.e. the material will retain a permanent elongation which is attributed to plastic deformation behavior. The applied stress is the so-called “yield stress”. With a further increase of the strain eventually the “ultimate or tensile stress” is reached, beyond which the stress steadily decreases until rupture. In contrast, a brittle material does not exhibit a permanent plastic elongation phase and rather breaks abruptly without any warning as soon as it is exposed to its tensile stress [Edeskuty 1996].

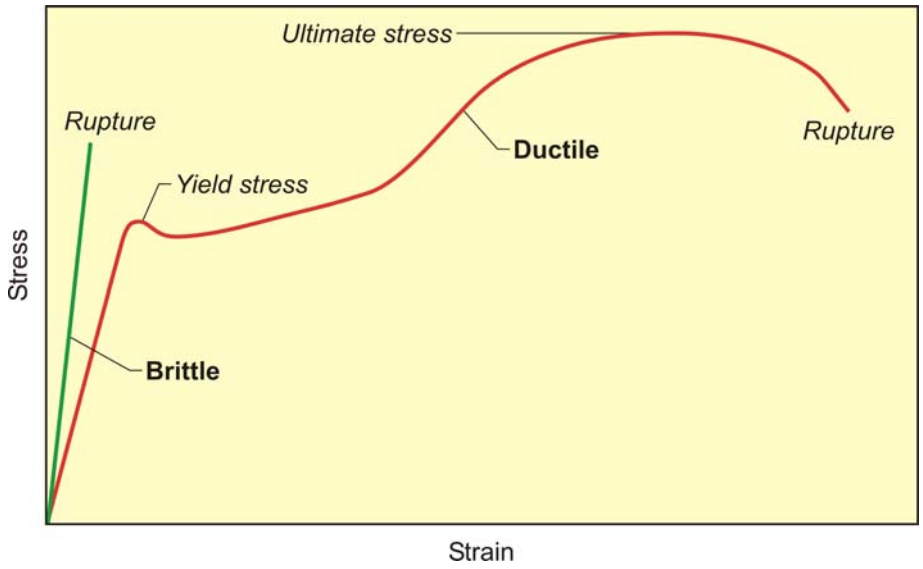

Figure 1-6. Ductile and brittle behavior of materials.

Hydrogen has long been recognized to have a deleterious effect on some metals by changing their physical properties. It is basically due to the presence of hydrogen atoms dissolved in the metal grid and accumulating in disturbed lattice regions. Apart from this hydrogen embrittlement effect, there is an additional influence on structural materials at cryogenic temperatures, which accounts for most service failures of brittle-type materials. With decreasing temperature, the yield stress and ultimate stress increase for most metals, generally connected with a corresponding drop in fracture toughness which is a measure of the ability of materials to resist crack propagation. The lower the toughness, the smaller is the tolerable crack length.

A material can change from ductile to brittle behavior as soon as the temperature falls below its so-called "nil-ductility temperature". This temperature is not a fixed value, but may vary as a function of prior heat or mechanical treatment and of the alloy composition and impurities, respectively. It is, in principle, the minimum temperature, at which a structural material is considered useful and can sometimes be significantly higher than the temperature of the cryogen. For some materials at cryogenic temperature, little stress is sufficient to break it, and it can occur very rapidly resulting in an almost instantaneous failure. This effect is a particular problem in cryogenic equipment exposed to periodic changes and was found in several accidents to have caused the failure of a cryogenic storage vessel, e.g. the rupture of a 4250 m^3 LNG tank in Cleveland, USA, in 1944 [Zabetakis 1967], when material behavior at cryogenic temperatures was not yet deeply understood.

The components of a cryogenic system usually undergo a thermal gradient, some only during cool-down or warm-up phases, others even at steady state operation. Strong gradients, particularly if non-linear, result in stresses which may lead to rupture. Thermal gradients are of significance in systems with stratified two-phase flows of cryogens.

Low temperatures can also affect materials by thermal contraction causing large thermal stresses, if the system cannot accommodate the differential thermal contraction of the materials. The thermal expansion coefficient is a function of the temperature. For many materials which are cooled down to cryogenic temperatures, more than 90% of the total contraction will have already taken place until 77 K. The coefficient is approximately 0.3% in iron-based alloys, 0.4% in aluminum, or more than 1% in many plastics

[Edeskuty 1996, NASA 1997b]. Cryogenic vessels or piping must account for this contraction to avoid large thermal stresses.

Materials with sufficiently high strength and high ductility, working successfully at low temperatures, including aluminum and most of its alloys, copper and its alloys, nickel and some of its alloys, as well as austenitic stainless steels, should be used in cryogen containing systems.

For many materials, specific heat exhibits a strong temperature dependence below 200 K showing that at cryogenic temperatures, much less heat is required to raise the temperature of a body than at ambient temperatures. An example: heat capacity of aluminium is reduced from about 950 J/(kg·K) at ambient temperature to less than 10 J/(kg·K) at 20 K.

1.4 Physiological Problems with Cryogenic Hydrogen

Hydrogen is classified as non-toxic and non-acid, non-carcinogenic, being a simple asphyxiant with no threshold limit value (TLV) or LD50 (lethal dose 50%) value established [NASA 1997a].

Vaporization of released liquid hydrogen affects the composition of the atmosphere, particularly in (partially) confined areas, carrying the risk of asphyxiation. The enormous liquid/ambient expansion ratio combined with condensation of O_2 from the ambient air and burning of flammable H_2-air mixtures leads to a significant dilution of the local atmosphere. An oxygen volume fraction of less than 19.5% is considered by NASA to be dangerous to humans; less than 8% will be lethal within minutes (Table 1-1). Alarm levels are generally set at 19% of oxygen.

Table 1-1. Impact on humans by an atmosphere with decreasing oxygen contents.

Oxygen contents in air (%)	Symptoms
~21 – 19	None
~19 – 15	Reduced reaction times, no visible effects
~15 – 12	Heavy breathing, rapid heart beat, impaired attention or coordination
~12 – 10	Dizziness, faulty judgement, poor muscular coordination, rapid fatigue, lips slightly bluish
~10 – 8	Nausea, vomiting, inability to move, loss of consciousness followed by death
~8 – 6	Brain damage after 4–8 min, death within 8 min
< 6	Coma after 40 s, respiratory failure, death

Direct contact with liquid hydrogen or with surfaces at very low temperature causes cryogenic “burns” similar to thermal burns. Living tissue will freeze except for very brief contact periods where the temperature difference between cryogen and skin is still high (film boiling regime) and heat transfer small. The freezing of skin onto a cold surface can lead to severe damage upon removal. Prolonged skin exposure to cold hydrogen may result in frostbite. A symptom is short-lived local pain. Frozen tissues are painless and

appear waxy, with a pale whitish or yellowish color. Thawing of the frozen tissue can cause intense pain. Shock may also occur. Prolonged inhalation of cold vapor or gas may cause serious lung damage. Particularly eyes are sensitive to cold. A longer exposure to cold temperatures after a large spill lowers the body temperature resulting in hypothermia, organ dysfunction, and respiratory depression [Edeskuty 1996].

There are no significant environmental hazards associated with the accidental discharge of liquid hydrogen due to its non-toxic character.

2 Applications and Safety Issues

2.1 Production of Liquid Hydrogen

Liquefaction of hydrogen is an energy-intense process as hydrogen has to be cooled to the boiling temperature of about 20 K. There is a minimum specific work (exergy), A_{min}, required for the liquefaction of hydrogen at ambient conditions. It is composed of three components [Vander Arend 1964]:

(a) Sensible heat, the work for cooling the gas to the boiling point determined by the Carnot cycle

$$A = (T_o - T_s) \times \Delta s = (T_o - T_s)/T_s \times \Delta Q$$

with $\Delta Q = T_s \times \Delta s$ the heat withdrawn at T_s;

(b) Latent heat, thework for condensation of the gas; and

(c) an additional amount of work necessary for the temperature dependent ortho-para conversion.

In total the minimum energy required amounts to

$$A_{\min} = \int_{T_o}^{T_s} \frac{T_o - T}{T} c_p \, dT + \frac{T_o - T_s}{T_s} \Delta H_v + \int_{C_1}^{C_2} \frac{T_o - T_s}{T_s} C_{o \to p} \, dC$$

$$= 5.8 + 6.2 + 2.2 = 14.2 \quad MJ/kg$$

where T_o – ambient temperature, K; T_s – boiling point, K; c_p – specific heat capacity (temperature dependent), J/(kg·K); ΔH_v – heat of vaporization, J/kg; C – concentration of ortho hydrogen; $C_{o \to p}$ – conversion energy from ortho to para hydrogen, J/kg.

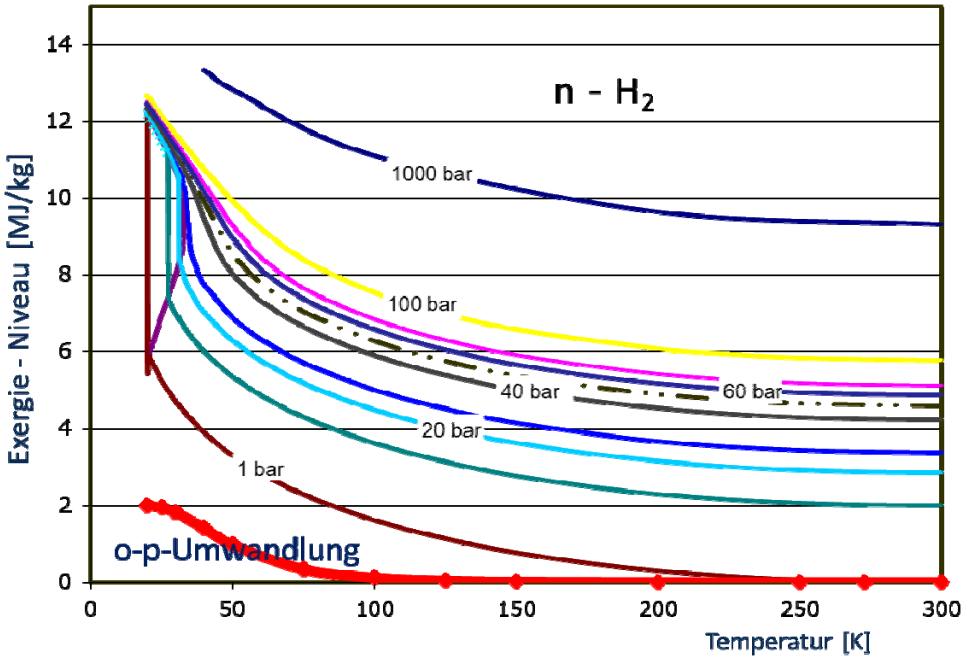

Figure 2-1. Minimum energy requirement for pressurizing and cooling normal hydrogen at standard conditions [Funke 2019].

So, at least 14.2 MJ of energy (11.8% of the lower heat of combustion) are required to liquefy 1 kg of normal-hydrogen (Fig. 2-1). As can be seen from Table 2-1, this value is larger than for any other gases.

Currently established technology requires in the order of 50 MJ/kg. Feasibility studies showed a potential to reduce this to 22 MJ/kg.

Table 2-1. Minimum energy requirement for liquefaction of different gases.

Gas	Boiling Point (K)	Heat of vaporization (kJ/kg)	Minimum Work (MJ/kg)		
			Cooling NTP → BP	Condensation	Total
Hydrogen	20.268	445.59	8.0*	6.2	14.2
Methane	111.632	509.88	0.3	0.8	1.1
Nitrogen	77.34	201.	0.2	0.6	0.8
Helium	4.216	20.9	6.9	1.4	8.3

* including ortho-para conversion

The principle available processes for cooling are grouped in external cooling by a colder medium in a heat exchanger and internal cooling, where the medium itself undergoes thermodynamic changes associated with a temperature drop. The latter are split in processes where the media provides mechanical work in expansion turbines “expanders” or in piston machines and in isenthalpic throttling in Joule-Thomson valves.

2.1.1 Linde-Hampson Process

The Linde-Hampson method is a thermodynamic process, where isothermal compression and subsequent isobaric cooling with the non-liquefied cold gas is done in a heat exchanger. Joule-Thomson expansion connected with an irreversible change in entropy is used as the refrigeration process. Because of the relatively low inversion temperature of hydrogen, a liquid nitrogen pre-cooling is needed. Despite its simplicity and reliability, this method has become less attractive (low efficiency, complex processing) compared to modern ones, where cooling is carried out in reversible processes (expander) at reduced energy consumption.

2.1.2 Claude Process

The commonly applied method in large-scale liquefaction plants is the Claude process combined with liquid nitrogen LN_2 pre-cooling where the necessary refrigeration is provided in four main steps (Fig. 2-2):

(1) Compression of hydrogen gas, removal of compression heat;

(2) Precooling with liquid nitrogen (> 80 K);

(3) Cooling of a part of the hydrogen in an expansion machine “expander” (> 30 K);

(4) Expanding of the residual hydrogen in a Joule-Thomson valve (20 K).

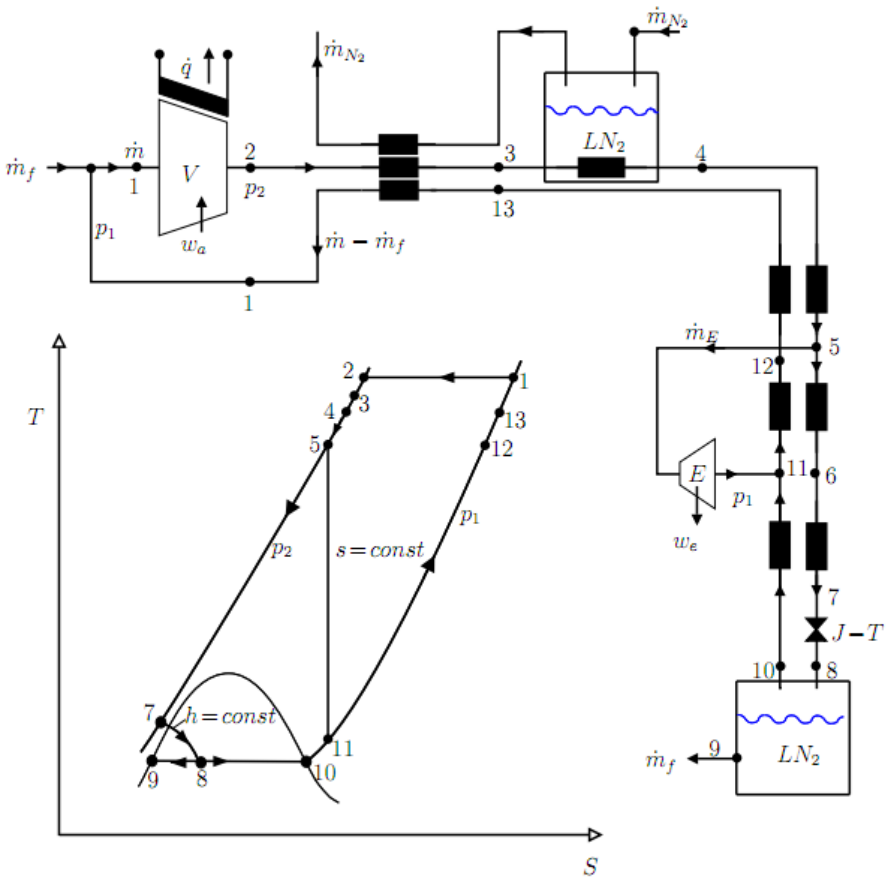

Figure 2-2. Schematics of a Claude Process with LN_2 precooling.

The first expansion step would already be sufficient for liquefaction. But the Joule-Thomson expansion is applied for the final step to avoid two-phase flow in the expander. Variations of the dual-pressure Claude process as a large-scale liquefaction method have proven to be the optimal solution.

The cooling stage (3) from 80 to 30 K represents the most energy-intensive step. Alternative techniques applied in this temperature domain are either the "classical" cascade refrigeration with cycles using different coolants (as was demonstrated by Dewar) or, a more economic method, the Brayton cycle with just one gaseous coolant which is sequentially expanded, before it cools down the hydrogen in a counter-current heat exchanger.

2.1.3 Magnetic Refrigeration Process

The magnetic refrigeration process takes advantage of the entropy difference and the adiabatic temperature change upon application or removal of magnetic fields in the working material, which either should have para- or ferromagnetic behavior. For efficiency reasons ferromagnetic material with appropriate Curie temperature should be applied. The actual cooling effect happens during the isentropic demagnetization of the ferromagnetic material. The magnetic refrigeration cycle consists of the steps:

(1) Adiabatic magnetization in an external magnetic field causing order of the magnetic dipoles (thus reducing entropy, thus increasing temperature);

(2) Transfer of the heat to a fluid (water, helium) at the same magnetic field strength;

(3) Adiabatic demagnetization with removal of the magnetic field at constant entropy, i.e. decreasing the temperature;

(4) Heat transfer from the gas (to be cooled) to the working material (solid).

Currently this method is relevant for temperatures below 5 K and for hydrogen liquefaction only relevant on a R&D level. It is expected that at least 15 separate cooling stages are necessary to cool down hydrogen to the boiling point, provided strong magnetic fields with a magnetic induction of about 10 T may be applied. Here it is assumed that a typical temperature decrease in the order of 1 K per Tesla may be achieved [Peschka 1992]. Suitable ferromagnetic materials with Curie point temperatures in the range of 20 to 300K have to be identified or developed.

However, the process appears promising because of its potentially compact design, long lifetime, low capital investment, and higher efficiency with an estimated liquefaction work of about 26 MJ/kg.

2.1.4 Liquefaction Plants Worldwide

One of the challenges in building a hydrogen economy is the establishment of an efficient production and supply infrastructure. Large scale distribution favors the relatively dense liquid phase LH_2, but liquefaction still suffers from low energy efficiencies. Reducing the energy consumption of liquefiers is an active subject of development for the LH_2 industry (see IDEALHy FCH JU project for instance).

Large scale installations are typically implemented with a Claude process with LN_2 pre-cooling providing acceptable efficiencies, at least for the past main application as rocket fuel. The complete process comprises an initial purification unit, additional external coolers with helium or mixed refrigerants as operating medium. The expansion is split in up to 6 stages and several ortho-para converters are integrated. All cold parts are mounted in a cold box, which is thermally insulated for instance with perlite.

Worldwide there are nearly 30 large scale liquefiers in operation with production capacities from 1 to ~35 t/d of LH_2 in a unit. Most and with the largest capacities are installed in the USA. But also in the European Union and in Asia, particularly Japan, H_2 liquefaction capability is existing and on the rise. Additionally, there are several laboratory-scaled liquefiers in operation with a capacity of a few kg/day [Asadnia 2018]. A list of currently operated liquefaction plants in the world is given in Table 2-2. Table 2-3 contains a list of liquefaction plants that were found to be under construction or planned to go into operation in near future.

Table 2-2. Operating commercial hydrogen liquefaction plants in the world.

Place	**Operator**	**Capacity (t/d)**	**Operation since**
Europe			
Rozenburg, Netherlands	Air Products	5.0	1987
Wazier/Lille, France	Air Liquide	10.5	1987
Kourou, French Guiana	Air Liquide	2.5	1990
Ingolstadt, Germany	Linde	4.5	1992
Leuna, Germany	Linde	5.3	2007
Total Europe		**27.8**	
America			
Ontario, CA	Linde-Praxair	20	1962
New Orleans, LA	Air Products	34 + 34	1977
Niagara Falls, NY	Praxair	38	1981/1989
Sarnia, ON	Air Products	29	1982
Bécancour, QU	Air Liquide	11	1986
Montreal, QU	Air Liquide	10	1986
Sacramento, CA	Air Products	5	1986
Magog, QU	Linde	15	1990
Pace, FL	Air Products	29	1994
McIntosh, AL	Praxair	24	1995
East Chicago, IN	Praxair	30	1999
Total America		**279**	
Asia			
Beijing, China	CALT	0.6	1995
Mahendragiri, India	ISRO	0.3	1992
India	Asiatic Oxygen	1.2	
India	Andhra Sugars	1.2	
Ooita, Japan	Pacific Hydrogen Co.	1.9	1986
Kimitsu, Japan	Nippon Steel Corp.	0.2	2004
Sakai (Osaka), Japan	Hydro Edge Co., Ltd.	5.1 + 5.1	2006
Ichihara (Chiba), Japan	Iwatani Industrial Gases Corp	5.1	2009
Shunan (Yamaguchi), Japan	Yamaguchi Liquid Hydrogen Corp	5.1	2013
Harima (Akashi), Japan	Kawasaki Heavy Ind.	4.2	2015

Baikonur, Kazakhstan	Cryogenmash	4 – 17	~1960
Plesetsk, Russia			
Total Asia		**~47**	
Total World		**~355**	

Table 2-3. Commercial hydrogen liquefaction plants in the world under construction/planning.

Place	**Operator**	**Capacity (t/d)**	**To be onstream in**
Leuna, 2nd plant	Linde	5	2021
Carson, CA	Air Products	10	2021
La Porte, TX	Air Products	~28	2021
Las Vegas, NV	Air Liquide	30	2022
USA	Chart Industries	14 + 14	2022
Haiyan/China	Air Products	30	2022
Weinan, China		8.5	
Chubu Pref, Japan	Ituchu-Air Liquide	30	~2025
Ulsan, ROK	Hyosung/Linde	35.6	
Changwon, ROK	Doosan Heavy Ind. / Air Liquide	5	2023
Total		**~210**	

The specific energy consumption, A, of today's hydrogen liquefiers is in the order of 12-15 kWh/kg of LH_2, 3 to 4 times higher compared to the minimum energy required (3.9 kWh/kg). This corresponds to an exergy efficiency (A_{min}/A) in the range of 25–33%. Target value for an optimized liquefier design is 6.2 kWh/kg [Funke 2019]. Improvement in efficiency is expected with the development of new materials and new compression/expansion technology. As an example, the recently established plant in Leuna, Germany, indicates a specific energy consumption of 10.3 kWh/kg (feed compression excluded) [Decker 2019a].

2.2 Storage of Liquid Hydrogen

2.2.1 Cryostat for Stationary Applications

Cryogenic vessels have been commonly used for more than 70 years for the storage and transportation of liquid hydrogen. Similar as for compressed storage there are two main classes of the LH_2 storage vessels. There are cryostats for stationary and for mobile applications. The vessel shown in Fig. 2-3 is the world's largest LH_2 tank located at the NASA Kennedy Space Center (KSC) in Florida. The tank is a 3800 m^3 (3218 m^3 of LH_2) double-wall vacuum perlite (1.3 m of thickness) insulated spherical (in/ex diameter = 18.75 / 21.34 m) storage vessel. The tank is operated at a pressure of 0.62 MPa and has a boil-off rate of 0.025%/d.

Figure 2-3. LH_2 storage vessel with 3800 m^3 capacity at KSC in Florida (Source NASA).

In order to manage storage at -253°C, for large storage (> 100 m^3 water volume) double-walled vacuum insulated pressure tanks are used. Such vessels consist of an inner pressure vessel and an external protective jacket. The volume between inner vessel and jacket is filled with compressed perlite under vacuum. Perlite is an inorganic amorphous volcanic glass that represents a good trade-off between cost and insulation properties.

Although many large-scale tanks are of spherical shape to minimize heat loss to the outside, the LH_2 tanks at production sites are typically horizontally arranged. At the Kourou Ariane launch site in French Guiana, Air Liquide operates five semi-mobile tanks of 320 m^3 each (0.39 MPa) and one tank of 110 m^3 (1.1 MPa). Total capacity is 22 t. Another example shown in Fig. 2-4 are the LH_2 storage tanks at the liquefaction plant in Waziers/France (Liquefaction unit = 10 t/d), AL operates four horizontal tanks of 250 m^3 each (in/ex diameter = 4.02 / 5.1 m - perlite thickness = 500 mm).

Figure 2-4. LH_2 stores at the Waziers liquefaction plant.

Modern tanks for liquid hydrogen production reduce boil-off losses to a minimum [Decker 2019b]. Nevertheless, it is assumed that roughly 1% of the liquefied hydrogen will be lost due to boil-off per day during hydrogen storage at the refueling station [Krieg 2012]. An average storage period of approximately three days is assumed.

For smaller storages (< 100 m^3), also single-walled pressure tank with multi-layer insulation coating are used (so-called MLI). This technology is described in more detail in chapter 2.3.1 on LH_2 trailers.

2.2.2 Cryostat for Mobile Applications

The heat absorption for the small automotive cryostat shown in Fig. 2-5 with an internal volume of about 100 ℓ is so reduced to about 1 W. This heat input leads to evaporation and via a pressure limiting valve to the boil-off. The boil-off corresponds to a loss of 1.5% of the stored energy per day for small cryostats. Thus, the typical stored mass of about 7 kg will be lost in two months if the car were not used in this phase.

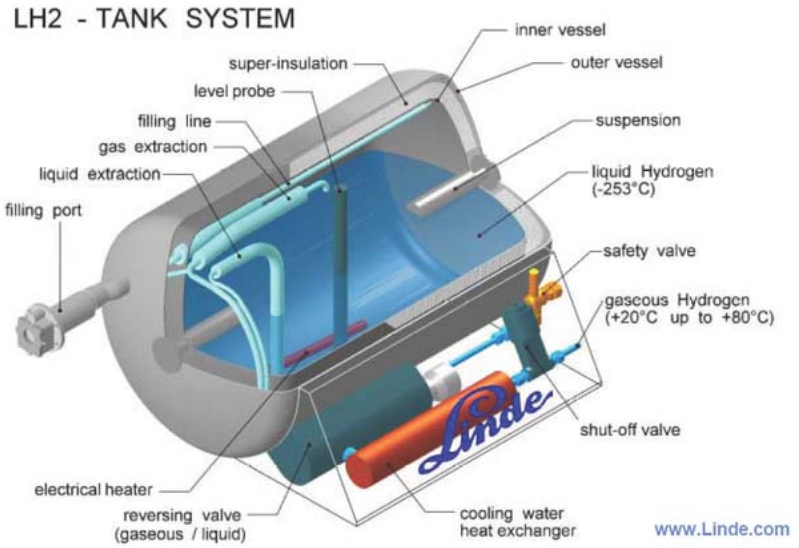

Figure 2-5. Schematic presentation of an LH_2 tank for automotive application (BMW 750h) produced by Magna Steyr (Source: Linde).

The boil-off management may reduce these losses or at least reduce the associated risk with released hydrogen by

- cold combustion with air in catalytic recombiners
- storing the boil-off gases in metal hydride storages
- re-cycling in a re-liquefaction
- direct energetic use, in a fuel cell for instance.

Of course the involved temperatures are demanding not only regarding the design of the actual storage but also regarding the compatibility of all connected technologies, like measurement techniques, armatures, valves, piping. The typical liquid hydrogen storage system as shown in Fig. 2-5 consists of the following regulatory elements:

(a) Liquefied hydrogen storage container(s);

(b) Shut off devices(s);

(c) A boil-off system;

(d) Pressure Relief Devices (PRDs);

(e) The interconnecting piping (if any) and fittings between the above components.

2.3 Transportation

Depending on the scale and the desired use, hydrogen batch transport is based either on compressed or liquefied hydrogen. Despite the higher efficiencies rooted in the higher densities of LH_2, in most cases high-pressure gaseous hydrogen is preferred over liquid hydrogen. This is because of the small numbers of liquefiers available worldwide and the higher energies required for liquefaction. So typically for long distance transport liquid hydrogen is the preferred option.

2.3.1 Road Transport

Road transport of gaseous hydrogen is presently carried out using trucks with steel cylinders of up to 90 ℓ at 20–30 MPa pressure or large seamless cylinders called “tubes” of up to 3000 ℓ at 20–25 MPa. For transport at a larger scale, pressures of 50–60 MPa or even higher may be employed. A 40 t truck carrying compressed hydrogen can deliver only 400 kg because of the weight of the 20 MPa pressure vessels.

Over longer distances, road transportation of liquid hydrogen is more attractive than gaseous hydrogen. Cryogenic liquid hydrogen trailers can carry up to 5000 kg of hydrogen and operate up to 1.2 MPa. Hydrogen boil-off can occur during transport despite the super-insulated design of these tankers, potentially on the order of 0.5%/d. Hydrogen boil-off up to roughly 5% also occurs when unloading the liquid hydrogen on delivery.

The LH_2 tanks on the trailers are insulated using a vacuum super insulation. This insulation is also used for transfer piping systems (Vacuum MLI Insulated Piping). The Vacuum Super Insulation is a system of thermal insulation which includes:

- A double-shell insulation space (interspace) where static or dynamic (for large storage) high vacuum is limiting heat transfer by conduction and convection.
- A blanket of alternate layers of highly reflecting shields (aluminum for instance) and insulating spacers (Lydall for instance) to prevent heat transfer by radiation as well as conduction between shields.
- An adsorbent (molecular sieve) placed in the vacuum space in order to achieve an adequate level of vacuum at low temperature by adsorption of residual gases and moisture.

Two examples for LH_2 trailers as shown in Fig. 2-6 are rather limited by the maximum dimensions of the transport vehicles. They come typically with a weight of ~25 metric tons for the empty tank plus a load of 2–3 t of LH_2.

Figure 2-6. Examples of LH_2 road truck transportation [Zittel 1996].

2.3.2 Pipeline Transport

Similar to the extensively installed natural gas networks, the transportation of hydrogen at high pressure through pipeline systems has been realized already at a broad scale. In contrast, pipeline transportation of liquid hydrogen is existing at a small scale only. Pipes for transferring cryogenic liquid hydrogen must comply with the extreme low temperature of LH_2 and the associated insulation requirements. Similar to LH_2 storage tanks, pipelines are of double-wall design and vacuum-jacketed. A prototypical transfer pipe for LH_2

therefore consists of at least two concentric tubes combined with superinsulation material in the vacuum space. Stainless steel is usually taken for the inner line with low heat conduction spacers as a support in the vacuum jacket. Because of the high cost increasing linearly with distance LH_2 pipelines are economically attractive only for short distances. The transfer is done by pressure difference rather than by pumps. There are rigid or flexible variants. Major concerns, apart from heat leakage, are the mechanical stress imposed on the inner line due to contraction/expansion, pressure oscillations upon cool-down, or two-phase flow. Therefore cryogenic pipes must be sufficiently flexible which can be done by appropriate pipe routing and expansion joints.

During the period of chill-down of an LH_2 line, a two-phase flow develops which is stratified for horizontal flows as is schematically shown in Fig. 2-7 [Mei 2006] exhibiting a vapor layer above the liquid due to vaporization and also a thin film underneath the liquid layer. This phenomenon is encountered particularly in refueling lines where chill-down is required before the fueling process itself begins to avoid the gaseous phase to enter the tank.

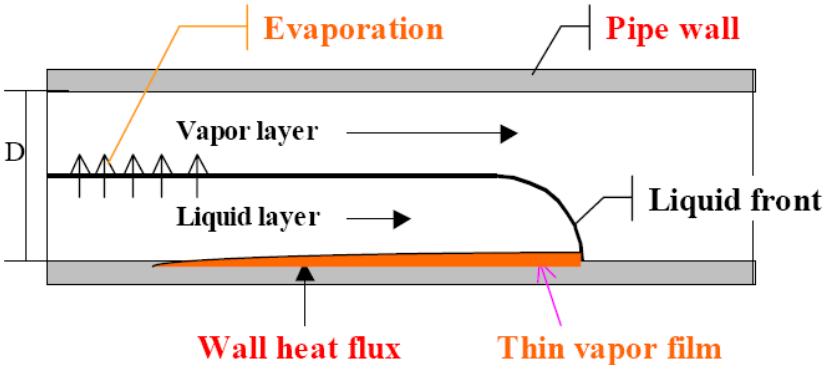

Figure 2-7. Two-phase flow in a horizontal line.

Figure 2-8 shows test and operations support contract engineers and technicians at the NASA Kennedy Space Center inspect an LH_2 supply hose at Launch Pad 39B. They are reviewing procedures preparing for a fit check of the new LH_2 transfer flex hose from its supply truck to the LH_2 tank at Pad 39B to confirm that the hose fits and functions properly.

Figure 2-8. Inspection of an LH_2 supply hose at NASA's Kennedy Space Center (Photo credit: NASA/Frankie Martin).

The space center's Ground Systems Development and Operations Program is overseeing upgrades and modifications to Pad 39B processing facilities to ensure all is in readiness to support Exploration Mission 1, the first flight of Space Launch System rocket and Orion spacecraft, currently planned for November 2021. Both are being developed for NASA's Journey to Mars.

For transferring LH_2 via pipeline from one storage to another (for instance from a large stationary storage to a truck or from a trailer to a storage tank at user's site), there are two methods:

- pressure buildup (natural pressure build up or voluntary vaporization of LH_2 via a small external heat exchanger). Hence, the pressure in the "mother storage" becomes more than the pressure in the "daughter storage" and LH_2 transfer is easy. The main drawbacks of this method are a long operating time and an increase of the pressure of the "mother" storage leading sometime to the need of a pressure venting;
- pumping in the "mother storage" using an appropriate transfer centrifugal cryogenic pump. The main drawbacks of this method are the cost of the pump and the need of frequent maintenance of the pump mostly due to cavitation (low available NPSH - Net Positive Suction Head: difference between liquid pressure and saturation vapour pressure of the considered compound - due to low density of LH_2).

At an LH_2 based hydrogen fueling station, the LH_2 is typically delivered by an LH_2 truck. This LH_2 truck is composed of a 40 m^3 horizontal tank operating between 0.1 and 1.2 MPa. The connection between the storage and the truck is done by a flexible transfer line (Fig. 2-9). The transfer is performed without a pump. A small vaporizer is present on the trailer to produce a pressure build up in the truck tank and to allow the transfer of liquid H_2 in the stationary vertical storage.

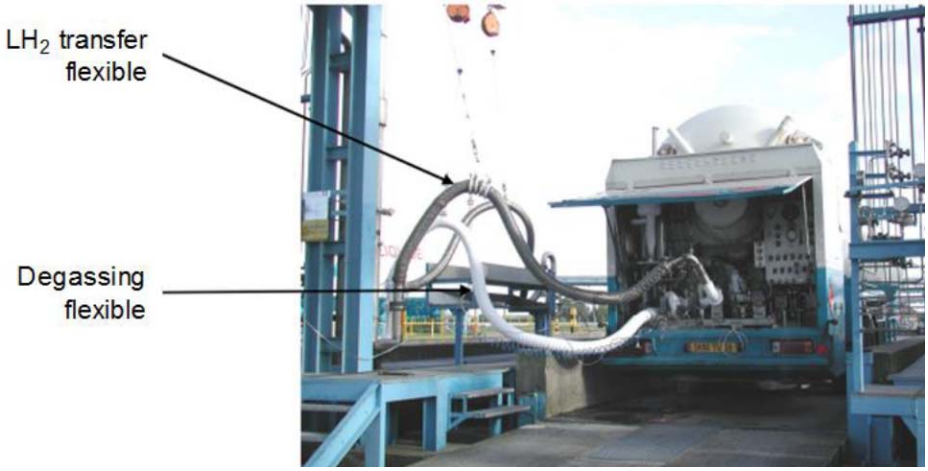

Figure 2-9. LH_2 transfer line from LH_2 trailer.

In a research and development project called icefuel, with the industry lead partners Evonik and LEONI, a flexible plastic pipe for combined transport of LH_2 and electricity via high temperature superconductor was tested (Fig. 2-10). For insulation, superinsulating material and a liquid nitrogen shield was used. The flexible pipeline could be used to supply residential area with chemical and electrical energy and information with an outer diameter of 40 mm only. Maximum transport capacity is 100–200 kW (LHV). [Markowz 2010].

Figure 2-10. icefuel cable (Courtesy LEONI, Nuremberg).

2.3.3 Ship Transport

Barges carrying liquid hydrogen have been used for fuel supply within the US and French space programs. Storage containers with a capacity of 947 m^3 of LH_2 (Fig. 2-11) are being used on the way from Louisiana to Florida since the NASA Apollo project, today serving the space shuttle. The European Ariane project was supplied with LH_2 by maritime transportation from New Orleans to Kourou, French Guiana, in 20 m^3 storage vessels with vapor or LN_2 cooled multilayer insulation [Peschka 1992]. These transports were discontinued with the operation of the 5 t/d capacity, on-site liquefaction plant since 1990.

Figure 2-11. NASA liquid hydrogen barge fleet.

As an important project in the development of a "CO_2-Free Hydrogen Supply Chain", HySTRA, Kawasaki Heavy Industries (KHI) is planning the demonstration of all necessary technologies on a 2017 pilot scale, and the examination of optimized locations, scales, configurations and cost efficiencies of the single chain components [Oyama 2013].

These include

- hydrogen production in Australia through both brown coal gasification and electrolysis with an overall capacity of 2660 t/yr;
- hydrogen liquefaction at a rate of 4.2 t/d;
- liquid hydrogen carrier ship with cargo capacity of 2500 m^3 for maritime transportation of 873 t/yr from Australia to Japan (corresponding to five roundtrips per year);
- liquid hydrogen stationary storage facility for 3400 m^3;
- hydrogen gas turbine power generation plant with a fuel consumption of 4.2 t/d.

An essential milestone of the HySTRA project was recently achieved with the construction, and completion of the world's first LH_2 carrier ship SUISO FRONTIER launched in December 2019 in Kobe, Japan (Fig. 2-12). The ship has an overall length of 116 m, a width of 19 m, a tonnage of 8000 t and is equipped with a diesel-electric propulsion system reaching a speed of 13.0 kn (~24 km/h) [KHI 2019]. The cargo ship has currently installed a single LH_2 tank with a capacity of 1250 m^3 featuring a double-shell structure with vacuum insulation in between [KHI 2020a].

Figure 2-12. SUISO FRONTIER, the world's first LH_2 carrier ship launched in 2019 with LH_2 storage tank [KHI 2020a].

Another major milestone was reached with the completion of an LH_2 receiving terminal in Kobe (Fig. 2-13), also a world's first-of-its-kind, designed to discharge a 2500 m^3-LH_2 cargo. The terminal includes a 2500 m^3 capacity stationary spherical LH_2 tank for longer-term storage [KHI 2020b].

The terminal was built for the CO_2-free Hydrogen Energy Supply-chain Technology Research Association (HySTRA). The Hydrogen Energy Supply Chain (HESC) is a joint Japanese-Australian venture.

Figure 2-13. KHI LH_2 receiving terminal in Kobe [KHI 2020b].

Commercial scale would need to develop much larger vessels, similar to today's LNG carrier ships of 160,000 m^3 and higher capacity. Various ship designs have been developed within the Euro-Quebec project for future maritime transportation (between Canada and Europe) [Giacomazzi 1993, Petersen 1994]. The barge carrier considered in the first stage was designed as a dock ship with a total length of 180 m and a width of 29 m carrying five barges (see also previous chapter) to contain a total of 15,000 m^3 of LH_2. Follow-on LH_2 tank ships are the dock ship and the so-called SWATH ship (Small Waterplane Area Twin Hull) developed by the German companies Howaldtswerke Deutsche Werft, Noell-LGA Gastechnik, and Germanischer Lloyd [Petersen 1994]. Both were designed for a load capacity of 125,000 m^3 to take up 8150 tons of LH_2. With a length of more than 300 m, the SWATH ship carries four spherical LH_2 tanks. The hydrogen propulsion system proposed, for which the LH_2 as well as the boil-off losses (~0.1 %/d) is to be used, is a gas turbine with steam injection of 41 MW.

2.3.4 Rail Transport

The transportation of cryogens in railway tank cars started in the beginning of the 1940s, where LOX was increasingly needed for the steel production. Liquid hydrogen transports in rail cars began in the 1960s by the Linde company using a 107 m^3 tank. The annular space between the inner and outer tanks has a vacuum drawn and is equipped with an insulation system using granular perlite or an alternating wrap of multiple layers of aluminum foil and paper. Measured boil-off rate was 0.2%/d. The US company Praxair is operating a fleet of 16 hydrogen rail cars. They are operated at a working overpressure of 55 kPa with a pressure control system to open the safety relief valve at an overpressure of 117 kPa. The quantities of LH_2 transported in rail cars over long distances (> 1000 km) are about 70 tons [Hudders 1963].

An extensive railway system exists at Baikonur where the cryogenics are moved from the storage tanks to the launch pad by rail cars.

Figure 2-14 depicts the design of a rail car for liquid hydrogen (and other cryogenic commodities) transports manufactured by the Chinese company CRRC Xi'an Co.,Ltd., a traditional enterprise in railway transportation equipment. The thermally insulated tank with a total volume of 85 m^3 to carry a payload of 5 t can be used for direct loading, unloading, or transfer filling [CRRCGC 2016].

Figure 2-14. T85-type liquefied hydrogen tank rail car.

2.4 Liquid Hydrogen Applications in Industry and Science

2.4.1 Mobile Applications

2.4.1.1 Cars

The German car company BMW started as early as 1978 its research on hydrogen-driven cars with a prototype internal combustion engine (ICE). There had been liquid hydrogen storage solutions demonstrated by BMW including safety testing under accidental conditions. Latest H_2 car generation is the BMW Hydrogen 7 (basis: BMW 760iL) of 2006, the first H_2 driven car for which series development process has been applied (Fig. 2-15).

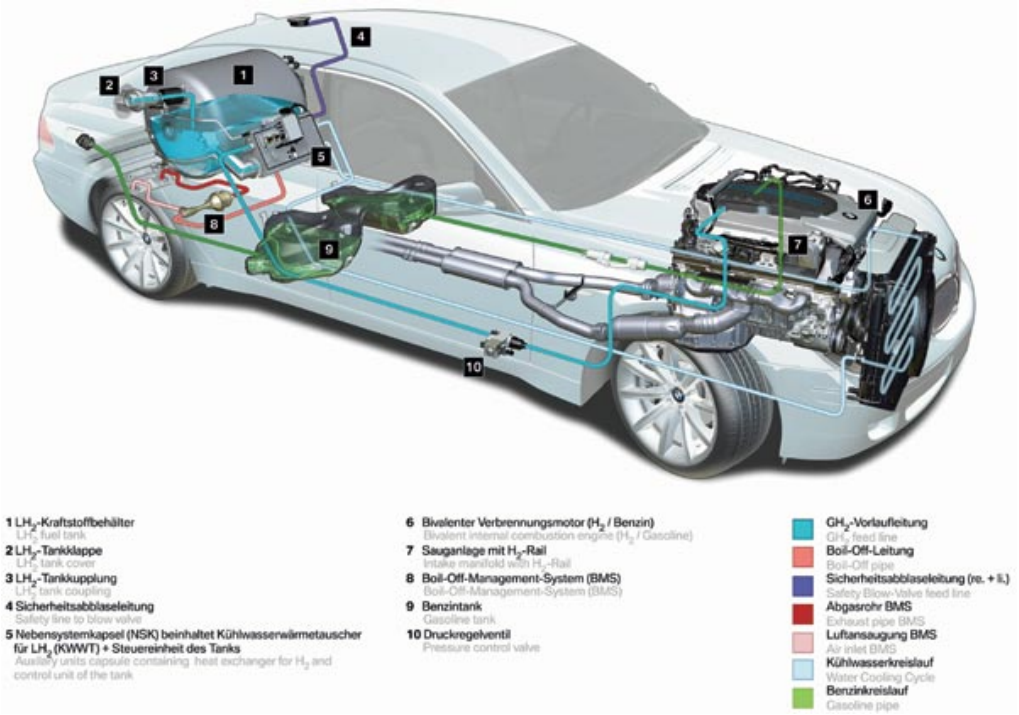

Figure 2-15. BMW 7 series with LH_2 storage tank and dual fuel (H_2 and gasoline) internal combustion engine (Courtesy of BMW CleanEnergy).

The BMW Hydrogen 7 is equipped with an 8 kg LH_2 tank for a cruising range of about 200 km and an average H_2 fuel consumption of 3.6 kg per 100 km. Although offering certain advantages with the low pressure and high densities the boil-off represents a considerable problem.

Present fuel storage concepts for hydrogen-driven vehicles include both the high-pressure gaseous storage and the cryogenic liquid storage, which requires an appropriate infrastructure including refueling devices for both modes.

In 2004, GH_2 and LH_2 dispensers have been fully integrated into a conventional service station in Berlin (Fig. 2-16) utilized by 17 H_2 driven vehicles (as of May 2007), but with a total capacity of 100 vehicles per day. While the gaseous H_2 is generated on-site by electrolysis, the liquid H_2 is delivered by tank truck. This H_2 filling station is operated by the CEP, a 5-years project of public and private partners to demonstrate production, storage, and distribution of H_2 and the operation, refueling, and maintenance of H_2 vehicles.

Figure 2-16. Refueling station for both GH_2 and LH_2 in Berlin (Courtesy BMW Group).

A liquid hydrogen supply system has the advantage of being capable to dispense the H_2 either as liquid or as high-pressure gas avoiding space consuming GH_2 storage. Only one LH_2 storage tank located underground with several tens of tons capacity is employed to serve both modes. Advantages are that separate storage devices for gaseous and liquid H_2 can be avoided as well as separate truck delivery for both modes. Another aim is to reduce filling time. High-pressure gas (70 MPa) is obtained by using newly developed cryogenic pumps which push the liquid into a heat exchanger where it heats up to ambient temperature. This key component is more compact, less noisy and needs less maintenance than a compressor which would be necessary in the case of gas delivery.

The first public station to offer liquid and gaseous hydrogen was opened in 1999 at the airport Munich in Germany and operated until 2006 (when the "ARGEMUC" project was terminated). The LH_2 delivered by truck was filled into a 12 m^3 storage vessel. Refueling of the vehicle was done automatically by a robot system. In the first two years, ~ 49 m^3 of LH_2 in more than 4000 refueling processes have been transferred into vehicle tanks. A new public filling station for LH_2 was opened in Munich in 2007 with the storage tank located underground. This station is one of the three mainly dedicated to the BMW Hydrogen 7 fleet.

"Weakest link" in the transfer lines between car tank and dispenser, i.e., the location with the maximum H_2 loss, is the cryogenic coupling. As the tank, it must have a double wall and vacuum insulation. Special constructions are necessary to transfer the cryogenic fuel and making sure that air ingress is avoided. Today's couplings are working with a floodgate which is purged and purified with helium to remove all air, before the valves on either end open at the same time. The refueling is made through an insulated pipe ("cold finger") inside the dispenser, which is pushed pneumatically into the filling line of the tank. The gaseous H_2 is removed from the tank and could be – as is the case in the Berlin filling station – routed to a fuel cell plant for electricity generation.

In principle, the problem related to the boil-off might be mitigated with a cryo-compressed storage, typically operated at 50 K and 35 MPa nominally. Such a system might be filled with cryo-compressed hydrogen, LH_2, or with compressed 35 MPa and represents a quite versatile solution.

Solid storage solutions, in particular conventional metal hydrides (Fe and Ti based storage material), are considered to be too heavy for light duty and cars. Although the light metal hydrides come close to the 7% weight performance (mass hydrogen / mass storage system) they require complex thermodynamic management for heat generated during refilling and required for extracting hydrogen.

2.4.1.2 Bus

Most buses carry the hydrogen as compressed gas. There are, however, a few examples where the hydrogen was stored in liquid form. From the three city buses tested within the Euro-Quebec project in the period 1995–1997, two were based on ICEs using LH_2 as fuel. One was a MAN bus with three superinsulated elliptical cryo-tanks with 200 ℓ geometrical volume each to contain a total of 570 ℓ of LH_2 in an underfloor arrangement allowing a cruising range of 250 km (Fig. 2-17). Starting 1996 the bus was test-operated over two years at the airport Munich and in Erlangen, Germany, since 1996. The other bus was of the Van Hool type equipped with two 200 ℓ roof-top-mounted LH_2 tanks as fuel supply system. As part of the EU project EUREKA, a hydrogen bus demonstrator was operated since 1995 using a 700 ℓ LH_2 tank in the rear of the bus to operate a 78 kW fuel cell power system for a 200 km cruising range.

Figure 2-17. MAN hydrogen-driven fuel cell bus of 1996 with LH_2 storage tanks.

2.4.1.3 Truck

The Musashi Institute of Technology as part of the Tokyo City University has already a long history (since 1970) in the development and testing of hydrogen-fueled vehicles with internal combustion engine. Shown in Fig. 2-18 is the 9th generation from 1996, Musashi-9, an LH_2 refrigerator truck where the cold hydrogen is also used to keep the cargo cool [Yamane 1996].

The world's first hydrogen-driven truck was Musashi-7, a modified medium duty truck, presented in 1986. The truck was equipped with a hydrogen-powered engine and with a 150 ℓ LH_2 tank. A high pressure LH_2 pump would provide the fuel to the engine. The pump delivered 8 MPa high pressure hydrogen gas to the engine and the fuel was injected to a hot surface igniter in DI combustion chamber [Takiguchi 1987].

Figure 2-18. Musashi-9 LH_2 truck Musashi Institute of Technology.

For storage of up to 100 kg of hydrogen currently compressed gaseous hydrogen at 35 to 70 MPa, cryo-compressed hydrogen and liquid hydrogen are investigated. The reference solution is the gaseous form with a 35 MPa Type 4 vessel which are typically integrated behind the driver cabin or above the rear axis. The LH_2 cryostats might be positioned at the same locations where the conventional fuel Diesel is stored. Two cryostats, each with about 500 ℓ empty volume have to be installed. For energy conversion either PEM fuel cells or an H_2 ICE might be chosen depending on the actual application and further criteria. In principle the technologies may be easily derived from the bus application, where more experience is available.

In June 2017 the Zurich engineering company ESORO received the road approval for the world's first fuel cell heavy-duty vehicle. It developed and built a fuel cell truck in the 35-tonne category. On-board storage of high-pressure hydrogen gas is made with seven tanks on a rack with a capacity of totally 34.5 kg of hydrogen [FCB 2016].

Daimler Trucks announced in 2020 the development of a fuel cell truck, GenH2 (Fig. 2-19), using on board storage of liquid hydrogen. The GenH2 Truck is designed to operate two fuel stacks each comprising 200 cells, for a total power output of 300 kW. Cruising ranges are expected to be in the order of 1000 km on a single tank filling. In cooperation with Linde, the next generation refueling technology will be developed based on subcooled liquidrogen (sLH_2). Daimler Truck AG plans to begin customer trials of the GenH2 Truck in 2023; series production may start in the second half of the decade.

Figure 2-19. Mercedes FC truck GenH2 concept with LH_2 storage.

2.4.1.4 Ship

Following an idea of 2014 to substantially reduce pollution in the San Francisco Bay by replacing the diesel-driven ferries with CO2 emission free, hydrogen-fueled ships, the Sandia National Laboratory conducted a study on the feasibility of a zero-emission, hydrogen fuel cell, high-speed passenger ferry, called the SF-BREEZE [Pratt 2016]. The ship is designed as a commuter ferry for 150 passengers to travel four 50 nm (~93 km) round-trip routes each day at a top speed of 35 knots (~65 km/h). Figure 2-20 shows a schematic of SF-BREEZE [Pratt 2016]. The on-board storage of fuel was selected to be liquid hydrogen to minimize the weight and thus enhance the ship's performance. A total of 1200 kg (or 17 m3) of LH2 are stored in a single tank installed on the roof. Power is provided by 41 PEMFC racks, each rack composed of four 30 kW FC stacks amounting to a total of 4.92 MW.

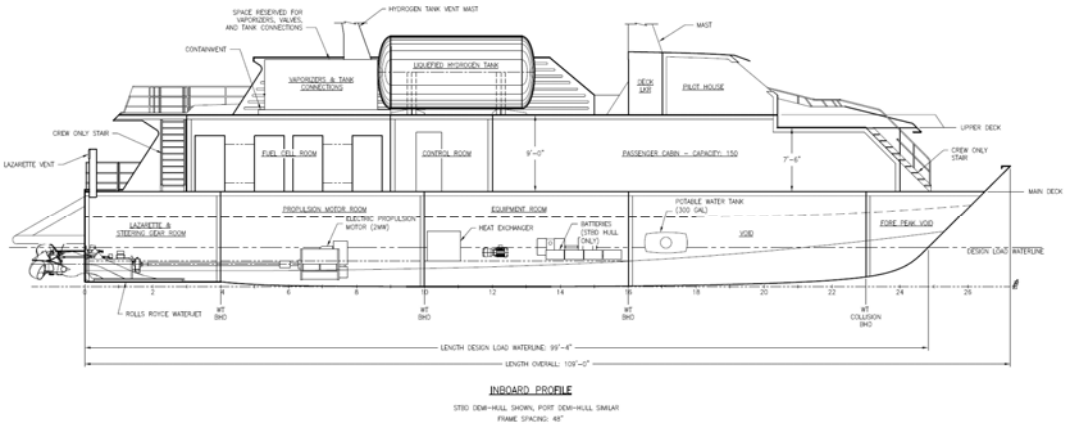

Figure 2-20. SF-BREEZE, a Zero-Emission, Hydrogen Fuel Cell, High-Speed Passenger Ferry [Pratt 2016].

The Norway-based shipping company Norled has started the development of hydrogen-powered car ferries considering two options for the storage of the hydrogen fuel, as liquid or as compressed gas (Fig. 2-21). For the cryo-version, Linde will supply both the liquid hydrogen and the related infrastructure. Power is provided by two 200-kW fuel cell modules. The LH_2 tank will be installed on the roof [Moore 2019].

Figure 2-21. On-deck arrangement of LH_2 storage, fuel cell and vent mast on the NORLED ferry [NORLED 2019].

Starting in 2021 the EU project HySHIP with 14 partners and led by the Norwegian shipping operator Wilhelmsen targets at the development of a zero-emission prototype ship with hydrogen propulsion. It is based on the so-called 'Topeka" concept (Fig. 2-22) planned to operate between the offshore supply bases on the Norwegian west coast. The ship will be equipped with a 3 MW PEM fuel cell stack and supported by a 1 MWh battery pack for the purpose of optimization of load and efficiency of the fuel cells. On-board storage of hydrogen will be a single LH_2 tank installed on the roof.

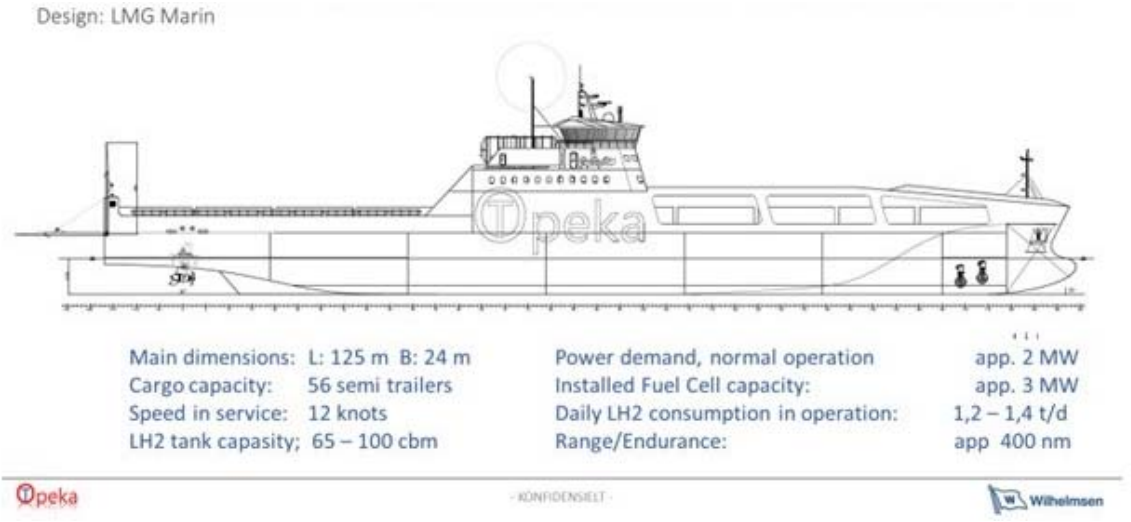

Figure 2-22. Design of the TOPEKA prototype FC ship with on-board storage of LH_2 [Turner 2020].

2.4.1.5 Aircraft

The idea to use LH_2 as aircraft fuel was considered since the early 20th century stressing that H_2 had a greater heat content than any other fuel, higher fuel flight efficiency, lighter weight, less noise, and reduced pollution. Also in terms of safety, LH_2 is expected to be safer than the conventional kerosene due to smaller endangered areas and shorter fire duration.

The first successful in-flight test of an experimental hydrogen-propelled aircraft was made in the USA. In a B-57B twin-engine aircraft, one turbojet engine was converted to run on both JP-4 and hydrogen fuel (Fig. 2-23). The stainless steel tank for the LH_2 on the left wing tip was 6.2 m long, had a volume of 1.7 m^3 and a 50 mm plastic foam insulation. The aircraft was supposed to start with the conventional JP-4 fuel, be switched to H_2 fuel at an altitude of ~ 16,400 m, before switched back to JP-4 and return to the ground under normal operational conditions [Sloop 1978]. Due to the significant loss of LH_2 fuel during chill-down of all LH_2 lines, it was considered wise to have the chill-down process made with liquid helium on ground prior to the flight [Dawson 2004]. On Feb. 13, 1957, the first of three successful flights took place. The one engine operated on H_2 for about 20 min at a speed of Mach 0.72 before the fuel tank was running empty [Sloop 1978].

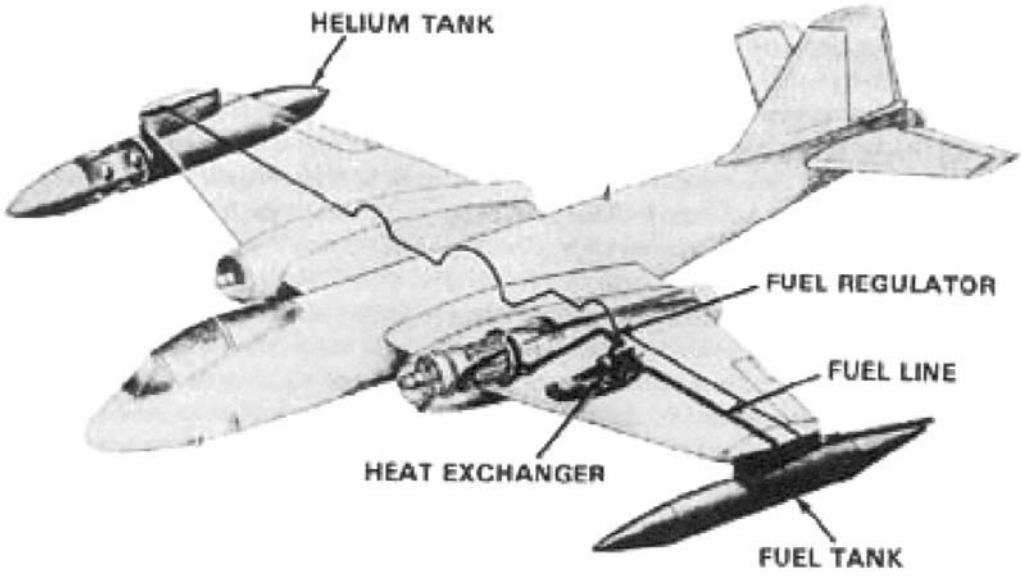

Figure 2-23. B-57B twin-engine aircraft with one engine fueled by LH_2 successfully operated first in 1956 [Sloop 1978] (Courtesy of NASA).

In 1988, a four-seater Grumman Cheetah with an LH_2 fueled internal combustion engine became the first and sole, so far, airplane to take off, cruise, and land by means of hydrogen power only [Peschka 1992], although it was a 36 s flight only.

In the same year, the Russian company ANTK-Tupolev has operated the “Flying Laboratory” Tu-155 (Fig. 2-24), which is a hybrid version of the Tu-154 airplane [DASA 1992]. One of the three engines (“NK-88”), the one in central position, could be fueled with either hydrogen or natural gas stored in a 17.5 m^3 capacity tank. The maiden flight on April 15, 1988, lasted 21 min; total operating experience with LH_2 accumulated to 10 hours [Tupolev 2008].

Figure 2-24. Tupolev 155 "Flying Laboratory" of 1988 with the central engine fueled by LH_2 or LNG (Courtesy of PSC Tupolev).

The project CRYOPLANE was launched in 1990 by a joint German-Russian consortium (DASA as the lead with main partners MBB, MTU, Tupulev, Kuznetsov) with the objective to study the feasibility of an aircraft propelled by cryogenic fuels [DASA 1992]. An Airbus A310-300 was selected as the baseline aircraft to be converted to LH_2 propulsion. For the new fuel tank concept, the most favorable design was seen in the top-mounted tank configuration with four tanks, two active ones with 40 m^3 each for either engine, and two passive ones with 80 m^3 each to refill the active tanks (Fig. 2-25).

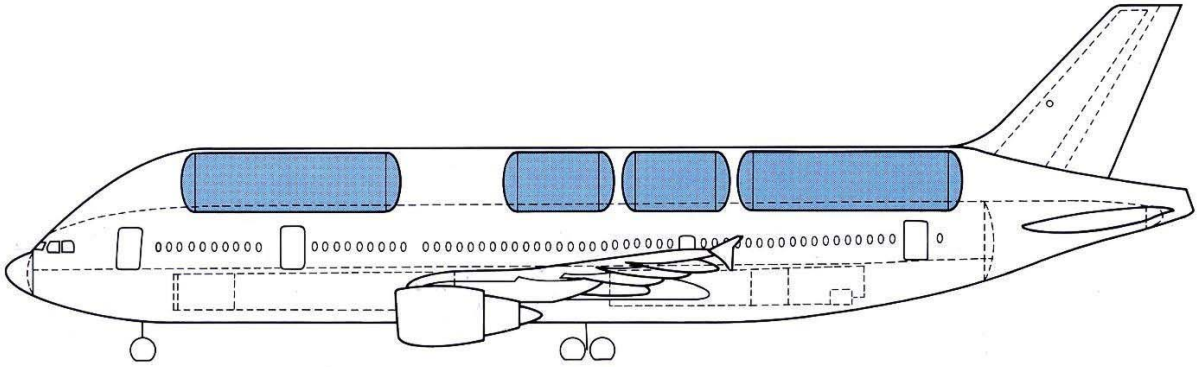

Figure 2-25. Schematic of the Cryoplane demonstrator based on an Airbus A310-300 with the top-mounted LH_2 tank arragement [DASA 1992] (Courtesy of Airbus Deutschland GmbH)

A technological development program for the fuel system components began in 1993 including the selection of materials for tanks and piping, control system and sensors for hydrogen leak detection, fuel pumps, LH_2 gasifier, combustion chamber. The first generation of LH_2 aviation was foreseen to require a fleet of 400-500 airplanes and the respective modification of ~70 European airports. The fuel consumption was assessed to be about 2 million t/yr of LH_2 or ~170 t/d for an average airport.

Recently, Airbus unveiled three concepts for a hydrogen-fueled "ZEROe" aircraft that utilize liquid hydrogen to power modified gas turbine engines. Shown in Fig. 2-26 is the turboprop concept for short-range flights and a cruising range of more than 1000 nautical miles (~1852 km).

Figure 2-26. One design of the Zero Emission Airbus [Airbus 2020].

2.4.1.6 Spacecraft

The application of liquid hydrogen as a fuel in space rockets was suggested, because it was expected to provide high exhaust velocity due to its high heating value and low molecular mass, its rapid conversion of energy to heat, and its cooling capacity. Due to the need of saving weight on the one hand and very short lifetimes on the other hand, LH_2 tanks for rockets or space ships usually consist of thin-walled stainless steel tank structures.

The Atlas–Centaur rocket was the first rocket to use the combination of liquid hydrogen/oxygen (LH_2/LOX) for propulsion. This rocket's second stage, Centaur, used the RL10 LH_2/LOX rocket engine manufactured by Pratt and Whitney. The lightweight and very reliable RL10 used liquid hydrogen to cool the engine nozzle, and the heat absorbed by the liquid hydrogen caused the hydrogen to expand, after which it flowed through a turbine. The rotation of the turbine was mechanically coupled to the LH_2 and LOX pumps which pump the propellants to the combustion chamber.

The NASA programs Apollo and Space Shuttle applied liquid hydrogen at a large scale. In the Apollo program, it was used in the secondary stage of the Saturn rockets. Fuel for the Space Shuttle was a combined system of external tank with LH_2/LOX fuel (Fig. 2-27) and rocket boosters containing solid fuel. The three main engines were running on LH_2/LOX reaching a thrust of ~1.8 MN each and designed for a burning time of about 9 min. Low-pressure and high-pressure turbo pumps pressurized the fluids to 30 MPa (oxygen) and 45 MPa (hydrogen), respectively, before injected at rates of 424 kg/s and 70.3 kg/s, respectively, into the combustion chamber and spark-ignited. The quantities of fuel on-board a space shuttle before start are 2380 m^3 of LH_2 with a weight of 106.3 t and 946 m^3 of LOX with a weight of 629.3 t.

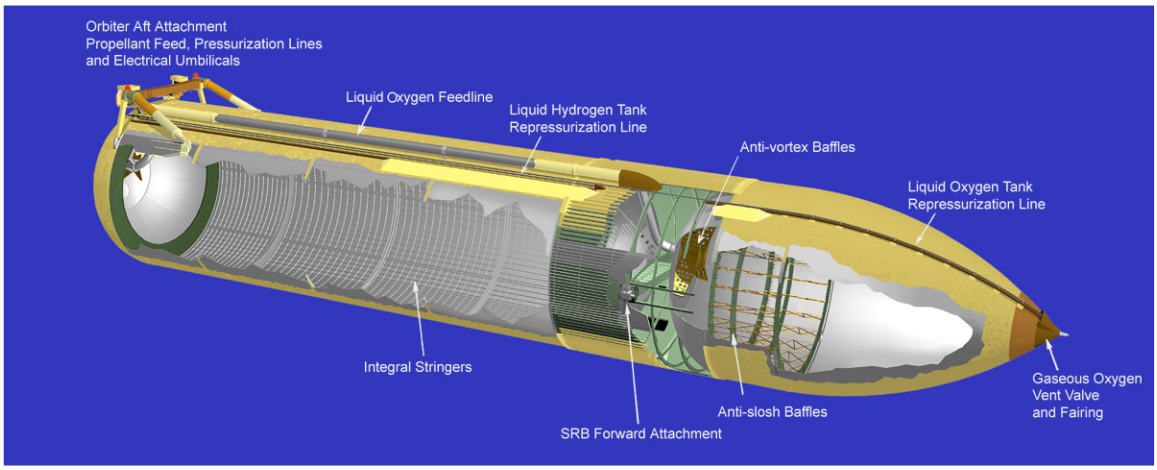

Figure 2-27. External Tank of the Space Shuttle (Courtesy of NASA).

Today its use is expanding to include government and commercial organizations like United Launch Alliance, Boeing, and Blue Origin.

2.4.2 Use of LH_2 in Industries

2.4.2.1 Chemical and Petrochemical Industries

By far the largest amount of hydrogen is consumed in the chemical and petrochemical industries. A non-energetic utilization of hydrogen is mainly given as raw material in the synthesis of ammonia (NH_3) for fertilizer and plastic production, methanol, polymers, or solvents. It is required in the direct reduction process of iron to iron sponge or raw iron and in the production of alcohols via oxo-synthesis. An indirect energetic utilization is given in refineries where the H_2 is used in catalytic cracking operations or hydro-treating to upgrade heavy and unsaturated compounds into lighter and more stable species. It is also needed in the production of synthetic fuels via Fischer-Tropsch synthesis, of methanol, or of synthetic natural gas. Furthermore, it is used in the hydrogenation of coal and heavy crude oil.

Hydrogen is also taken to remove sulfur from crude oil and gasoline, and to purify gases, e.g. by capture of oxygen traces in argon. In power plants, LH_2 can be used for the cooling of large electric generators. Sites where no H_2 production plant is available, delivery is preferably in form of liquid hydrogen.

2.4.2.2 Metal Industries

In the metal industries, LH_2 is used in the metal production process directly (e.g., tungsten, tungsten carbide, molybdenum metal powder), and also, if mixed with inert gases, in secondary processes to act as reducing atmosphere in heat treating, sintering, copper brazing.

2.4.2.3 Electronic Industries

Highly pure hydrogen is mainly needed as a carrier gas for active elements as arsine and phosphine in the manufacture of integrated circuits, polycrystalline silicon for semiconductors, optical fibers for communication, or fused quartz. Pure water vapor

required is generated from mixing oxygen with vaporized LH_2. The hydrogen is either used as atmosphere or as a clean burning fuel.

2.4.2.4 Food Industries

The properties of fats and oils are changing through hydrogenation of organic intermediate products like amines and fatty acids making food less susceptible to oxidation and spoilage.

2.4.3 Use of LH_2 in Scientific Research

2.4.3.1 H_2/O_2 Steam Generator

A research project with a high potential for application in the power generation industries is a hydrogen-oxygen fueled steam generator developed by the DLR and other German companies from 1989 to 1993. This component is actually the re-configuration of an H_2/O_2 rocket engine which allows the instantaneous provision of steam of any desired quality. H_2 and O_2 are compressed and injected in a combustion chamber.

Stoichiometric mixture is necessary to generate superheated steam of high quality without any side products. The combustion gas with a temperature of 3000°C can be cooled by adding water to achieve exactly the desired steam condition for injection into the power plant process. Such a steam generator can act as a backup system for fast power-up of steam generation plants to serve as a cold stand-by spinning reserve in decentralized power production.

In a first step, totally 285 combustion tests were conducted in 1991/92 with a prototype operated in the power output range between 25 and 70 MW. The second step was the construction of the demonstration facility for H_2/O_2 instant reserve, HYDROSS, consisting of a modified H_2/O_2 steam generator of 2 m length and 0.4 m outer diameter plus storage and supply system [Kusterer 1995]. Full power was obtained after 1 s, and after 3–5 s, there was stable steam production. The experimental version of the steam generator produced steam of 560–950°C at 4–9 MPa. This compact, soot-free, and low-cost component is principally ready for the market. The facility and a schematic are shown in Fig. 2-28 [Haidn 1996].

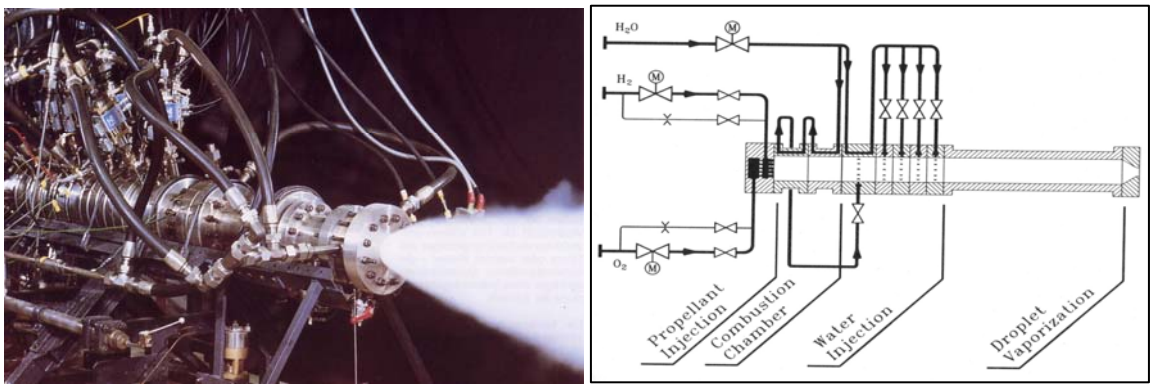

Figure 2-28. Schematic of the DLR LH_2-LOX steam generator [Haidn 1996] (Courtesy of DLR).

2.4.3.2 Bubble Chamber

The bubble chamber was invented in 1952 as an instrument to detect and visualize moving electrically charged elementary particles. It is a cylindrical vessel filled with a transparent liquid just below its boiling point. A piston is used to suddenly decrease pressure, by which the liquid goes into a superheated metastable phase. When a particle passes through, the liquid is warmed up to the boiling point along the track of ions created. In the wake remains a trail of microscopic bubbles that can be photographed. Bubble density around a track is proportional to the particle's energy loss. The resolution achieved is down to a few micrometers. Also, the recovery time is short; bubble chambers could be operated at 20 pulses/s. Liquid hydrogen is used because it offers the possibility of simple particle interactions, as hydrogen nuclei consist only of single protons. The magnetic field applied serves to curve the tracks of charged particles to ease their identification. The schematic of a bubble chamber is given in Fig. 2-29.

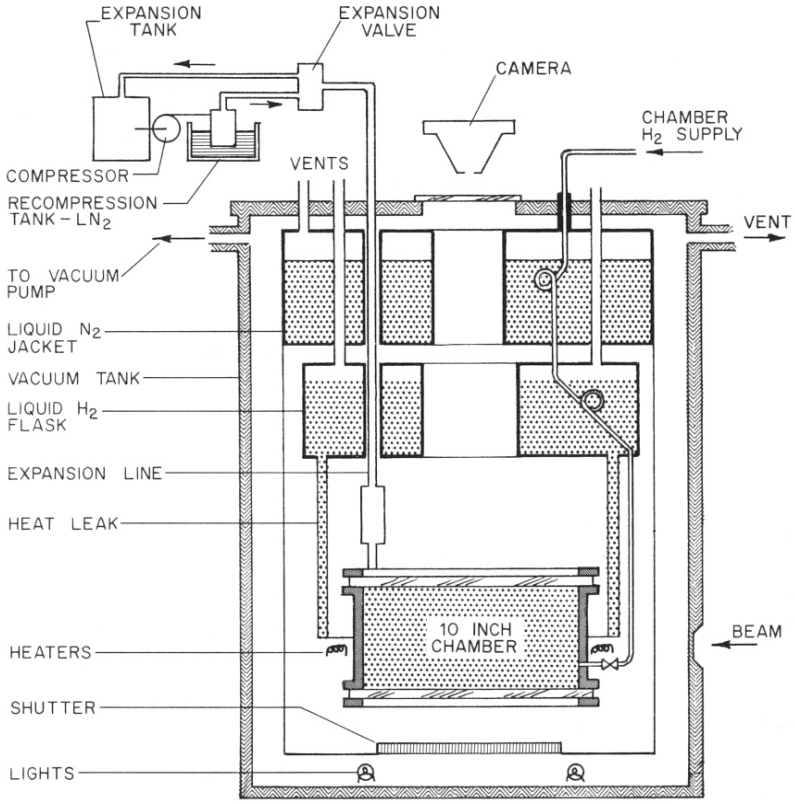

Figure 2-29. Schematic of a bubble chamber[Sittig 1963].

Early bubble chambers were very small. The first fabricated was a 100 mm long glass tube of 0.25 mm diameter filled with diethyl ether. The first device to work with LH_2 built in 1954 was a chamber of 37 mm in diameter. Successor models were rapidly growing in size. In 1959, a 180 cm long bubble chamber filled with 500 ℓ of LH_2 (also LD_2) was erected in Berkeley, where the liquid was kept at a temperature of 26 K and at an overpressure of about 0.4 MPa. More than 100 bubble chambers were built throughout the world operating on liquid hydrogen or deuterium, but also propane, argon, or helium were used as working fluids.

Among the largest chambers was the Big European Bubble Chamber (BEBC) at CERN in Geneva installed in the early 1970s. It consisted of a stainless-steel vessel measuring 3.7 m in diameter and 4 m in height, and was filled with 35 m^3 of liquid hydrogen (or

deuterium or a neon-hydrogen mixture). Its sensitivity was regulated by means of a huge piston weighing 2 t. The chamber remained filled over longer periods of up to one year. In case of too high pressures, a safety relief valve was activated to dump the leaking gas into a large sphere. A critical issue was the tight sealing of the glass window in larger bubble chambers due to different shrinkage rates of the glass and metal materials. BEBC operation ended its active life in 1984. After a 30 year long bubble chamber era, this detection technique came to an end and was gradually replaced with spark chambers.

2.4.3.3 Neutron Moderator

Hydrogen is one of the most attractive materials for cold moderators in steady or pulsed neutron sources. These are devices to generate slow neutrons with energies < 0.005 eV and respective wavelengths in the order of inter-atomic distances, an ideal investigation tool for scattering experiments in material sciences. Depending on the user's requirements, the neutrons generated in either a nuclear material test reactor or a spallation source are slowed down by passing through a moderator. The lower the temperature of the moderator, the higher is the yield of slow neutrons. LH_2 or LD_2 is in use as cold moderator material in MTRs since 1957.

The European Spallation Source, ESS, a joint European project and currently under construction in Lund, Sweden, was – according to its concept in 2002 [ESS 2004] – designed as a 10 MW facility with a linear accelerator producing a proton beam to serve two target systems. The type of the target was flowing mercury (it will be solid tungsten in Lund). Cold moderator systems (two for each target) were to be employed to slow down the liberated neutrons to a desired energy spectrum, before they are routed into the instruments of the users.

Supercritical hydrogen and liquid hydrogen are considered ideal moderators in that they offer a high cross section and large energy transfer per collision and, as a liquid, allows easy heat removal. The advantage of supercritical hydrogen over sub-cooled liquid is the total absence of problems with two-phase flow especially during cool-down, warm-up, stand-by, or other transient conditions. Ortho H_2 is the stronger neutron scatter than para H_2 and is ideal to maximize the production of cold neutrons showing the higher integrated intensity.

An advanced cold moderator system which was foreseen for the ESS project is shown in Fig. 2-30 [ESS 2004]. Dimensions of the chamber are 120 mm in length, 150 mm in height, and 50 mm in thickness. Moderating material is a flow of supercritical H_2 at 1.5 MPa (which is 0.2 MPa above the critical pressure) with inlet/outlet temperatures of 25 K and 28 K, respectively, to remove the power of maximum 7.5 kW produced in the chamber. Flow obstacles inside the chamber were to create a temperature distribution as homogeneous as possible (Fig. 2-30, bottom left).

Due to the need of permanent heat removal, a self-sustained, closed-cycle refrigeration system is required. Insulation of the cold helium and hydrogen systems is made by a vacuum containment. All H_2 containing systems including transfer lines (Fig. 2-30, bottom right) are surrounded by a helium blanket to serve the purpose of detecting leakages in the vacuum containment and preventing air ingress. This safety concept corresponds to a "triple containment" system to avoid pumping of air and thus oxygen to the cold surface in the case of a small leak in the outer shell. The triple containment is a characteristic – and crucial – feature of all cold moderator systems.

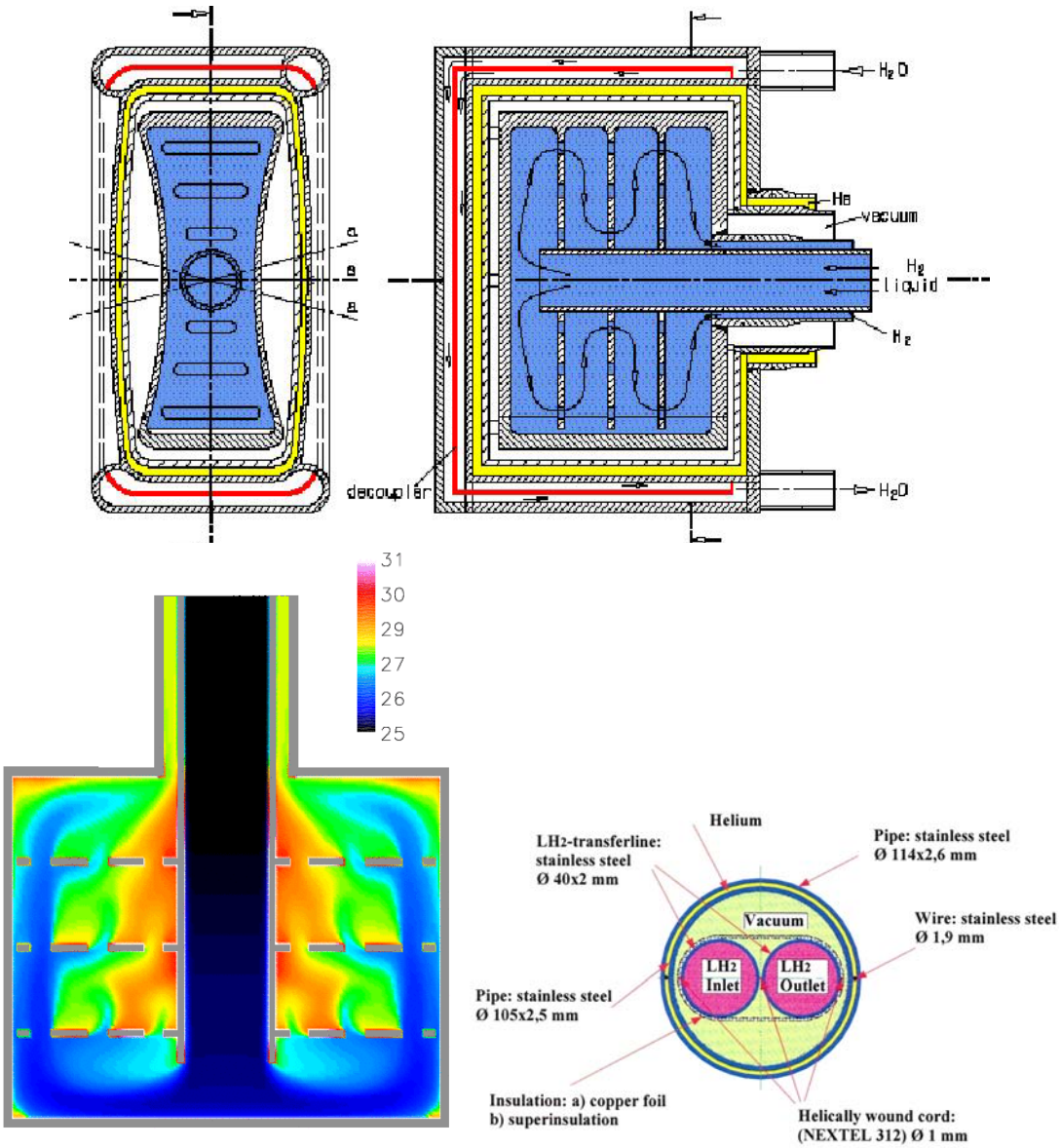

Figure 2-30. Supercritical hydrogen moderator system of the European Spallation Source Top: horizontal and vertical cut through chamber (walls and gaps enlarged) Bottom, left: fluid temperature distribution in chamber during normal operation Bottom, right: Cross section of the hydrogen transfer lines (rigid sections) [ESS 2004].

2.4.3.3 Heavy Water Production by LH_2 Distillation

The fractional distillation of liquid hydrogen and subsequent conversion of the deuterium to heavy water is an efficient method based on the fact that boiling points are different for H_2 (20.3 K) and D_2 (23.5 K) and HD (22.1 K), respectively. As the hydrogen gas above the liquid is slightly depleted in deuterium, the D_2 can be gathered by simple vaporization of liquid hydrogen. Reactions of the form

$$2\ HD \quad \rightarrow \quad H_2 + D_2$$

result in a ternary mixture with fractions in the order of 25% each for H_2 and D_2, with still 50% remaining HD. The separation process is conducted in several subsequent stages. In

a separate column, the pure D_2 is extracted from the mixture. Advantages of the refrigeration process are a separation factor (ratio of D_2 concentration in the liquid over concentration in the vapor) of ~1.5 and a moderate energy demand. Major drawback is the need for a highly pure H_2 feed [Miller 2001].

The former Soviet Union was successful in the construction of an industrial-scale plant for D_2 production in 1958 [Malkov 1958]. The distillation columns had typical sizes of up to 10 m in height and 1–2 m in diameter. The columns were insulated by a vacuum jacket and an LN_2-cooled heat barrier or installed inside an LN_2-cooled vacuum cold box. Operating conditions were in the ranges of < 35 K and 0.5–5 MPa. An important safety-related aspect was the necessary removal of impurities (N_2, O_2) which may plug lines upon freezing.

3 Behavior

3.1 Release and Dispersion

Most experimental work to investigate the safety of cryogenic liquefied gaseous fuels began in the 1970s concentrating mainly on LNG and LPG, commodities which were shipped around the world to a tremendously increasing extend. Main goal of these works was the investigation of accidental spill scenarios during maritime transportation. A respective experimental program for liquid hydrogen was conducted on a much smaller scale, initially by those who considered and handled LH_2 in larger quantities (space programs). Main focus was on the combustion behavior of the LH_2 and the atmospheric dispersion of the evolving vapor cloud after an LH_2 spill. Only little work was concentrating on the cryogenic pool itself, whereby vaporization and spreading never were examined simultaneously.

3.1.1 Cryogenic Release Modes

The processes of release and subsequent distribution of a gas are strongly dependent on its thermodynamic state during storage. Pressurized gases form a free jet or will be flash-released, if there is a complete failure of the storage vessel. For cryogenic storage, the substance will be liberated - depending on the leak location - as saturated vapor or as a liquid which starts to vaporize immediately. Parameters of concern are the expansion of a flammable vapor cloud, the height that it could attain, the time until it becomes sufficiently diluted below the flammability limits, and the total quantity of fuel in the cloud.

3.1.1.1 Single-Phase Releases

Experiments were carried out on releases of cryo-compressed hydrogen with temperatures 50, 200 and 300 K, and pressures up to 90 MPa [Kobayashi 2018]. Release diameter was in the range 0.2–1 mm. Results showed that for decreasing supply temperature, there is an increase in leakage flow rate and hydrogen concentration. The results of hydrogen distribution were used to build an empirical relationship to determine the 1% concentration distance based on the hydrogen mass flow rate.

Ulster University analyzed the applicability of notional nozzle theory [Molkov 2009] in CFD simulations to predict concentration decay in cryogenic under-expanded jets (PRESLHY D3.2, 2021). The CFD model employed a RANS approach with realizable κ-ε model for turbulence. Simulation results well predicted experiments by [Hecht 2019] with release pressure up to 0.5 MPa and temperature in the range 50–61 K (Fig. 3-1). CFD results showed that for the given scenario the presence of a co-flow of air to the jet did not affect the axial hydrogen decay. The extraction velocity at the hood was found to not affect results when varied in the experimental range 2–8 m/s.

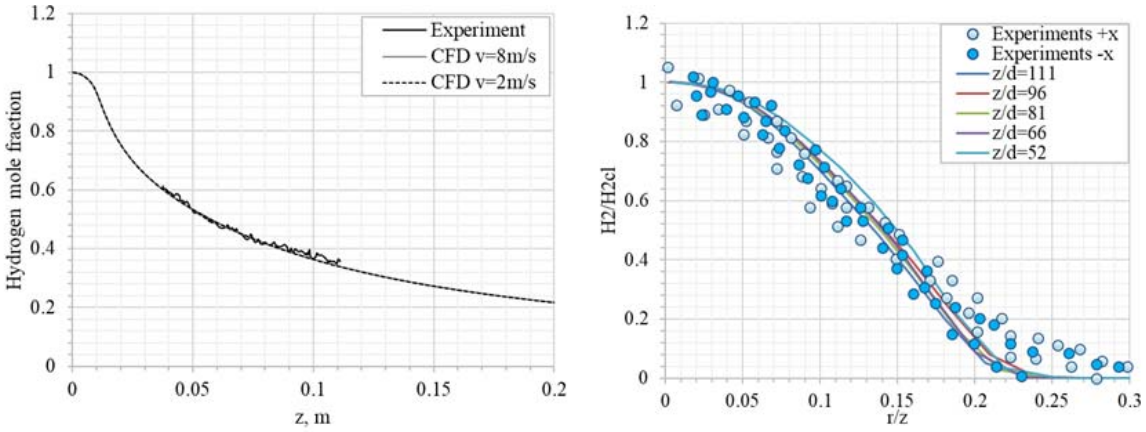

Figure 3-1. Hydrogen concentration along the jet axis (left) and normalized radial distance (right): simulation results versus experiments for test with T = 61 K, P = 0.2 MPa, and d = 1.25 mm.

A CFD benchmark study on [Hecht 2019] was conducted among partners Air Liquide, National Center for Scientific Research "Demokritos", Ulster University and Karlsruhe Institute of Technology (PRESLHY D3.2, 2021). The different approaches employed RANS and DES simulations and compared CFD predictions to experimental hydrogen and temperature distributions to assess the different models capabilities.

The properties of the cryogenic flow at the nozzle can be significantly affected by heat transfer through the wall of a non-insulated pipe connecting the storage system to the nozzle. This was investigated numerically by Ulster University (PRESLHY D3.2, 2021) and results showed that even in a release pipe as short as 60 mm exposed to external ambient temperature air, the inclusion of heat transfer effect can cause a decrease of 9% of the hydrogen mass flow rate and significant variation of the flow temperature and properties at the nozzle.

3.1.1.2 Multi-Phase Releases

Experiments were carried out on cryogenic hydrogen choked releases through an elliptical converging-diverging nozzle with 2.934 mm throat diameter [Simoneau 1979]. Examined hydrogen stagnation conditions were in the sub-cooled liquid regime. Pressures were in the range 1.29–5.89 MPa and temperatures in the range 27.2–32.3 K. The NASA experiments were used in several modeling studies to assess the capability of multiphase release models to predict the hydrogen mass flow rate and properties at the nozzle.

A Homogeneous Non-Equilibrium Flash Model (HNEM) was used [Travis 2012] which accounts for liquid superheat through a constant, prescribed “non-equilibrium” parameter. The approach implements the NIST EoS [Leachman 2009]. Calculations resulted in consistently larger mass fluxes than experimentally measured, but within a 10% variation.

The Homogeneous Equilibrium Model (HEM) was used to model NASA releases [Venetsanos 2017]. Also in this case, NIST EoS was used and mass flow rate was predicted with a 10% accuracy.

A Homogeneous Non-Equilibrium model (HNEM) was proposed [Venetsanos 2018] which is an intermediate between HEM (homogeneous equilibrium) and HFM (homogeneous frozen) models. The model does not present any sound speed discontinuity when crossing the liquid saturation (bimodal) curve. The HNEM model was seen to

improve predictive capability for the NASA experiments with low mass fluxes in comparison to HEM.

3.1.1.3 Blowdown of a Storage System

During blowdown of pressurized hydrogen storage systems, temperature in the tank decreases due to the gas expansion. This process competes with the tendency of the gas temperature to increase due to the heat transfer through the tank wall. A study [Schefer 2007] highlighted the importance to include heat transfer effect on blowdown dynamics. This may further gain significance in the case of cryo-compressed storage tanks with a damaged insulation. A non-adiabatic blowdown model accounting for heat transfer through the wall of high pressure hydrogen tanks was developed and validated [Dadashzadeh 2019]. The under-expanded jet theory [Molkov 2009] was employed to calculate parameters at the real and notional nozzle exits. Abel-Noble EOS was used to take into account the non-ideal behavior of hydrogen gas.

In the frame of PRESLHY project (PRESLHY D6.5, 2021), the theoretical model was further developed to extend its application and validation to cryo-compressed hydrogen. In this formulation, the non-ideal behavior of cryogenic hydrogen is taken into account by using NIST EOS by implementing CoolProp database to evaluate hydrogen thermodynamic parameters [Bell 2014]. The model takes into account convective heat transfer at the internal and external interfaces: hydrogen/wall and wall/external ambient, respectively. Nusselt correlations are employed to calculate the convective heat transfer coefficients in either natural or forced convection regimes. Conduction through the wall is calculated by solving an unsteady heat transfer one-dimensional equation though the finite difference method. The model can be applied to cryogenic hydrogen storages as it has been validated against experimental tests performed within PRESLHY project with initial storage temperature of 80 K and pressure up to 20 MPa. The model well represented pressure and temperature dynamics during blowdown for releases with diameter in the range 0.5–4 mm. As an example, Fig. 3-2 shows the comparison between simulated and experimental pressure and temperature dynamics in the tank for a release test through a 1 mm diameter with initial conditions p = 20 MPa and T = 80 K.

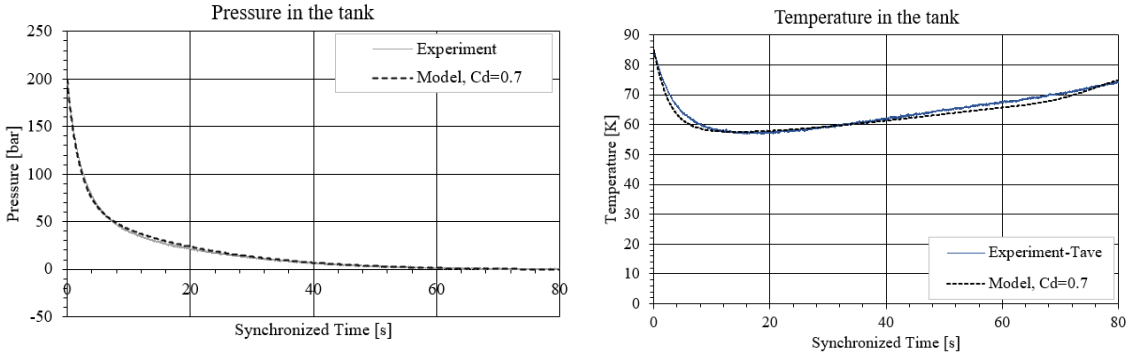

Figure 3-2. Blowdown of a tank with initial storage pressure and temperature 20 MPa and 80 K, nozzle diameter of 1 mm. Pressure and temperature dynamics in the tank: experiments versus simulations using a discharge coefficient (C_d) equal to 0.7.

CFD modeling of transient hydrogen releases during a storage tank blowdown may be challenging in terms of numerical efforts. Employing a notional nozzle as inflow boundary with specified flow velocity would require a change of the numerical grid because of transient in time release conditions and notional nozzle diameter during

blowdown process. A different approach was employed by Ulster University to simulate numerically Pro-Science experiments on cryogenic hydrogen releases (PRESLHY D3.2, 2021). This is the volumetric source approach and it employs source terms for mass, momentum, energy, turbulent kinetic energy and turbulent dissipation rate depending on the dynamics of properties at the notional nozzle.

3.1.2 Liquid Pool Spreading/Vaporization

3.1.2.1 Phenomenology

The release of hydrogen as a liquefied gas usually results in the accumulation and formation of a liquid pool on the ground, which expands, depending on the volume spilled and the release rate, in radial direction away from the release point, and which also immediately starts to vaporize [Verfondern 2007]. The most dominant heat source is heat transport from the ground. This contribution is based on the relationship between heat flux density and the temperature difference between cryogen and surface ("Nukiyama curve") [Brentari 1965]. Figure 3-3 shows the comparison of experimentally derived heat flux densities with correlations recommended for the film boiling regime ("Kutateladze") and the nucleate boiling regime ("Breen & Westwater") [Dienhart 1995]. Upon contact with the ground, the cryogen will in a short initial phase slide on a vapor cushion (film boiling) due to the large temperature difference between liquid and ground. The vaporization rate is comparatively low and if the ground is initially water, no ice will be formed. With increasing coverage of the surface, the difference in temperatures decreases until – at the Leidenfrost point – the vapor film collapses resulting in enhanced heat transfer via direct contact (nucleate boiling). On water, there is the chance of ice formation which, however, depending on the amount of mass released, will be hindered due to the violent boiling of the cryogen.

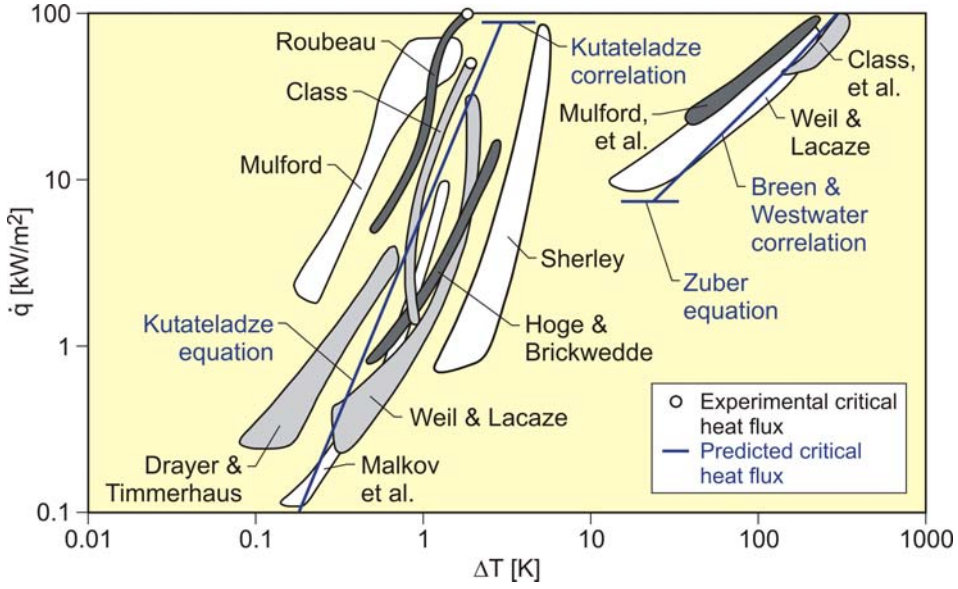

Figure 3-3. Correlations of the Nukiyama curve for hydrogen based on experimentally covered ranges for the heat flux density [Dienhart 1995].

Above a certain amount of a cryogenic liquid released, a pool on the ground is formed. Both diameter and thickness of the pool are increasing with time until an equilibrium state is reached. After termination of the release phase, the pool is decaying from its

boundaries. It breaks up in floe-like islands when the thickness drops below a certain value. This minimum thickness is determined by the surface tension of the cryogen and is typically in the range of 1–2 mm. The development of a hydraulic gradient results in a decreasing thickness towards the outside.

The spreading of a cryogenic pool is influenced by the type of ground, solid or liquid, and by the release mode, instantaneous or continuous. In an instantaneous release, the release time is theoretically zero (or release rate is infinite), but practically short compared to the vaporization time. Furthermore the cryogen spreading on the surface penetrates the water to a certain degree, thus reducing the effective height responsible for the spreading and also requiring additional displacement energy at the leading edge of the pool below the water surface. The reduction factor, δ, is given by the density ratio of both liquids:

$$\delta = 1 - \frac{\rho_{liquid}}{\rho_{water}}$$

telling that only 7% of a liquid hydrogen pool will be below the water surface level compared to, e.g. more than 40% of LNG or even 81% of LN_2. The factor δ is 1 for a solid ground.

A special effect was identified for a continuous release particularly on a water surface. The equilibrium state is not being reached in a gradually increasing pool size. Before reaching the equilibrium state, the pool sometimes forms a detaching annular-shaped region which propagates outwards ahead of the main pool (see Fig. 3-4, left) [Brandeis 1983].

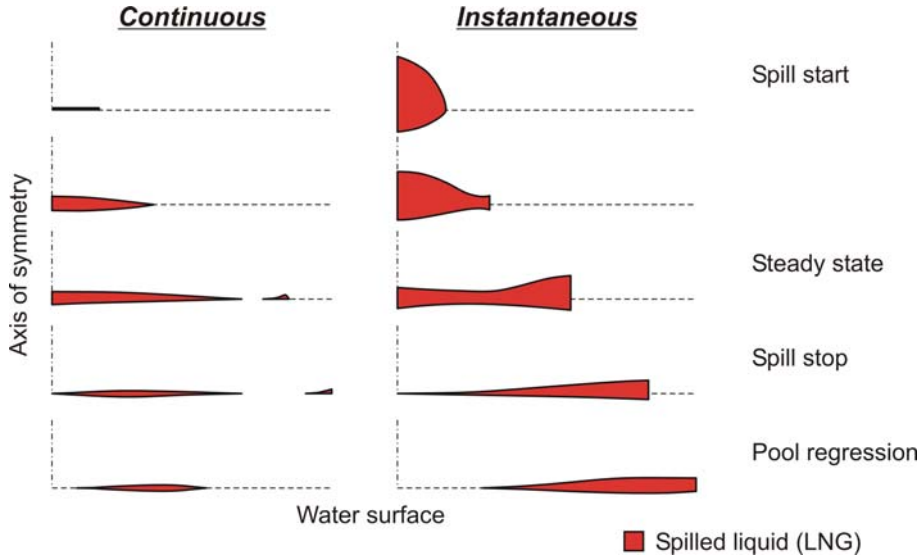

Figure 3-4. Comparison of the transient pool shape of a continuous (left) and instantaneous (right) release on a water surface [Brandeis 1983].

This phenomenon, for which there is hardly any experimental evidence because of its short lifetime, can be explained by the fact that in the first seconds more of the high-momentum liquid is released than can vaporize from the actual pool surface; it becomes thicker like a shock wave at its leading edge while displacing the ground liquid. It results in a stretching of the pool behind the leading edge, where the thickness becomes very small, until the leading edge wavelet eventually separates. Realistically the ring pool will certainly break up soon in smaller single pools drifting away as has been observed in release tests. Whether the ring pool indeed separates or only shortly enlarges the main

pool radius, is depending on the cryogen properties of density and vaporization enthalpy and on the source rate.

Another widely observed phenomenon for cryogenic spills on a water surface is the so-called "rapid phase transition" (RPT). RPTs are physical ("thermal"), non-combustive vapor explosions resulting from a spontaneous and violent phase change of the fragmented liquid gas at such a high rate that shock waves may be formed. Although the energy release is small compared with a chemical explosion, it was observed for LNG that RPTs with observed overpressures of up to 5 kPa were able to cause structural damage.

3.1.2.2 Experimental Work on LH_2 Pool Spreading and Vaporization

Arthur D. Little (1960)

Arthur D. Little (1960), under the sponsorship of the US Air Force, performed large LH_2 releases [Cassut 1960]. Tests consisted of 1¼, 32, 600, and 5000 gallons spills (corresponding to ~5–19,000 ℓ) of atmospheric LH_2 on the ground.

LH_2 pool vaporization rates were measured to be initially 130–180 mm/min before decreasing rapidly to a steady state value of ~38 mm/min.

For the small-scale tests, LH_2 was stored in Dewar vessels and spilled into pits from the fall of the Dewars on the floor. For the two largest tests, the LH_2 was transferred from a truck to insulated storage which were emptied by opening a bottom valve. For all tests, the cloud remained close to the ground for a few seconds and then gradually rose. For instance, the evaporation of 120 ℓ of LH_2 took 30 seconds. Unfortunately, the experiments were poorly instrumented for concentrations and/or temperature measurements.

The tests also consisted of continuous LH_2 releases (2 ℓ/s over 16 min or 16 ℓ/s over 1 min at wind speeds between 1.8 and 7.6 m/s) imitating a pipeline rupture. These experiments revealed a dense visible cloud up to 200 m distance.

Bureau of Mines (1961)

Zabetakis and Burgess (1960) determined the evaporation rate of LH_2 from the surface of a block of paraffin wax cast at laboratory scale [Zabetakis 1960]. They used a 2.8-inch Dewar flask and measured the rates of gas evolution following release of LH_2 into the Dewar. They showed that the vaporization rate of liquid hydrogen can be calculated after the initial period of violent boiling. They then investigated the influence of the ground on the vaporization rate and spreading of the pool by spilling ~6.8 ℓ of LH_2 from a Dewar on gravel and smooth macadam. The high specific surface of the gravel causes a faster vaporization than the macadam, leading to a higher visible cloud for the same elapsed time.

They also spilled 56 ℓ of LH_2 on smooth steel and gravel surfaces, the cloud was subsequently ignited. The rapid vaporization due to the gravel surface caused the centre of the base of the flame to be closer to the Dewar than observed when using the smooth steel plate.

They also determined experimentally the distribution of flammable volumes from liquid hydrogen spillage from open-mouths Dewar for various quantities of hydrogen from 0.5

to 7.4 ℓ. They tried to correlate the position of the visible cloud to the flammable cloud and found that the visible cloud could not be used as an accurate measure of the position of the flammable zone since the flammable mixtures could be ignited both outside and within the visible cloud.

NASA (1980)

In the 1980 NASA LH_2 spill trials [Witcofski 1981, Witcofski 1984], the liquid hydrogen was released from a 5.7 m^3 dewar, passing a horizontal spill line of about 30 m length, which was curved at its end vertically towards the ground. A 1.2×1.2 m^2 steel plate was located directly under the line exit to prevent earth erosion. The spill line dumped the LH_2 into a 9.1 m diameter spill pond with compacted sand as ground. The pond had an earthen side, about 60 cm in height. Pool spreading on the "compacted sand" ground was not a major objective, therefore only scanty data from just one test (#6) became available. From the thermocouples deployed at 1, 2, and 3 m distance from the spill point, only the inner two were found to have gotten contact with the cold liquid, which would mean a maximum pool radius not exceeding 3 m. Visual recordings, however, seem to indicate full coverage of the prepared diked area (radius 4.6 m) during the spill.

The nominal release rate of 134 ℓ/s of LH_2 reduced by the flash-vaporized fraction leads to an estimated 87 ℓ/s rate over 38 s contributing to pool spreading. The maximum pool radius was calculated to be about 6.5 m, more than twice the measurement range for the radius observed in the test. The calculated pool lifetime is 43.5 s which is about the figure of 43 s estimated by the NASA experimenters. The discrepancy in pool size is most certainly due to percolation of the liquid into the sand and furrows developing on the test site enlarging the surface area. Also the release process itself with the LH_2 first splashing on a deflection plate before hitting the ground certainly increased the vaporization rate. These all are aspects which were not simulated in the calculation and which may have significantly reduced the pool size [Verfondern 1997].

Research Center Jülich (1994)

In 1994, the first spill tests with LH_2 were conducted in Germany under the direction of BAM, Berlin, in which pool spreading was investigated in further detail. In four of these tests, FZJ studied the pool behavior by measuring the LH_2 pool radius in two directions as a function of time [Schmidtchen 1994, Dienhart 1995]. The release of LH_2 was made both on a water surface using a circular swimming pool with 3.5 m diameter (two tests) as depicted on the left of Fig. 3-5, and on a solid ground (visible on the outer left side) represented by a square aluminum sheet with 2 m side length and 20 mm thickness. A cross-shaped trestle was arranged above the respective ground. On two perpendicular branches of the trestle, a total of 18 thermocouples were fixed every 0.1 and 0.2 m, respectively, in radial direction. They were adjusted approximately 1 mm above the surface of the ground and served as indicator of the presence of the spreading cryogen.

Figure 3-5. LH_2 pool spreading on water during spill tests in 1996 with ice layer visible at test end (Courtesy of BAM).

The spill tests on water were performed over a time period of 62 s each at an estimated rate of 5 ℓ/s of LH_2, a value which is already corrected by the flash-vaporized fraction of at least 30%. After contact of the LH_2 with water surface, a closed pool was formed, clearly visible and hardly covered by the white cloud of condensed water vapor. The "equilibrium" pool radius did not remain constant, but moved forward and backward within the range of 0.4–0.6m away from the center. This pulsation-like behavior is probably caused by the irregular efflux due to the violent bubbling of the liquid and release-induced turbulences. After cutting off the source, a massive ice layer was identified where the pool was boiling. Also long-shaped ice tracks leading radially away could be observed. In the two tests on the aluminum sheet, conducted at an LH_2 release rate of (corrected) 6 ℓ/s over 62 s each, the pool front was also observed to pulsate showing a maximum radius in the range between 0.3 and 0.5 m.

Mitsubishi Heavy Industries (MHI) (1994)

In release experiments conducted by MHI the vaporization rates of liquid hydrogen and liquid oxygen spilled on different ground surfaces contained in a vacuum-insulated cylindrical glass Dewar were measured (Figs. 3-6 and 3-7). The different ground surfaces investigated were (i) limestone concrete, (ii) dry layer of sand, and (iii) a layer of sand with 7% water content to imitate rainfall conditions.

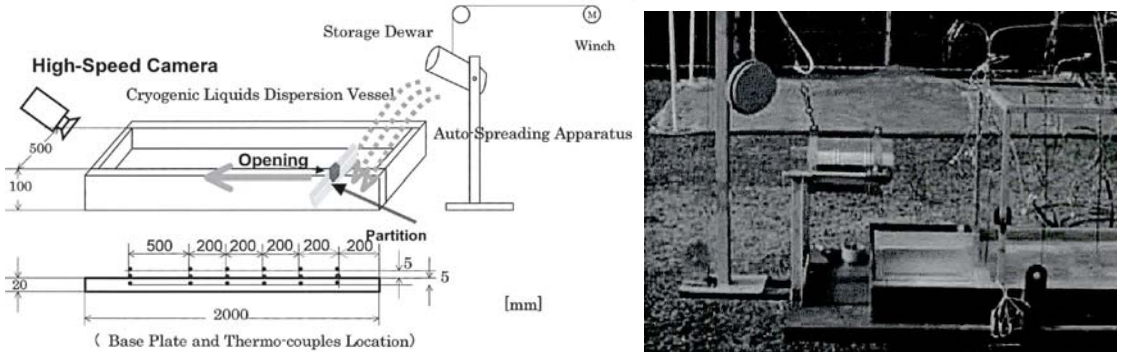

Figure 3-6. MHI LH_2 spill test experimental setup [Takeno 1994].

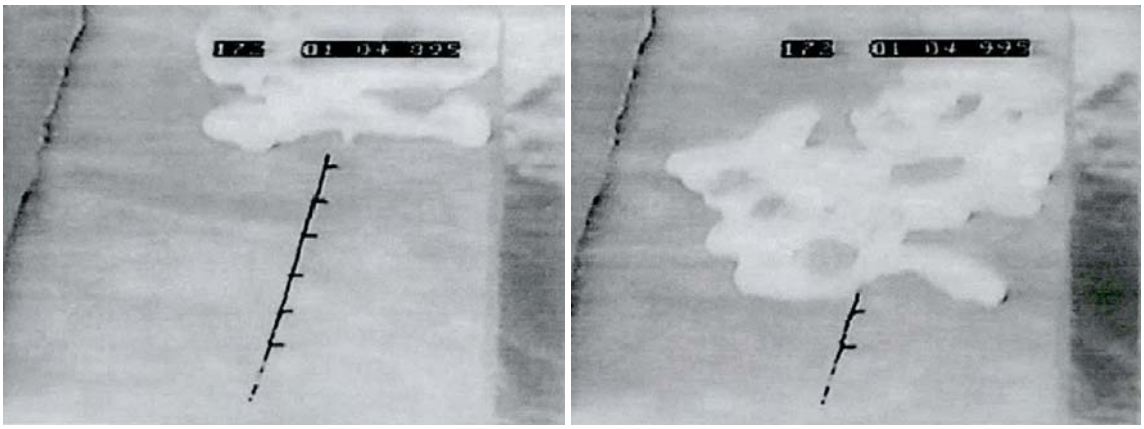

Figure 3-7. MHI LH_2 spill test results [Chitose 2002].

Two vessel sizes were used for the experiments with liquid hydrogen: 50 mm diameter and 600 mm length and 100 mm diameter for 200 mm length. The volume of liquid used were 0.5 ℓ, 1 ℓ, and 1.5 ℓ, respectively. The vessel dimensions and the quantity of fuel were varied to investigate the thermal influence of the vessel wall and the gravitational influence of the liquid.

They found out that in both wet and dry sand, the liquid hydrogen would not soak into it due respectively to the water and the air freezing creating a thin layer on top of the sand. For the concrete layer, the liquid just vaporized above it. In all cases, the variation of vaporization rate with time was proportional to $t^{-1/2}$, except in the starting phase of vaporization.

Health and Safety Laboratory (2010)

During 2009-2011 the Health and Safety Laboratory (HSL) in UK performed experiments on large-scale unignited releases of LH_2 with the aim of determining the range of hazards from a realistic release of LH_2 [Royle 2010b, Hooker 2012]. The work involved releasing LH_2 (from a 2.5 ton capacity LH_2 tanker) at fixed conditions of 1 barg in the tanker through 20 m of 25.4 mm (1") diameter hose, corresponding to a rate of 60 ℓ/min for different durations. The release height and orientation were varied and the sensor positions were changed.

The release height and orientation were varied and the sensor positions were changed. There were horizontal releases just above the ground (about 10 cm) as well as 86 cm above the ground. The extent of the pool was measured using thermocouples and visual records. Thermal gradient in the ground – three thermocouples were embedded into the concrete substrate at depths of 10, 20 and 30 mm. The tests were conducted on a 32 m diameter concrete pad.

Four tests were conducted:

- Tests 6 and 10 consisted of a vertically downward release 100 mm above the ground,
- Test 7 was a horizontal release 860 mm above the ground,
- Test 5 was a horizontal release onto the ground.

A significant and relatively thick layer of solidified air was formed during the spill (Fig. 3-8).

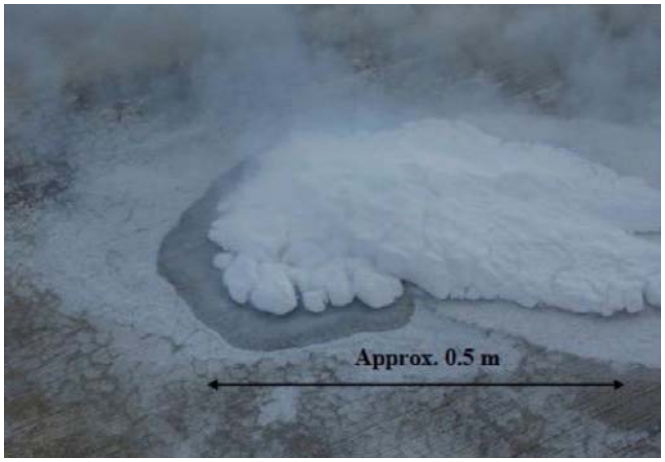

Figure 3-8. Solidified air formed during the LH_2 spill experiments.

The release of hydrogen in contact with a concrete surface produces a solid deposit of oxygen and nitrogen once the substrate is sufficiently cooled.

Pro-Science (2020)

The experimental campaign carried out by Pro-Science aimed at the generation of LH_2 pools above different substrates as concrete, sand, water and gravel and the investigation of the vaporization rate from the LH_2 pool above these substrates. The substrate was placed within a 0.5 × 0.5 × 0.2 m open stainless steel box (Fig. 3-9)., up to a substrate layer height of 0.1 m. In the remaining box height of 0.1 m, the LH_2 pool was intended to form above the substrate. Twenty-six thermocouples were employed to monitor the temperature within the substrate material, but also within and above the LH_2 pool. The experimental setup included hydrogen concentration sensors and a scale to assess the weight of the LH_2 pool. Measurements also aimed to investigate oxygen, nitrogen, moisture carry-over within the pool. An experiment usually comprised three subsequent pool formations with the same substrate filling. This approach allowed investigating the vaporization rate for different initial temperatures of the substrate, starting from ambient temperature (for the first LH_2 pool in an experiment) to much lower temperatures in the subsequent fillings, depending on the substrate. It was observed that the vaporization rate for the first LH_2 pool formation above the gravel substrate was significantly higher than for the other materials, which behaved rather similar. Experimental tests with a fan introducing a side wind ventilation rate of 5 m/s above the box surface did not show any significant effect on the vaporization rate.

Figure 3-9. Experimental set-up for LH_2 pool investigation on different substrates: concrete, sand and gravel.

3.1.2.3 Modeling of Cryogen Pool Spreading and Vaporization

A concomitant effort to experimental cryogenic pool spreading studies is the modeling of the physical phenomena that occur. FZJ has developed the computer code LAUV [Dienhart 1995] also based on the shallow-layer equations, which allows for the description of pool height and velocity as a function of time and location. It addresses the relevant physical phenomena in both instantaneous and continuous (at a constant or transient rate) type releases onto either solid or liquid ground. Heat conduction from the ground is deemed the dominant heat source for vaporizing the cryogen, determined by solving the one-dimensional or optionally two-dimensional Fourier equation. Other heat fluxes are neglected.

Heat Transfer from the Ground

The heat conduction in a homogeneous medium can be described by the Fourier differential equation:

$$\frac{\partial T}{\partial t} = a * \nabla^2 T + \frac{\Phi}{\rho c_p}$$

where a – thermal diffusivity, m^2/s; Φ – volume-related heat production rate in the ground, kW/m^2; ρ – density of the ground, kg/m^3; c_p – specific heat capacity, J/(kg·K); T – temperature, K; t – time, s.

A simple 1D solution of the above equation is the heat flux density [Carslaw 1959]:

$$\dot{q}(z,t) = -\lambda \frac{\partial T}{\partial z} = -\sqrt{\frac{\lambda \rho c_p}{\pi t}} * \Delta T * \exp\left\{-\frac{z^2}{4at}\right\}$$

where ΔT – difference between boiling point of the cryogen and the initial ground temperature, K; λ – thermal conductivity, W/(m·K); z – coordinate in depth, m.

Various authors have been investigating theoretically and experimentally the heat flux density for LH_2 (and other cryogens) at the surface. For the film boiling regime, heat flux density can be determined according to [Brentari 1965] by the following relationship:

$$\dot{q}_{FB} = 4.95 \frac{(\Delta\rho)^{0.375}}{\sigma^{0.125}} * \left[\frac{\lambda_g^3 \Delta H_{v,eff} \rho_g}{\eta_g}\right]^{0.25} * (\Delta T)^{0.75}$$

with the effective heat of vaporization $\Delta H_{v,eff} = \frac{(\Delta H_v + 0.34 c_p \Delta T)^2}{\Delta H_v}$

where σ – surface tension, N/m; λ_g – thermal conductivity of gas, W/(m·K); ρ_g – density of gas, kg/m^3; η – dynamic viscosity, $N·s/m^2$.

With decreasing temperature difference, a limit is given by the minimum film boiling heat flux density described by a correlation according to [Zuber 1959]:

$$\dot{q}_{MFB} = \frac{\pi^2}{60} * \left(\frac{4}{3}\right)^{0.25} * \rho_g * \Delta H_v * \left[\sigma \frac{\rho_l - \rho_g}{(\rho_l + \rho_g)^2}\right]^{0.25}$$

where index l – liquid; index g – gas.

For the nucleate boiling regime, Kutateladze has deduced the following relationship [Brentari 1965]:

$$\dot{q}_{NB} = 4.87 * 10^{-11} \frac{c_{p,l}^{1.5} \lambda_l \rho_l^{1.282} p_o^{1.75}}{(\Delta H_v \rho_g)^{1.5} \sigma^{0.906} \eta_l^{0.626}} * (\Delta T)^{2.5}$$

where p_o – ambient pressure, Pa.

The critical heat flux density or "departure of nucleate boiling", DNB, describes the point where the space between the bubbles is filled with just as much liquid as is needed to form new bubbles:

$$\dot{q}_{DNB} = 15.7 * \Delta H_v * \rho_g^{0.5} * (\sigma \Delta\rho)^{0.25}$$

The areas shown in above Fig. 3-3 represent the experimentally determined heat flux densities of LH_2 covering both nucleate boiling and film boiling regimes. The solid lines (in blue) indicate curves calculated according to the above equations for $\dot{q}_{FB}$ and $\dot{q}_{NB}$.

Considering the volume of an incremental pool element, the mass conservation equation is given by balancing the volume change in time with the sum of all volume fluxes passing the element's boundaries. For a pool with cylindrical geometry,

$$\frac{\partial(rh)}{\partial t} + \frac{\partial(urh)}{\partial r} + r(v - w) = 0$$

where h = h(r, t) – pool height, m; r – radius, m; t – time, s; u = u(r, t) – horizontal (depth-averaged) pool spreading velocity, m/s; w – liquid fuel source rate, m/s; v – liquid fuel vaporization rate, m/s.

From the simple one-dimensional analytical solution of the Fourier equation, the vaporization rate per unit surface can be derived as

$$v = \frac{\lambda \Delta T}{\rho_l \Delta H_v \sqrt{\pi a} \sqrt{t - t'}}$$

where λ – thermal conductivity of ground, W/mK; ΔT – temperature difference between liquid and ground, K; ρ_l – density of liquid, kg/m^3; H – vaporization enthalpy, J/kg; a – thermal diffusivity, m^2/s; t' – time moment from which surface element gets into contact with pool, s.

The momentum conservation equation is determined by the balance of forces attacking the incremental pool volume taking account of buoyancy and friction forces:

$$\frac{\partial u}{\partial t} + \frac{\partial}{\partial r}\left(\frac{u^2}{2} + \delta g h\right) + \frac{F}{h} = 0$$

where g – acceleration of gravity, m/s^2; F = F(u, h) – friction force per mass unit, kg; δ – reduction factor (=1 for solid ground).

The above shallow-layer differential equation system (3-7) and (3-9) is solved by applying an explicit finite-difference scheme. It is valid under the following initial and boundary conditions:

- Spreading is horizontal in radial direction (1D) in unobstructed terrain.
- For instantaneous release, the pool is initially at rest (zero momentum), i.e. purely gravitational spreading. The initial pool height h(r) is assumed to be a (negative) square function of the radius.
- For continuous release, the source is a volume flow per unit surface downwards and perpendicular to the spreading. Source is always in the center.
- Vaporization is a volume loss per unit surface upwards through the pool surface.
- There is no vertical velocity profile within the pool (which is realistic for shallow layers and low friction).
- Densities of ground and cryogen remain constant, i.e. no influence by bubble formation.

During the initial release phase, the surface area of the pool is growing which implies an enhanced vaporization rate (Fig. 3-10). Eventually a state is reached which is characterized by the incoming mass to equal the vaporized mass. This equilibrium state, however, does not necessarily mean a constant surface area of the pool. For a solid ground, the cooling results in a decrease of the heat input which, for a constant spill rate, will lead to a gradually increasing pool size. In contrast, for a water surface, pool area and vaporization rate are maximal and remain principally constant despite ice formation as was concluded from lab-scale testing.

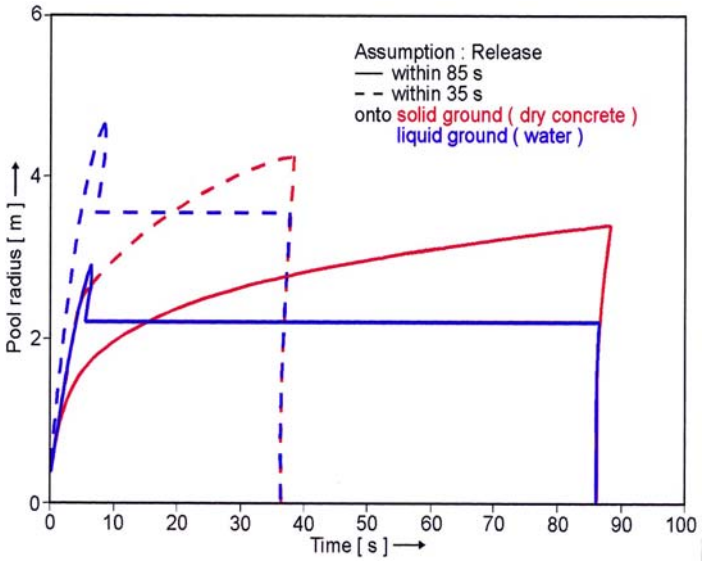

Figure 3-10. LH_2 pool spreading on solid and liquid ground.

Postcalculations of the FZJ experimental investigation of LH_2 pool spreading with the LAUV model are shown in Fig. 3-11. The symbols represent the outermost positions which had definite contact with the cryogen, meaning that the principal uncertainty for the pool radius is given by the distance to the next measuring position (see error bars). The shaded area describes the pulsation range according to what was observed from the video recording. Both measurement and calculation reveal the pool front at the beginning to have shortly propagated beyond the steady state presumably indicating the phenomenon of a detaching pool ring typical for continuous releases. The radius was then calculated to slowly increase due to the gradual temperature decrease of the ice layer formed on the water surface. Equilibrium is reached approximately after 10 s into the test,

until at time of 62.9 s, i.e. about a second after termination of the spillage, the pool has completely vaporized. Despite the given uncertainties, the calculated curve for the maximum pool radius is still well within the measurement range. The ice layer thickness could not be measured during or after the test; according to the calculation, it has grown to 7 mm at the center with the longest contact to the cryogen.

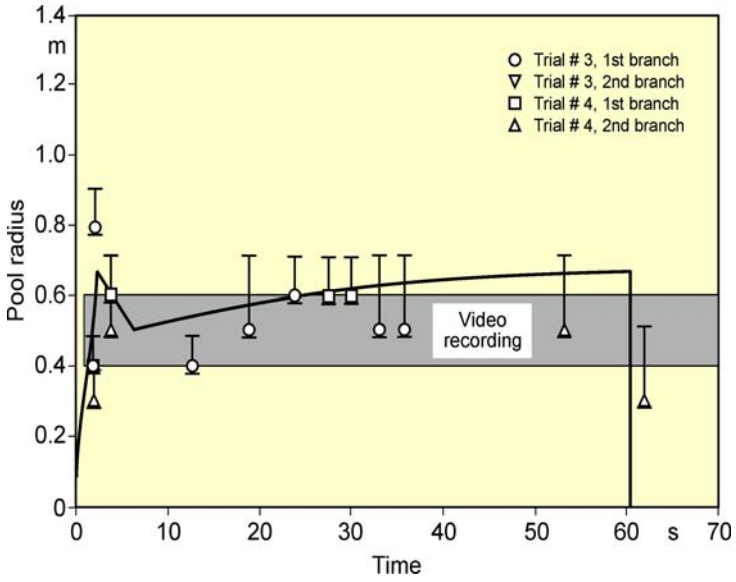

Figure 3-11. Continuous release of LH_2 over 62 s at a rate of 5 ℓ/s onto water [Dienhart 1995].

A 3 mm water layer on the concrete leads again to a longer vaporization time due to an insulation effect of the – then – ice layer, but the time was still shorter than in the "dry" case [Dienhart 1995].

A predictive study with the LAUV code was made to analyze the differences in the spreading behavior of the cryogens LH_2, LOX, LNG, and LN_2 on solid ground (macadam) for the case of a 40 m^3 volume that is a typical size of a tank truck load. Results are shown in Fig. 3-12 for a continuous spill at a rate of 1 m^3/s.

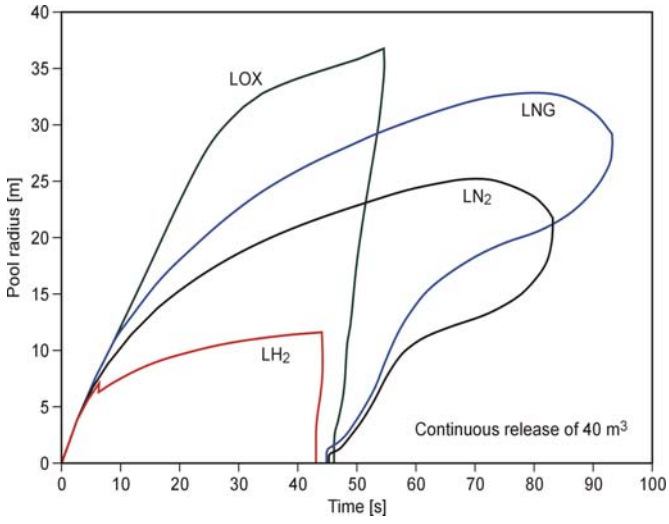

Figure 3-12. Comparison of pool spreading behavior of 40 m^3 (road truck load) of a cryogen in a continuous release over 40 s [Verfondern 2007].

A remarkable difference among the cryogens considered is the small size and the short lifetime of the LH_2 pool compared to all other pools. The maximum LH_2 pool radius will be ~12 m with the total pool completely vaporized after ~45 s, or ~5 s after end of the spill. In contrast, all other cryogen pools, with their much higher weight and thus much higher kinetic energy used for spreading, are much longer-lived. The LNG pool will survive longest with 54 more seconds after the cessation of the spill [Verfondern 2007].

Further approaches and codes for CFD modeling of an LH_2 spill were proposed in [Venetsanos 2007, Middha 2011] and recently by [Jin 2017] and by [Jäkel 2017]. The model performances were tested against the experimental trials on 5110 m^3 spills by NASA in 1980.

[Venetsanos 2007] used ADREA-HF with a dispersed mixture approach. The model applies the HEM model to characterize the two-phase flow. This assumes that phases have same velocities (homogeneous), same pressure and temperature (thermodynamic equilibrium). Raoult's law for ideal mixtures was employed to calculate the phase distribution. Best agreement with the concentration measurements was found by modeling the source as a jet, accounting for the small fence around the spill and including heat transfer from the ground.

[Jin 2017] used the dispersed mixture approach with thermodynamic equilibrium and slip velocity between phases. The phase distribution was assessed by explicit modeling of vaporization rate along with a transport equation for the gas phase.

[Jäkel 2017] developed a new multiphase multicomponent CFD model capable of simulating liquid and gaseous distributions.

[Middha 2011] used a separated phases approach: a pool model for the liquid phase and CFD only for the vapor phase. With this approach, they were able to provide pool spreading predictions well agreeing with experiments.

3.1.3 Dispersion of Cold Vapor Cloud

3.1.3.1 Phenomenology

The spreading and dispersion behavior of a gas is significantly influenced by the density difference to the ambient air. In case of the release of a neutral or negatively buoyant gas, mixing with air is poor and slow. The cloud must be picked up by the ambient flow before it can be carried downstream and diluted. If the source rate is larger than the removal rate, a vapor blanket can accumulate on the ground until a certain size is reached with steady-state conditions.

The initial phase after release of a heavy gas is characterized by a slumping of the gas cloud under gravitation with a behavior similar to a liquid. It shows a spreading behavior which is – at least in the initial phase – independent of the wind direction. It forms a shallow pancake-shaped plume with resistance to vertical dispersion. The spreading of the gas cloud is further influenced by factors such as surface area, type of ground, thermal effects from the interaction with the ambient atmosphere which can either enhance or dampen the turbulence by buoyancy. Air entrainment from the upper surface and the edges due to atmospheric turbulence eventually results in dilution to effectively neutral density. Top entrainment of air into heavy gases is significantly smaller than for neutral gases.

Hydrogen gas at its boiling point is slightly heavier than air. Small quantities of LH_2 released tend to rise almost immediately. In case of the release of a large amount of LH_2, however, the vaporized gas will remain near the ground for a longer time because of only gradual air entrainment from the outside into the vapor cloud.

Gas at cryogenic temperatures causes the moisture in the air to condense and make the vapor cloud visible which is of advantage in case of accidental releases. The presence of droplets, either liquefied gas resulting from the release process or water from the moisture, result in vaporization and condensation processes with removal of heat from or addition of heat to the gas. Low moisture content thus means a longer lifetime of a heavy gas cloud.

It is known from the experience that a hydrogen-air gas cloud evolving from the inadvertent release of hydrogen upon the failure of a storage tank or a pipeline liberates only a small portion of its thermal energy contents in case of an explosion, which is in the range between 0.1 and 10%, in most cases < 1% [Lind 1975].

3.1.3.2 Experimental Work on Cold Cloud Dispersion

Arthur D. Little (1960)

Spill experiments with LH_2 amounts ranging between 5 ℓ and 19 m^3 were conducted by Arthur D. Little Inc. [ADL 1960] simulating the conditions of storage and transport with the objectives to test safe handling, to observe the dispersion behavior, to establish quantity-distance relationships, and to compare with hydrocarbon fuels. The vaporized, still cold hydrogen was found to remain close to the ground for a few seconds and then gradually rise. It also showed the tendency of horizontal spreading in all directions in a semi-spherical shape. Tests with continuous LH_2 release of ~ 2 ℓ/s over 16 min or 16 ℓ/s over 1 min at wind speeds between 1.8 and 7.6 m/s revealed a dense visible cloud up to 200 m distance [Cassut 1960]. Observed areas with H2-air mixture within the flammability limits are plotted in Fig. 3-13.

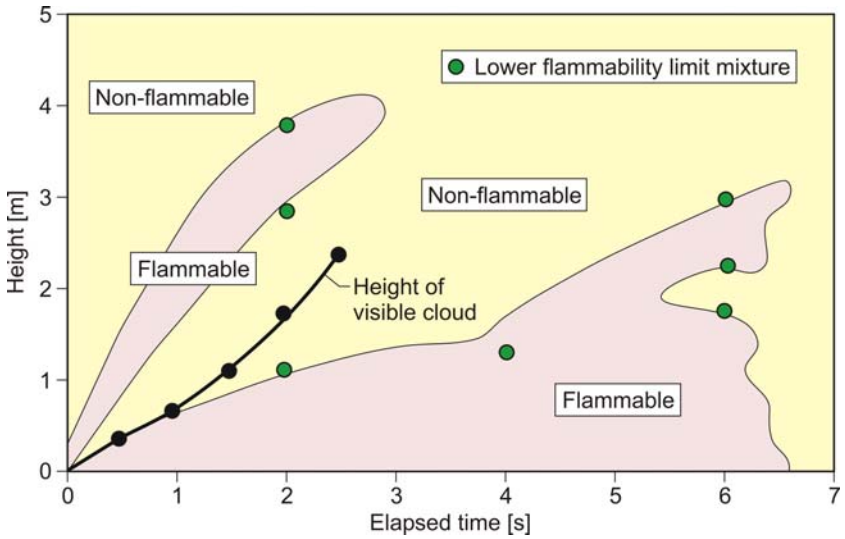

Figure 3-13. Observed flammable areas and visible gas cloud after the instantaneous release of 3 ℓ of LH_2 at 15°C ambient temperature and quiescent air as a function of time after spillage [Zabetakis 1960].

NASA (1980)

The NASA LH_2 trials conducted between August and December of 1980 [Witcofski 1984, Chirivella 1986] were initiated when trying to analyze the scenario of a bursting of the 3000 m^3 LH_2 storage tank at the Kennedy Space Center at Cape Canaveral and to study the propagation of a large-scale hydrogen gas cloud in the open atmosphere. The spill experiments consisted of a series of seven trials, in five of which a volume of 5.1 m^3 of LH_2 was released near-ground within a time span of 35–85 s.

The developing hydrogen gas cloud and the visible cloud, respectively, could be observed over several hundreds of meters, when the ground was able to sufficiently cool down. The visible cloud was initially steeply rising, before it later remained longer near the ground (Fig. 3-14). This behavior was explained with the high impulse when opening the valve showing a high sensitivity of the type of release for LH_2. Unlike LH_2 pool vaporization with typical vaporization rates of 0.4–0.8 mm/s, high release rates lead to intensive turbulences with violent cloud formation and rapid mixing with the ambient air. Figure 3-15 shows for test 6 the concentration distribution as was derived from the temperature measurements assuming adiabatic mixing of hydrogen with the ambient air [Witcofski 1984].

Figure 3-14. Cold hydrogen vapor cloud dispersion during NASA spill test #6. (Courtesy of NASA).

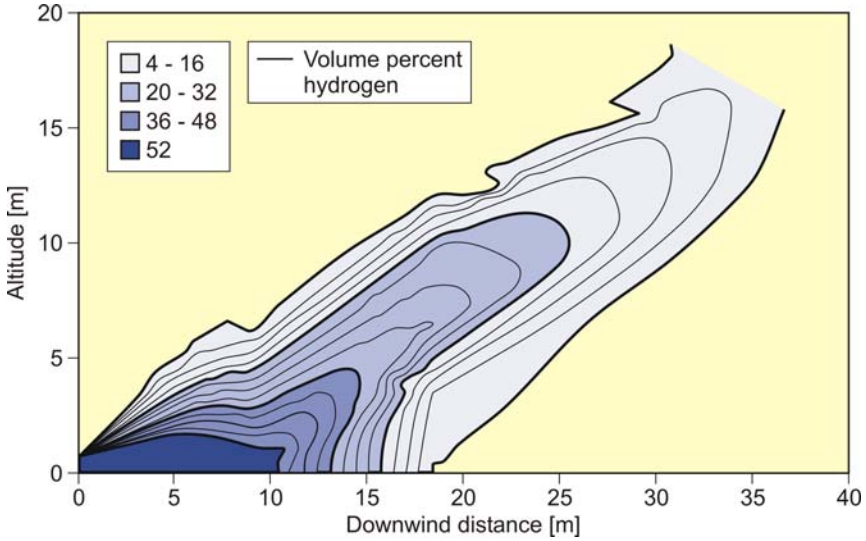

Figure 3-15. Measured concentration distribution after 21 s of test #6 of the NASA spill tests.

Battelle/BAM (1994)

The objective of the liquid hydrogen spill tests conducted in 1994 in a deserted barrack area was to investigate the LH_2 pool formation and vaporization (see chapter 3.1.2), and the subsequent dispersion behavior of the cold vapor cloud in the vicinity of buildings simulating a residential area. Hydrogen release rates were approximately 0.8 kg/s over a period of about 1 min. The cloud dispersion behavior was recorded by continuously measuring hydrogen concentrations and temperatures at specified locations near the source, as well as the weather conditions. Respective spill experiments with LPG were made (release rate ~0.25 kg/s over ~7 minutes) to reveal the significant difference in spreading and dispersion behavior of the two fuels. Shortcomings during the test were the poor weather conditions, wind with no prevailing direction and rain which caused the visible gas cloud to be larger than expected.

What, however, could be demonstrated by the tests, was that, different from LPG, the gasified hydrogen quickly traveled upwards (Fig. 3-16) and disappeared in the atmosphere, and in this regard behaved safer than other fuels [Schmidtchen 1994].

Figure 3-16. Screenshots from the evolving vapor cloud following LH_2 spill.

Karlsruhe Institute of Technology (2009)

The experiments at Karlsruhe Institute of Technology (KIT) conducted in the framework of the ICEFUEL project [Breitung 2009] consisted of release and ignition of horizontal liquid hydrogen jets at temperature of 35 to 65 K and pressures from 0.7 to 3.5 MPa. They performed a total of 37 experiments (Fig. 3-17), divided in three campaigns, of liquid hydrogen releases through a small orifice of 0.5 or 1 mm (from 2 to 8 g/s). They studied the distribution process (temperature and concentration) in cryogenic unignited jets. The hydrogen concentrations were measured for different nozzle diameters and reservoir conditions (pressure and temperature). It is interesting to notice that the distance to 4% is larger for cryogenic release than for cold or ambient gaseous release.

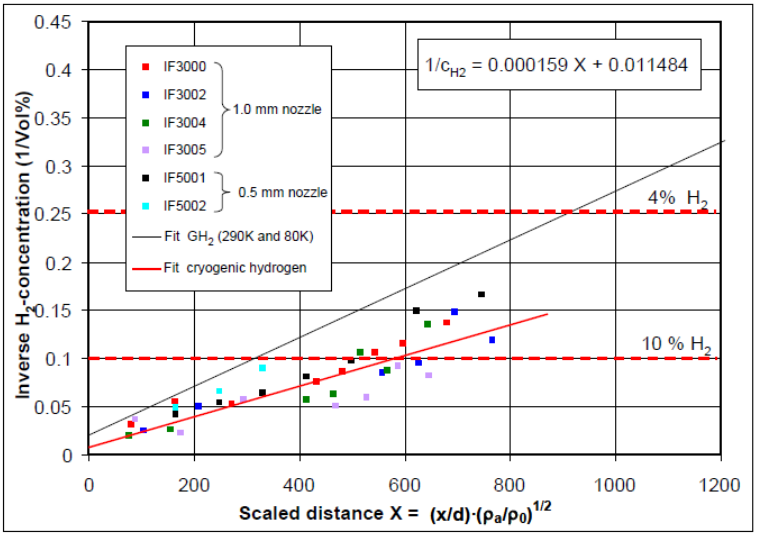

Figure 3-17. Summary of measured axial hydrogen concentrations in case of cryogenic and gaseous hydrogen release.

Winters (2011)

Winters and Houf [2011] studied steady-state leaks with large amounts of pressure drop along the leak path such that hydrogen enters the atmosphere at near atmospheric pressure (i.e. very low Mach number). They developed a three-stage buoyant turbulent entrainment model to predict the properties (trajectory, H2 concentration and temperature) of a jet emanating from the leak depending if the leak occurs from the saturated vapor space or saturated liquid space.

In the first stage of the entrainment model, ambient temperature air (295 K) mixes with the leaking hydrogen (20–30 K) over a short distance creating an ideal gas mixture at low temperature (~65 K). During this process, states of hydrogen and air are determined from equilibrium thermodynamics using models developed by NIST. In the second stage of the model the radial distribution of H_2 concentration and velocity in the jet develop into a Gaussian profile characteristic of free jets. The third and by far the longest stage is the part of the jet trajectory where the flow is fully established.

While trajectories for ambient temperature jets depend solely on the leak densimetric Froude number, results from the present study show that cold jet trajectories depend on the Froude number and the initial jet density ratio. Obviously, results show that flammability envelopes for cold hydrogen jets are generally larger than those of ambient temperature jets. For the same diameters and pressure, the largest distance to 4% H_2 concentration is for the subcooled liquid leaks (possibly even worst if there is rainout) followed by saturated liquid leaks and saturated vapor leak (the shortest distance to 4%).

Sandia National Laboratory (2018)

Recently vertical cryogenic hydrogen releases (1 and 1.25 mm diameter) at low pressure (0.2 to 0.5 MPa) and low nozzle temperature (50 to 61 K) were performed using spontaneous Raman scattering [Hecht 2019]. They studied the distribution of concentration (average centerline and half-width of mass fraction, radial profiles) and

temperature decay. They compared the radial mass fraction and temperature at selected distances with two fits based on their releases and one based on the available literature (room temperature jets). They also used the mole fraction and temperature fields for comparison with the ColdPlume model which gave good predictions. It should be interesting to compare these results with the correlation proposed by KIT.

Health and Safety Laboratory (2020)

HSE investigated the release characteristics and dispersion of elevated spills of LH_2 over a concrete pad, along with the propensity for rainout to form. The experimental campaign included 25 tests on releases from a tank with pressure of 1 or 5 barg and through nozzle diameters 6 mm, 12 mm and 25.4 mm (Fig. 3-18).

Measurements of pressure, mass flow rate and temperature in the pipework provided information of the phase of hydrogen at the release, which was multiphase for the majority of tests. This has been attributed predominantly to the heat transfer into the fluid in the final 3 m of pipework, which contained the instrumentation and therefore was not vacuum insulated. The dispersion from these releases was measured using hydrogen concentration and temperature measurements.

Figure 3-18. Visible cloud during dispersion and rainout tests at HSE facility.

Rainout did not occur during the established flow of these releases, but there was evidence of rainout soon after valve closure (probably liquid air). Further to this, condensed components of air formed around the release point and on impingements for releases from the 6 and 12 mm nozzles. Pools were only formed with low, vertically downward releases. These pools potentially comprised of LH_2, condensed components of air, or a mixture of the two.

The development and dispersion of the gaseous H_2 cloud that forms from a release of LH_2 was captured by the instrumentation and video footage. The jet is typically momentum dominated for the initial section, which ranges between 1.5 m and 6 m depending on the release pressure and nozzle size, but then becomes extremely dependent on the wind, including transient localized gusts. Transient ignitable pockets, with average H_2 concentration > LEL, were measured at 14 m distance from LH_2 releases through 12 mm holes or larger.

Pro-Science and Karlsruhe Institute of Technology (2020)

DisCha Experimental Campaign on Cryogenic Hydrogen Jets

Within the frame of PRESLHY project, partners Pro-Science (PS) and Karlsruhe Institute of Technology (KIT) and performed over 200 hydrogen blowdown tests on high to low pressure (0.5-20 MPa) releases at ambient and cryogenic temperature (80 K). The main purpose of the tests was to:

- investigate the blowdown behavior of cryogenic hydrogen stored at elevated pressure.
- investigate the dispersion of cryogenic hydrogen.
- provide validation and reference data for models defining or using a discharge coefficient; subsequent explosion tests where the released gases will be ignited.
- provide data on electrostatic field excitation and associated ignition potential of high pressure hydrogen gas jets at cryogenic temperatures.

Tests showed a good reproducibility, although the experimental facility was continuously improved and extended. The final test setup included 2 pressure sensors and 13 thermocouples, 5 hydrogen concentration probes, 2 field mills for electrostatic field strength, and 3 cameras. For the cold hydrogen jets (Fig. 3-19), it was observed the formation of ice crystals from air humidity at the nozzle prior to the test initialization. It is considered that crystals are then entrained in the jet under the form of particles. These ice crystals are thought to be the cause of the strong electrostatic fields measured for the cryogenic tests. However, none of tests showed spontaneous ignition. Tests with larger diameter and high pressure showed a strong temperature decay in the reservoir close to the hydrogen boiling point. However, it is not possible to say if hydrogen condensed because of further temperature reduction at the nozzle due to the gas acceleration.

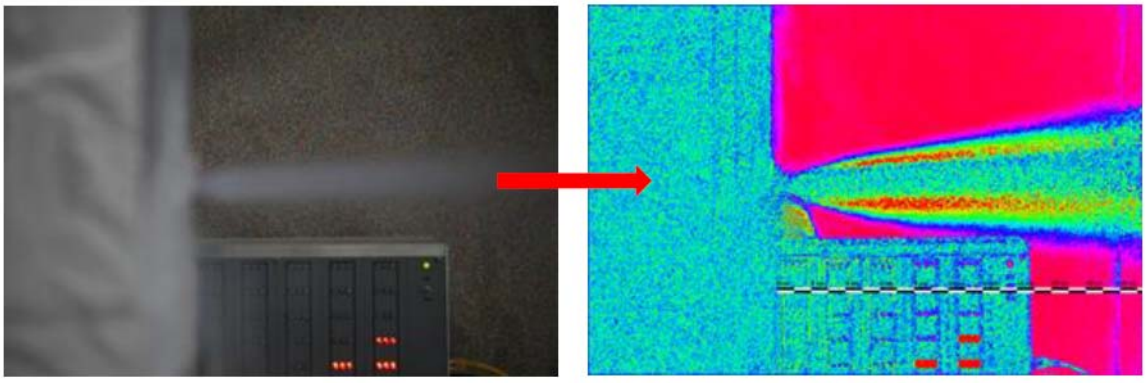

Figure 3-19. BOS post processing of cryogenic jets in DisCha experimental campaign.

Cryostat Experimental Campaign on Multiphase Releases

Project partners PS and KIT performed a series of experimental tests to characterize the release and dispersion of hydrogen multiphase releases from a 0.225 m^3 vessel at an temperature of approximately 30 K. Figure 3-20 shows the Cryostat vessel. The tests were performed for release nozzles with orifice diameters of 2–4 mm and initial pressures in the range of 0.2–0.45 MPa. The vessel was positioned on a scales and was equipped

with thermocouples and pressure sensors to monitor properties during the vessel blowdown. Thermocouples and video observation (including a thermo-camera) were used to give insights into the dispersion behavior of hydrogen.

Figure 3-20. CRYOVESSEL facility.

Optical observations showed the formation of a “finger like” structure at tip of nozzle (see Fig. 3-20, center), whose length grows with release duration. This “finger like” structure was seen to either be blown away by the jet or just fell down, but soon disappeared after reaching the ground as no traces were left on the ground after the test ending.

Figure 3-21. Optical observation from cold test with release diameter of 2 mm and pressure of 0.4 MPa.

3.1.3.3 Modeling of the Near-Field Region in Cryogenic Jet Release

In the event of potential liquid hydrogen leaks, the pressurized storage conditions will develop at the leaks, resulting in the formation of under-expanded hydrogen jets. Insight about the dispersion of cold hydrogen is of importance to safety analysis. While the subsequent dispersion of the released hydrogen can be simulated with the pseudo diameter/notional nozzle approach covered elsewhere in the handbook, the detailed near-field flow structures and transient physics of the under-expanded cryogenic hydrogen jets can be modeled with direct numerical simulations (DNS) [Ren 2020].

In DNS, the compressible Navier-Stokes equations with the transportation equations of multispecies are directly solved. The transport properties, such as viscosity, heat conductivity and diffusion coefficient of the chemical species can be obtained based on the kinetic theory [Poling 2001]. It is generally necessary to use higher-order numerical schemes, e.g. the adaptive central-upwind sixth-order weighted essentially non-oscillatory (WENO-CU6) scheme [Hu 2010] for the convection terms to facilitate the simulations of the main flow with low dissipation and achieve a proper resolution of the flow properties around the shock waves, the sixth-order symmetric compact difference scheme for the viscous diffusion terms. Time-integration can be realized by the explicit third order Runge-Kutta method.

As an example, Warwick FIRE has conducted such simulations for the experimental configurations of Hecht et al. [2019] with hydrogen (inflow) and air (coflow) injected from the bottom, as shown in Fig. 3-22. The non-reflected boundary conditions are applied on the left as well as the right boundaries. For the outlet conditions, the parameters are interpolated by assuming first-order derivatives. A slow coflow air with a streamwise velocity of 0.3 m/s is imposed at the inlet. The static pressure, P_a, and the static temperature, T_a, of the ambient air are 0.1 MPa and 297 K, respectively. The nozzle pressure increased from 0.3, 0.4 to 0.5 MPa as in the experiments and the respective cases are named as LP, MP, and HP. The grids with the size of Δ = 20 μm are applied in the numerical simulations after the grid sensitivity study.

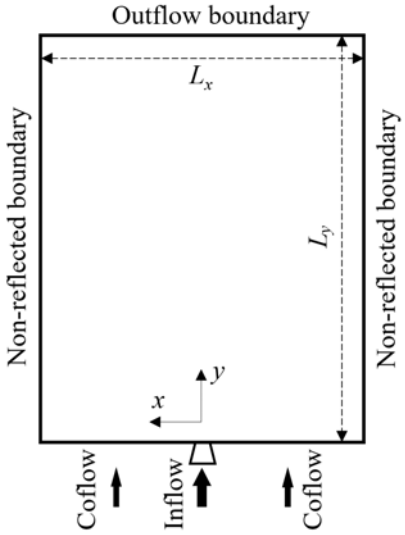

Figure 3-22. Computational domain and boundary conditions.

The early stages of the near-nozzle flow structures for cases LP, MP, and HP from time t = 10 to 40 μs are shown in Fig. 3-23. Complex waves are formed in the near-nozzle field. If the partial pressure of hydrogen (P_{H2}) is higher than its saturated vapor pressure (P_{vap}), the localized hydrogen liquefaction is expected to occur. Hydrogen liquefaction potentiality (HLP) is calculated as HLP = $P_{H2} - P_{vap}$. If HLP is greater than zero, the occurrence of liquefaction is expected to occur theoretically. The red dashed lines in Fig. 3-16(a) denotes the regions where HLP > 0, indicating that localized liquefaction can occur in the under-expanded jets of cold hydrogen gas due to the local expansion. For the low-pressure cases (LP and MP), the liquefaction cannot be formed.

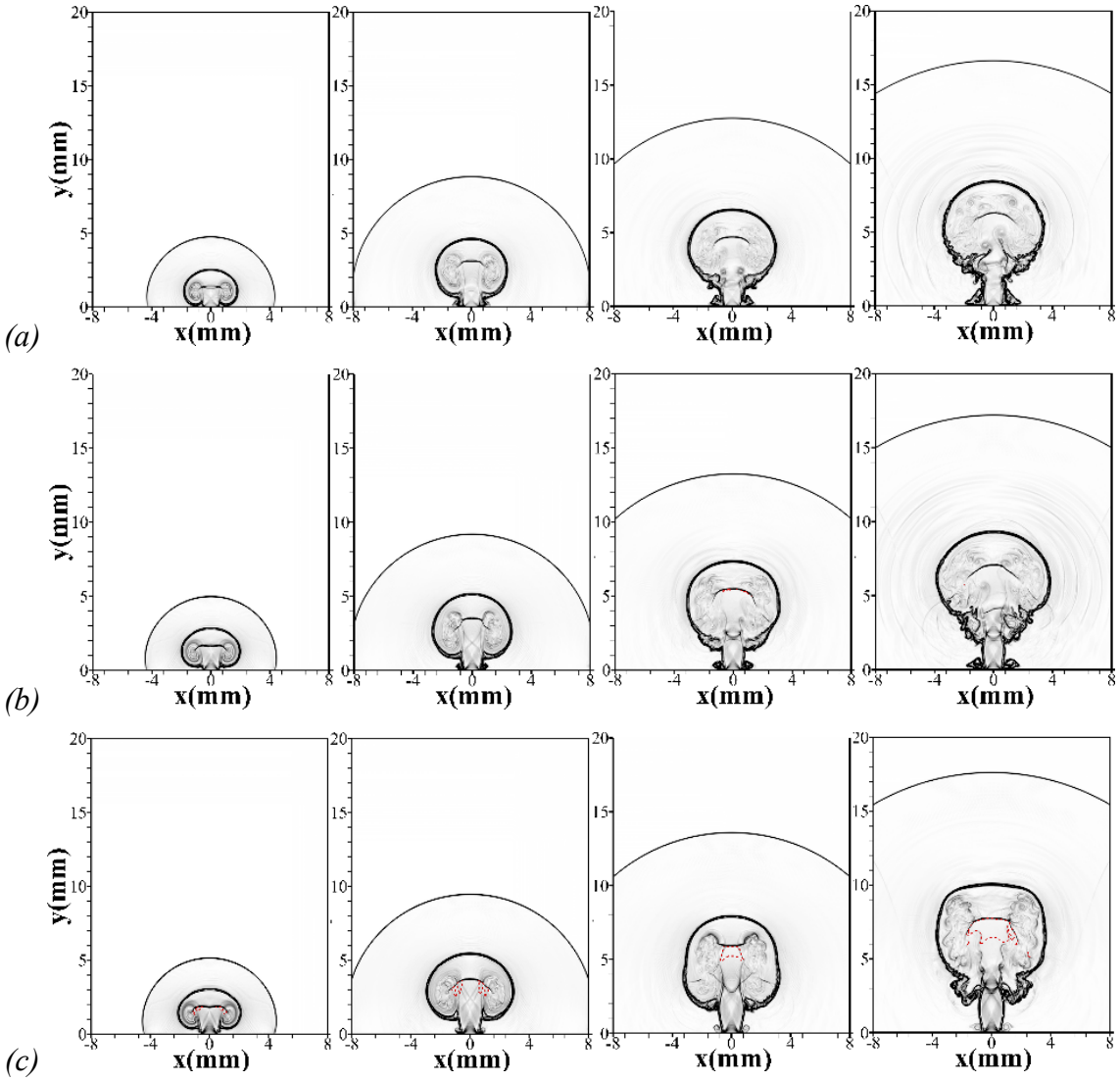

Figure 3-23. Transient development of the near-nozzle flow structure by density gradient for Case HP from t = 10 to 40μs shown in time interval of 10 μs: (a) Case LP, (b) Case MP and (c) Case HP.

The downstream development of the jets for Case HP is shown in Fig. 3-24. The strong shear results in the rolling and shedding of vortices, which is associated with a large amount of hydrogen entrained by the coflow air. The regime of the potential liquefaction region decreases continuously as the expansion wave weakens. For the other cases, the liquefaction cannot be formed.

In summary, DNS studies are power to characterize the near-field flow physics, which are difficult to capture in the experimental tests. The studies conducted by Warwick FIRE has revealed that strong expansion formed in the jet head can lead to localized liquefaction due to the difference between the partial pressure of hydrogen and the saturated vapor pressure of hydrogen. The variation in the nozzle pressure ratio not only affects the subsequent hydrogen dispersion but also the jet shapes in the near-field region. The jet head varies from a round shape for the low nozzle pressure ratio to a quasi-rectangle shape for the high nozzle pressure ratio. The observed influence may lead to related changes in the subsequent far field dispersion.

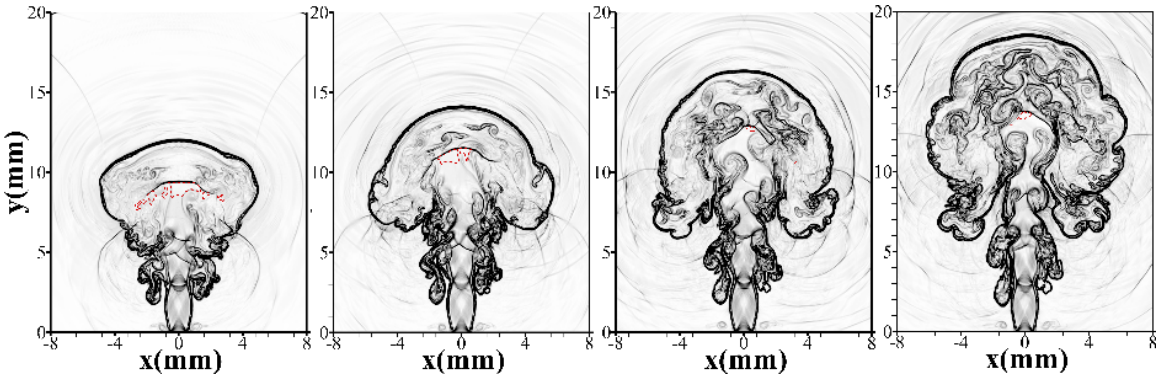

Figure 3-24 Instantaneous distributions of density gradient for Case HP from t = 50 to 80μs shown in time interval of 10 μs. The red dashed lines denote the region of HLP > 0.

3.1.3.4 Modeling of Cold Cloud Dispersion

Venetsanos et al. [2019] modeled the dispersion behavior of the experimental test by Proust et al. [2007] on a large scale release of 110 kg of helium in 52 s by using the CFD code ADREA-HF. Simulation results were compared against the temperature time histories at sensors deployed at various distances and heights downstream the source. Simulated temperature recordings were generally in good agreement with the experimental with a tendency to under-predict temperature as the source is approached.

Within the frame of PRESLHY project, HSE developed a model based on the adiabatic mixing approach to determine the final state when mixing liquid hydrogen and moist air in terms of temperature, hydrogen volume fraction and density. The method calculates the gas concentrations from measured temperature, humidity and temperature of ambient air in conditions of minimal exchange of heat except with entrained air.

3.1.3.5 The Similarity Law for Cryogenic Jets

The similarity law is a tool able to predict the distances where a dangerous hydrogen concentration in air is achieved, such as the Lower Flammability Limit (LFL) to determine the size of the flammable envelope produced by an unintended hydrogen release.

A similarity law was developed [Chen 1980] for evaluation of the axial concentration decay in momentum-controlled expanded jets, showing that for round jets, the mass fraction at a given distance x is linearly proportional to the orifice diameter d:

$$C_{ax} = 5.4 \sqrt{\frac{\rho_N}{\rho_s}} \frac{d}{x}$$

where ρ_N – density of hydrogen at the nozzle; ρ_s – density of surrounding air; x – distance from nozzle.

The similarity law formulation for under-expanded jets was attempted and applied to natural gas releases [Birch 1984].

The similarity law was employed for momentum-controlled hydrogen jets [Saffers 2013] using Ulster's under-expanded jet theory to calculate density at the nozzle [Molkov 2009]. The correlation was validated against experiments on hydrogen jets with release

temperature in the range 80–298 K and pressure 0.26–40 MPa. Validation range was further extended [Cirrone 2019a] to temperatures down to 50 K for release pressures up to 0.6 MPa abs, by comparison with nine experimental tests performed at Sandia National Laboratories (SNL) on releases with pressures of 0.2–0.5 MPa, abs, and temperatures of 50–61 K [Hecht 2019]. The similarity law was found to provide excellent agreement between experiments and calculations for the jets with release diameter equal to 1.25 mm and pressures above 0.2 MPa (deviation 5%), whereas deviation increases to 10% for the release at 0.2 MPa, abs. Predictions showed a larger deviation for the releases with 1 mm diameter nozzle which were characterized by a more unstable concentration decay in experiments. The effect of real gas EOS on the hydrogen concentration decay was found to be limited to 4.5% at the distance where a concentration of half the LFL is reached. Figure 3-25 shows the comparison between SNL experimental data and the similarity law, along with experimental data reported [Saffers 2013] and previously used for validation.

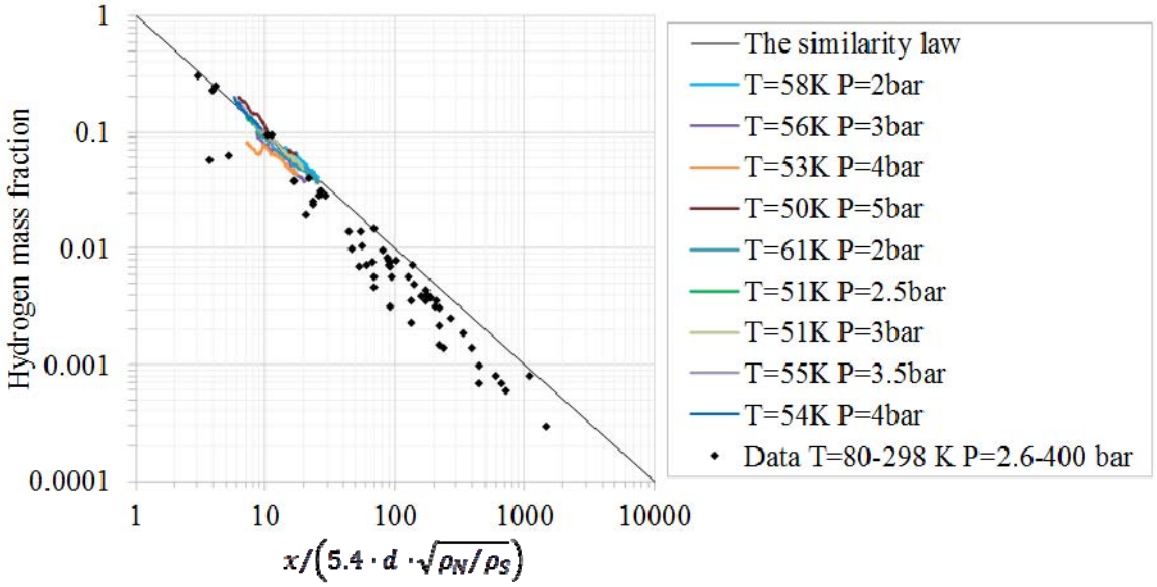

Figure 3-25. The similarity law and experimental data on axial concentration decay in momentum-controlled under-expanded jets from SNL tests and [Saffers 2013].

3.2 Ignition

3.2.1 Ignition of Liquid Pool

For open LH_2 pools, it needs to be considered that cold hydrogen gas is less volatile compared to ambient gas and thus more prone to the formation of a flammable mixture with air. Furthermore LH_2 in direct contact with the ambient air quickly contaminates itself due to condensation and solidification of air constituents. Solid particles may lead to plugging of pressure relief valves, vents or filters. In addition, due to the different boiling points of nitrogen (77.3 K) and oxygen (90.2 K), the oxygen condenses first upon cooling down or vaporizes last upon warming up, both situations always connected with an oxygen-enriched condensate forming shock-explosive mixtures. Also liquid or solid oxygen in combination with another combustible material, even if solid and thus not "flammable", may form highly explosive mixtures with drastically decreased ignition

energies. Examples are LH_2 plus solid air having an O_2 fraction of > 40%, or liquid oxygen spilled onto asphalt [Zabetakis 1967].

Main objective of the burning tests was the derivation of empirical relationships between the amount of spilled LH_2 and flame height/width to be used for setting standards for the definition of safety distances. Measurements of maximum height and width of the flames from rapid spillage and ignition with quantities of up to 89 ℓ of LH_2 were summarized in an empirical correlation between maximum flame height/width and the spilled volume as [Zabetakis 1960]

$$H_{max} \approx W_{max} \approx 2.1 \times \sqrt{V_l}$$

where H_{max}, W_{max} is the maximum flame height and width, respectively, m; V_l is the volume of spilled LH_2, ℓ.

Ignition of the vapor above the pool (depth: 50–300 mm) was by either spark or flame source in the range of up to 8 s after spillage. The later the ignition, the larger was the fire ball.

It was found from experiments that pools of LH_2 were difficult to ignite, and only accelerated flames were observed with hardly any tendency to detonation. A factor contributing to this effect is the inhibiting influence of the condensing moisture in the open atmosphere [Kreiser 1994].

In pool fires, the hydrogen flames principally remained limited to the pool size, but were largely extended, up to 50 m, in vertical direction. They were even able to ignite separated flammable gas pockets creating a new fire ball. The hydrogen vapor clouds evolving from LH_2 pools into the open atmosphere appeared to be inhomogeneously composed with a stoichiometric mixture being highly unlikely [ADL 1960]. The ignition of premixed LH_2 with condensed air significantly enhances burning rates with a large variation. The flame will become wider and taller, and the radiated energy increases [Urano 1986].

Pro-Science and Karlsruhe Institute of Technology (2020)

After investigating the formation and vaporization of LH_2 pools above different substrates as concrete, sand, water, and gravel, a second experimental campaign on the ignition of LH_2 pools was carried out by Pro-Science and KIT. In this campaign the same pool and substrates as described in 3.1.2.2 was used, but to save the instrumentation most sensors from above the pool were removed. To characterize the combustion behavior, pressure sensors were distributed on the ground around the pool facility. As in the unignited tests, the pool was filled and vaporized at least once to cool down the substrate, before, after the final filling, the ignition source (spark generated between two electrodes) in the cloud above the surface of the pool was turned on. By controlling time of ignition and the height of the ignition source above the pool it was aimed to induce the combustion in a position of the cloud where flammable mixtures of different H_2 concentration levels are present.

An ignition of the cloud above the pool was observed for all ignited tests, and the level of damage to the pool facility ranged from no/minor damage via significant damage to complete destruction of the facility (Fig. 3-26).

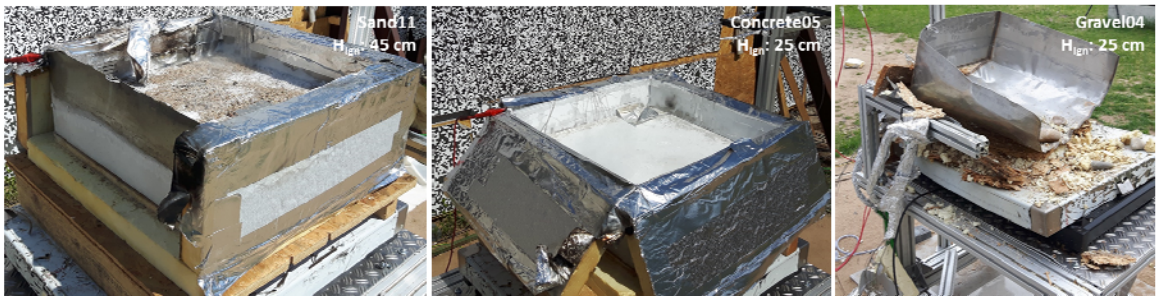

Figure 3-26. Different damage levels after ignition of LH_2 pools.

3.2.2 Ignition of Hydrogen-Air Cold Mixtures

Several potential mechanism of ignition were identified for hydrogen-air mixtures in [Astbury 2005]. The present chapter focuses on the research available for cryogenic hydrogen mixtures. Flammability limits for low temperature mixtures were presented in section 1.2 and are not repeated here.

3.2.2.1 Hot Surface Ignition and Minimum Ignition Energy (MIE)

INERIS Experiments (2020)

The device used to measure the hot surface temperature (T_{pcrit}) is a straight horizontal tube (Fig. 3-27), 10 cm diameter, 2.5 m long equipped with a flange in which gaseous hydrogen, gaseous nitrogen, gaseous oxygen and when required liquid nitrogen are admitted and mixed. This arrangement enables to vary independently H_2 concentrations, velocities U, and initial temperatures T_0. The hot body is a nichrome wire spiraled around a 10 mm alumina core (Fig. 3-28). It is electrically heated and the temperature can be varied. The whole flammable range could be explored with velocities ranging from nearly zero (0.5 m/s) to 30 m/s and temperatures between -120°C to ambient.

Figure 3-27. Details of the setup for T_{pcrit} measurements.

Figure 3-28. Hot coil arrangement (0.7 m nichrome wire of 0.0008 diameter spiraled over a 9 mm diameter and 30 mm long alumina cylinder) – electrically heated.

The influence of the reactivity seems very small (Fig. 3-29). Note also that this temperature is very close to the auto-ignition temperature. An optimum is found at 10% H_2 in air.

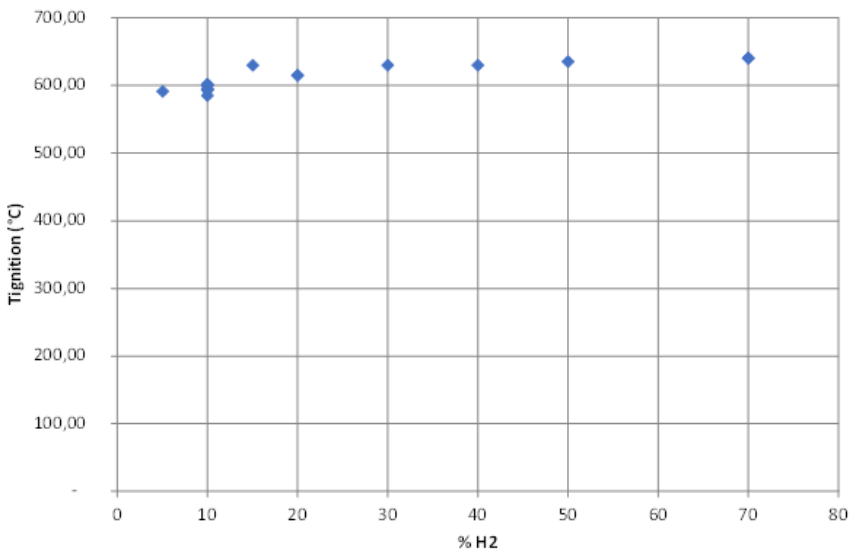

Figure 3-29. Influence of the proportion of H_2 in the mixture on the hot surface ignition temperature (ambient conditions and at rest).

The second point is about the influence of the temperature of the flammable atmosphere. The data of Figs. 3-30 and 3-31 were established for the optimum composition (10% H_2-air mixture). In the parametric range investigated, there is no significant influence of the flow velocity or of the temperature of the mixture.

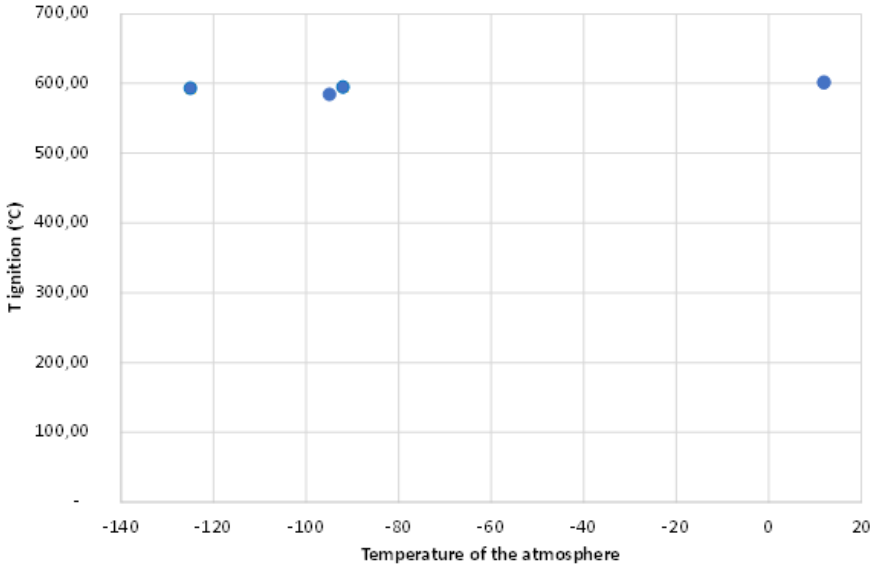

Figure 3-30. Influence of the temperature of the H_2-air mixture on the hot surface ignition temperature (at 10% H_2 in air at rest).

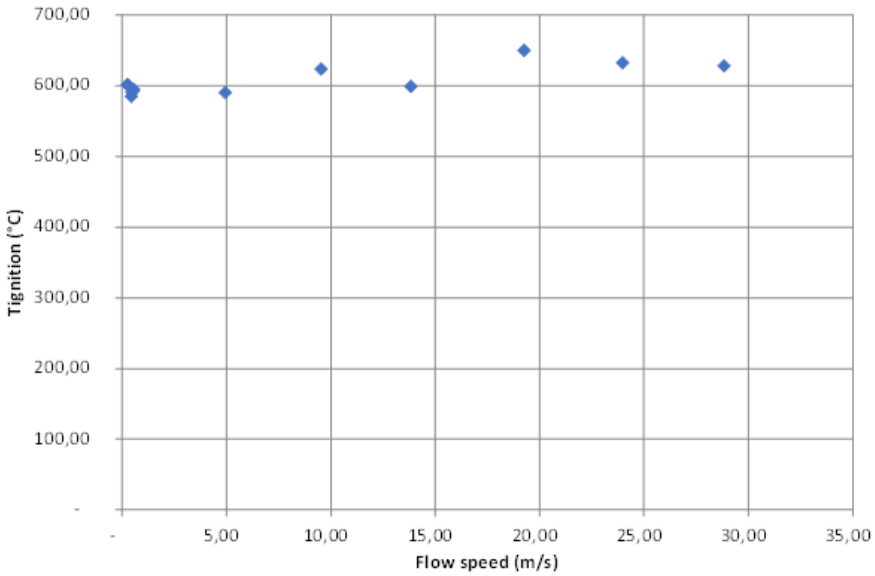

Figure 3-31. Influence of the velocity of the H_2-air mixture on the hot surface ignition temperature (10 % H_2, ambient conditions).

Zero-dimensional auto-ignition temperature calculations using Cantera code with Maas-Warnatz and Lutz detailed chemistry [Lutz 1988, Maas 1988] have been performed within PRESLHY project to model hot surface ignition with hypothetical infinite radius of hot surface. As Figure 3-32 shows, the calculations agree very well with experimental measurements on auto-ignition temperature under hot surface ignition of hydrogen-air mixtures performed at INERIS (Figs. 3-29–3-30). For instance, the calculations mechanism gives an auto-ignition temperature T_c = 607°C for stoichiometric hydrogen-air mixture. INERIS data give the value T_c = 630°C. Both calculations and experimental measurements demonstrate almost no dependence of ignition temperature on cryogenic initial temperature. Compared to the calculations, the INERIS measurements show a slightly increasing auto-ignition temperature from 595°C to 645°C with hydrogen concentration increase from 10% to 70% H_2 at ambient initial conditions.

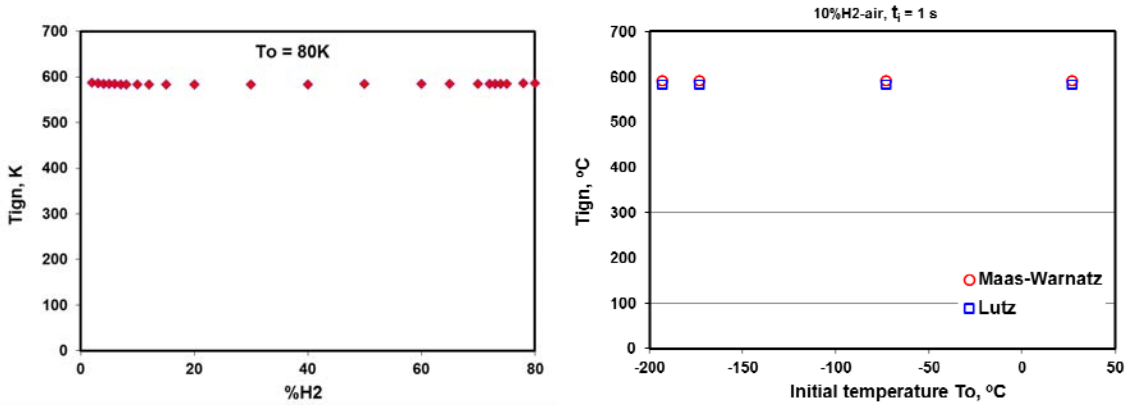

Figure 3-32. Influence of the velocity of the H_2-air mixture on the hot surface ignition temperature (10 % H_2, ambient conditions).

The Minimum Ignition Energy (MIE) is the lowest energy value of a high-voltage capacitor discharge required to ignite a hydrogen-air mixture at atmospheric pressure and room temperature. It is expected that this energy increases for decreasing initial temperature of the mixture. Semi-empirical correlations for hydrogen-air mixtures with

temperatures in the range 200–300 K were developed [Martín-Valdepeñas 2003]. A MIE slightly larger than 0.1 mJ was obtained for a stoichiometric mixture with temperature equal to 50 K.

The device used to measure the minimum ignition energy (MIE) is a vertical burner filled with glass beads (Fig. 3-32). The flammable mixture is introduced from the bottom and diffuses upwards. Ignition is produced just above the surface and the bed of particles quenches the flame. When cooled mixtures are desired the bed is cooled before the ignition tests by pouring about 2 ℓ of liquid nitrogen from the top.

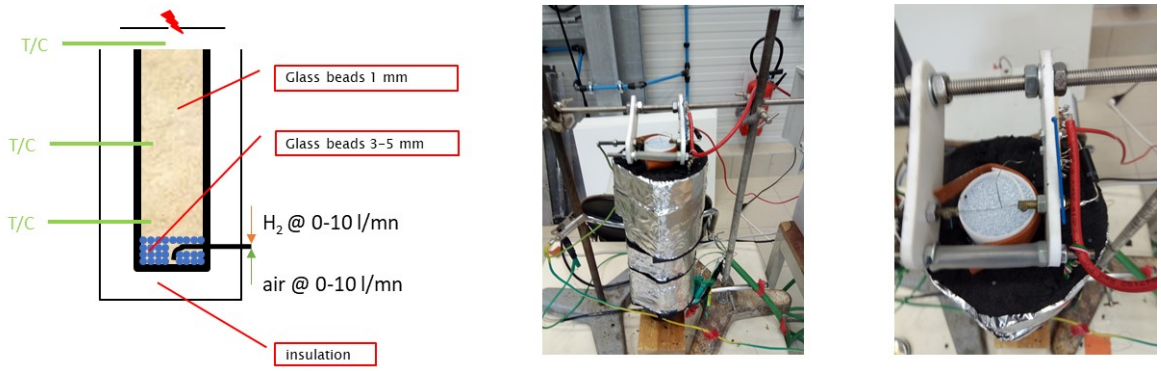

Figure 3-33. Burner (40 mm inner diameter and 400 mm high).

An innovative spark generator was developed and tested (Fig. 3-34). A significant effort was devoted to its development and to the control of the spark. A very weak high voltage spark triggers the discharge of a low voltage capacitor in series with a 1 mH inductance to prolongate the spark duration and limit the current.

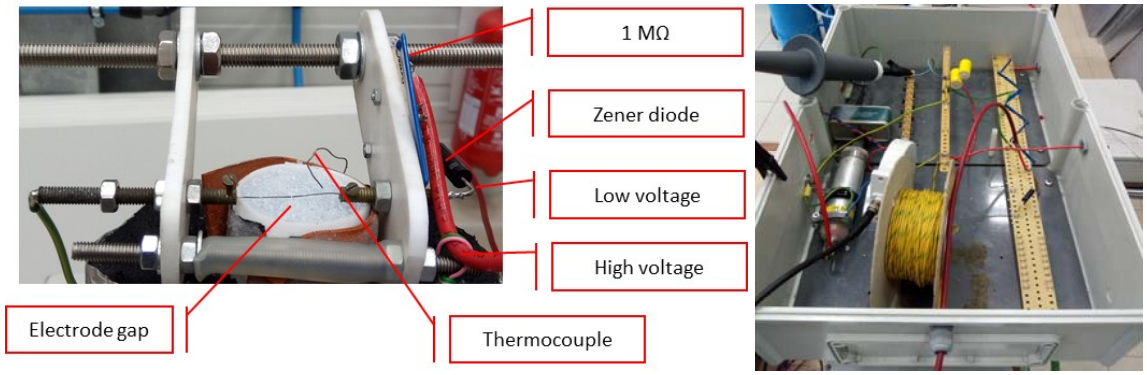

Figure 3-34. Spark gap arrangement (0.5 mm gap) and spark electronics.

Tests were performed with hydrogen-air mixtures at ambient temperature. As shown in Fig. 3-35, the MIE values are in line with the data from the literature with a minimum at 20% H_2 in air amounting 18 µJ.

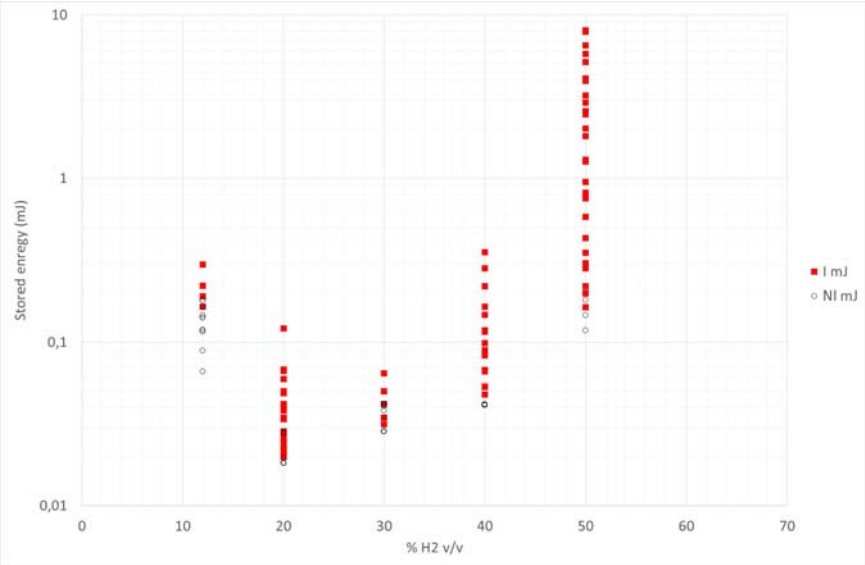

Figure 3-35. MIE for hydrogen-air mixtures at ambient temperature and atmospheric pressure.

MIE measurements were done at this optimum concentration between -120°C and ambient temperature at atmospheric pressure (Fig. 3-36). The MIE increases when the temperature drops, but this increase of MIE does not seem linear.

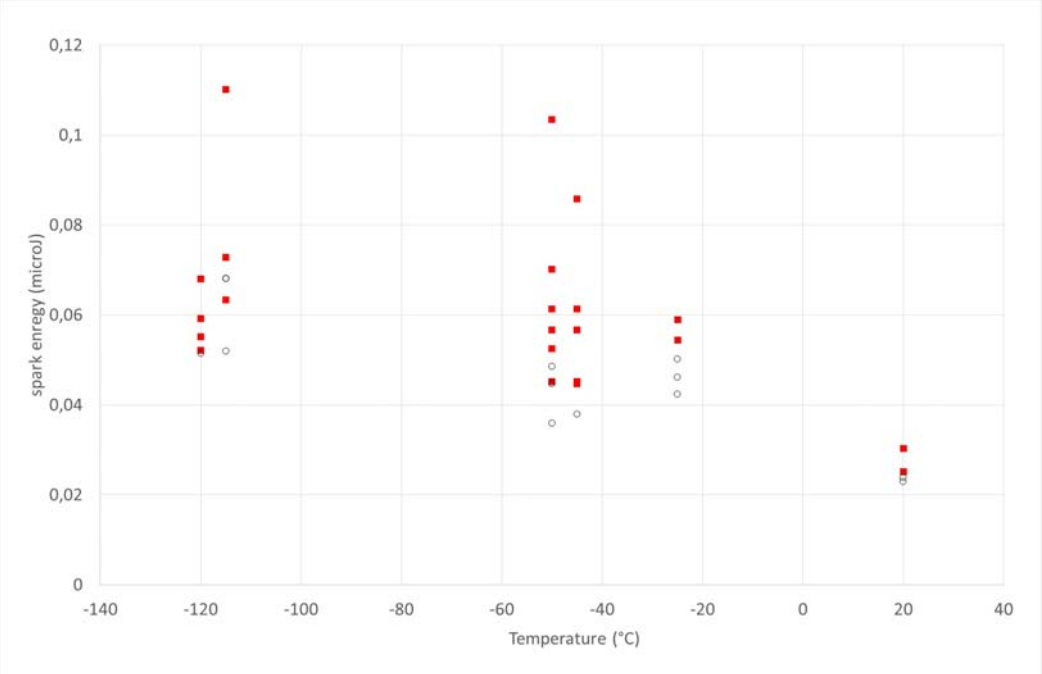

Figure 3-36. MIE of 20% H_2-air mixtures as function of the temperature at atmospheric pressure.

3.2.2.2 Modeling of Ignition and Determination of MIE

Several theoretical correlations have been developed based on the dependence of minimum ignition energy (MIE) on the quenching distance [Lewis 1961, Monakhov 1986, Law 2006, Kondo 2003]. It was found [Lewis 1961] that for strong flames, E_{min} is proportional to d^3, whereas for less strong flames proportionality was found for d^2. [Law

2006] confirmed proportionality of E_{min} to d^3, based on experimental results [Calcote 1952] for a variety of fuels including hydrogen. The author considered that the quenching distance should be of the same order of the laminar flame thickness δ_L, as this is the distance characterizing heat losses.

Models available in literature have been not validated against tests on cryogenic mixtures. Furthermore, their applications have been generally limited to mixtures of known and tabulated properties, e.g. experimental measurements of quenching distance. This would prevent the application of the model in conditions where experimental data are not available, such as mixtures with initial temperature different from ambient or with different hydrogen concentration. To overcome these shortcomings, Ulster University developed an engineering tool for calculation of MIE for mixtures at arbitrary temperature and hydrogen content (PRESLHY D6.5, 2021). Similarly to [Lewis 1961] the MIE is considered as the amount of energy required to heat up a sphere of flammable mixture at initial temperature T_u of the unburnt mixture, to that of the flame, T_b. The quenching distance, d, is considered as the diameter of the critical flame kernel:

$$E_{min} = \frac{1}{6}\pi d^3 \rho_{av} c_{p,av} (T_b - T_u)$$

The model employs the laminar flame thickness to determine the critical flame kernel. Cantera and Chemkin software is used to calculate the flame and mixtures parameters, and their performance are compared. The model implements a correction of the laminar flame speed to take into account flame stretch and selective diffusivity. To assess the validity of the correlation, results were compared against tests for ambient temperature mixtures [Lewis 1961, Ono 2007] and against tests for cryogenic mixtures with temperatures of -100°C performed by INERIS within the PRESLHY project. For a stoichiometric mixture at cryogenic temperature, the simulated MIE was found to be 40 μJ, predicting well the experimental MIE which was found to be between 40–50 μJ.

CFD modeling may be a further resourceful tool for predicting MIE for arbitrary conditions. A CFD approach was developed within PRESLHY project by partner Ulster University to model ignition by spark and flame kernel development in hydrogen-air mixtures (PRESLHY D4.2, 2021). It employs detailed chemical kinetics, including 13 chemical species and 37 elementary reactions for hydrogen-air combustion. The CFD model was used to investigate the flame kernel growth following ignition of a stoichiometric hydrogen-air mixture ignition for the MIE reported in literature, i.e. 17 μJ. Results showed a good agreement between the analytical and experimental flame kernel developments. The ignition energy (IE) in CFD simulations was progressively reduced to numerically determine the minimum energy level igniting the mixture. CFD modeling interested mixtures with hydrogen concentrations in the range of 10–55% and took account of the dependency of MIE on the gap in between electrodes. Figure 3-37 compares simulation results to experimental measurements [Lewis 1961, Ono 2007] for ambient temperature mixtures. Simulations calculated the absolute MIE as 15 μJ for hydrogen concentrations of 22–29% by vol and an electrodes' gap equal to 0.5 mm, which very well agrees with 17 μJ measured in experiments. Ignition was not numerically obtained for IE = 12 μJ. Even closer agreement was found for MIE in tests with 1 mm as electrode gap, where simulated MIE exactly coincides with experimental measurement at H_2 concentration of 14 and 35% by vol.

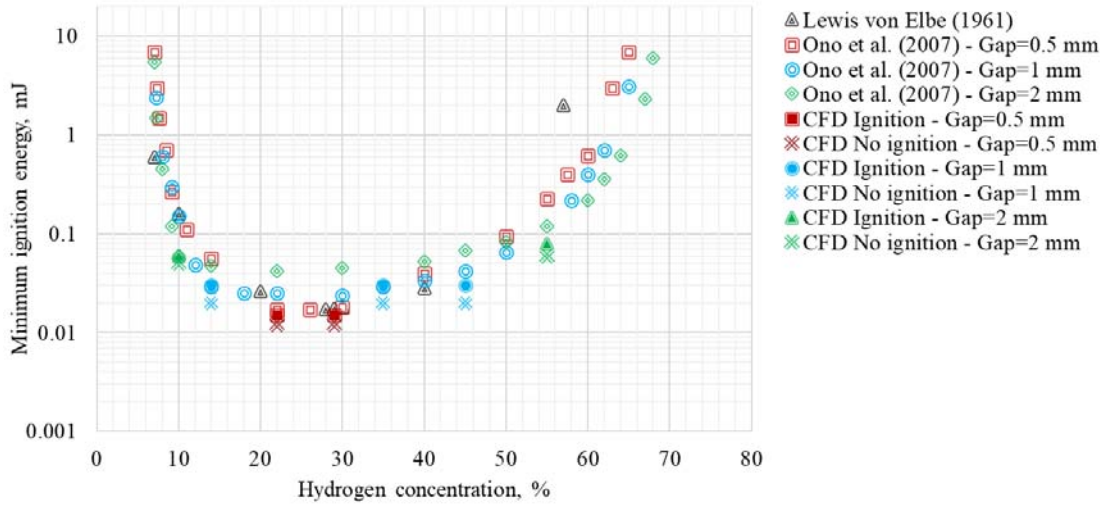

Figure 3-37. Determination of Minimum Ignition Energy (MIE): CFD simulation results versus experiments.

The same CFD model was applied to cryogenic hydrogen-air mixtures at -100°C. Simulated MIE was seen to increase with the decrease of temperature. For a hydrogen concentration in air equal to 20% and 30%, MIE resulted to be 30 μJ. CFD simulation results well agree with experiments by INERIS which recorded ignition in the range 40-50 μJ for H_2 = 20% and 30% by vol.

3.2.2.3 Electrostatic Ignition

During release of low temperature hydrogen, there could be condensation/freezing of humidity or other air components. The formed solid or liquid particles may lead to electrostatic charging of the jet and potential ignition. Experiments by [Merilo 2012] showed that electrostatic discharge of entrained particulate could ignite hydrogen releases at ambient temperature. Previous experiences in hydrogen production and storage facilities in the USA showed that hydrogen through unflared vent stacks could be ignited by a static charge in air. Lesson learnt to prevent this eventuality is to ensure a good and continuous ground connection. Several experimental campaigns have been conductive within PRESLHY project to investigate the electrostatic charging of low temperature hydrogen releases and their potential to ignite.

Health and Safety Laboratory (2020)

Health and Safety Executive carried out a series of experiments to assess the propensity for LH_2 to generate electrostatic charging capable of igniting the hydrogen cloud during a release or accidental spill scenario. The experiments found out that electrostatic charges can pose a hazard when considering LH_2 facilities.

LH_2 was released through nozzle diameters 6, 12 and 25.4 mm at a pressure within 0.1-0.5 MPa range. The experiments were designed to measure two distinct modes of charging:

- Thirty tests provided information on the charging due to charge separation near to the LH_2 / pipe interface. This was monitored by using an electrometer connected to an electrically isolated section of pipework prior to the release point (Fig. 3-38,

left).

- Seven tests assessed the charging of the cloud generated by a jet of hydrogen, which may be liquid, gaseous or two-phase, by measuring the electric field. In few trials, a Faraday cage was also employed to have a better characterization of the electric field geometry (Fig. 3-38, right).

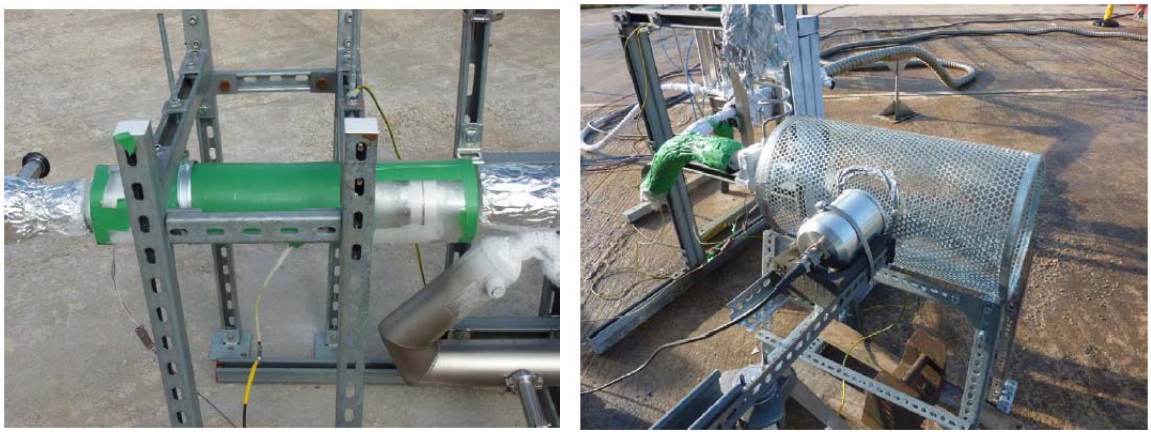

Figure 3-38. Experimental setup.
Left: isolated pipework. Right: Faraday cage and field meter.

The wall current measurements showed the ability for LH_2 to induce a current on a section of electrically insulated pipework. The produced charge depends on the phase of LH_2 in the pipework, the turbulence of the flow, and the resistance to ground of the section of the pipework. Frost formation on the outside of the pipework dynamically changed the resistance to ground throughout each trial, complicating the quantitative interpretation of results.

The experimental measurements of electric field in the plume showed intermittent spikes in field strength. This evidence indicates that the multiphase hydrogen jet itself does not create a significant charge, but the charging can be caused by interactions of hydrogen with air, other substances and objects. In particular, air in the pipework being ejected and solidified air forming around the release point, breaking off and flowing downstream appear to be the cause of the electrical fields measured in these experiments. This effect could be larger with different initial conditions either at the nozzle or in the tanker.

Pro-Science and Karlsruhe Institute of Technology (2020)

In the frame of the PRESLHY project more than 200 hydrogen blowdown experiments were made with the DisCha facility at KIT at ambient temperature and cryogenic temperatures (approximately 80 K). The reservoir pressure has been varied from 0.5 to 20 MPa, the tested release nozzle diameters were 0.5, 1, 2, and 4 mm, respectively. Extensive equipment was used to measure hydrogen mass, pressure and temperature in the pressure vessels and temperature, hydrogen concentration and electrostatic field in and around the released jets. Additionally all ambient conditions like temperature, pressure and relative humidity have been recorded.

No spontaneous ignition was observed in any of the performed tests. The generation of strong electrostatic fields was observed in the cold jets, especially for high initial

pressure, in the order of 5 kV/m. These values, 100–1000 times higher than the natural electrostatic background field, are considered to be provoked by the ice crystals formed at the release nozzle and subsequent entrainment during the initial phase of the gas discharge. Jets at normal temperature did not generate significant electrostatic fields.

Further seven tests were carried out on the release of LH_2 with the Cryostat vessel at an initial temperature of about 30 K, pressures up to 0.5 MPa, and inventories of up to 3.78 kg H_2. The fields measured with the CRYOSTAT facility during the release of LH_2 (Fig. 3-39) generally were considerably higher than the ones measured in the DisCha experiments at 80 K with pressures of 0.5 MPa. But in contrast to the DisCha experiments, the field values seem to decrease with increasing initial pressure level, however, the pressure range investigated (0.2 to 0.5 MPa) may not have been large enough to draw definitive conclusions.

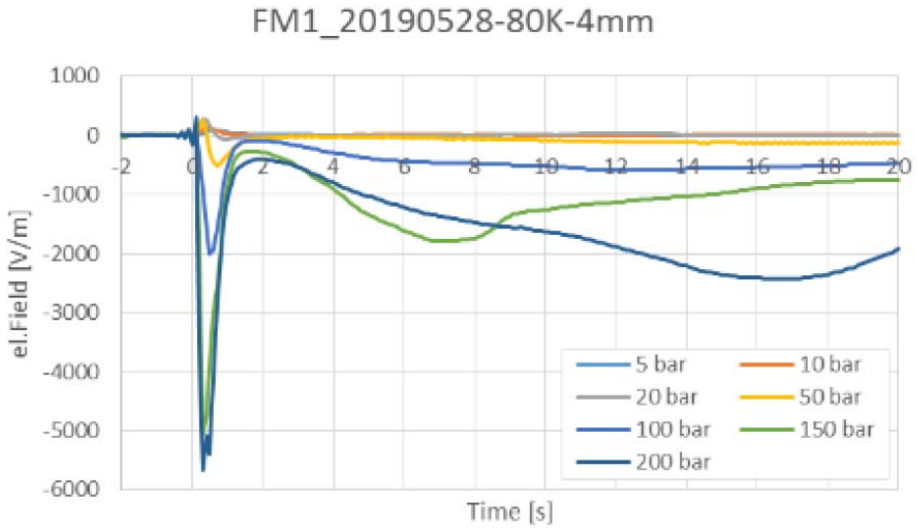

Figure 3-39. Electrostatic field measured with field mill FM1 for blowdown of up to 20 MPa of hydrogen at initial temperature equal to 80 K.

3.2.2.4 Diffusion Ignition

The spontaneous ignition mechanism has been first postulated in [Wolanski 1973], following the observations on ignition occurrence when high pressure hydrogen was admitted to a shock tube filled with air or oxygen. The authors suggested that ignition was caused by the high temperature gradient at the contact surface where the oxygen heated by the primary shock wave produced by the expanding gas, mixed and reacted with hydrogen due to diffusion. Experimental investigations on verification of spontaneous ignition by changing hydrogen pressure, temperature, release orifice size, etc. were performed in [Bazhenova 2006, Golub 2007, Golub 2008, Golub 2010]. Generally, it was observed that an increase of initial temperature may cause an earlier ignition and verification for lower pressures. Hence, it may be expected that for cryogenic hydrogen the pressure limit would increase with respect to ambient temperature storage. To the authors' knowledge, no experimental studies were yet available in literature on spontaneous ignition for cryogenic mixtures.

In the frame of PRESLHY project (PRESLHY D5.2, 2021), an LES approach was employed by partner UU to investigate numerically the effect of hydrogen temperature

decrease on pressure limit leading to spontaneous ignition in a T-shaped channel, following the work performed in [Bragin 2013]. Ignition and combustion dynamics were assessed by analyzing the temperature and hydroxyl mole fraction distributions. It was found that a pressure of 2.9 MPa is required for hydrogen at ambient temperature (300 K) to provide spontaneous ignition and likely sustained flame combustion outside the T-shaped channel. Lower pressures in the range 2.6–2.8 MPa were found to trigger ignition and to later result into self-extinction. For a pressure of 2.43 MPa, there was no recording of ignition. For cryogenic hydrogen (80 K), the limit pressure required to trigger ignition and sustain combustion outside the T-shaped channel was determined to be 9.4 MPa. This limit pressure is approximately 4 times larger than for ambient temperature hydrogen. Numerical simulations with initial pressures equal to 8.75 and 7.5 MPa results showed that there was ignition within the T-shaped channel, but this later self-extinguished.

3.2.2.5 Water Spray and Deluge Tests

An unintended release of liquid hydrogen on water may lead to a sudden and violent vaporization of liquid hydrogen, known as Rapid Phase Transition (RPT). Experimental work by Health and Safety Executive within the frame of PRESLHY project investigated whether rapid phase transitions and associated pressure effects are to be expected if water from sprinklers or hose jets is applied on liquid hydrogen in a tray with dimensions 800 mm x 800 mm x 100 mm. The experimental equipment (Fig. 3-40) included pressure transducers to capture any overpressure produced and assess the verification of RPT.

Figure 3-40. Experimental facility for rapid phase transition investigation.
Left: fully developed water spray from sprinklers.
Right: water jet application into the centre of the tray (right).

Experiments carried out with the sprinkler systems showed that most of the vapor production was complete within approximately 30 seconds (Fig. 3-41).

Figure 3-41. Vapor production after 5, 10, 20 and 30 s of water spray impingement.

For both sprinkler and water jet systems tests there was no significant recorded overpressure and no sign of rapid phase transition during the experiments. In the case of the test with sprinklers, there was significant formation and deposition of ice in the pool tray. Temperature records suggest there was an accumulation of condensed air at the bottom of the tray. On the contrary, at the end of test with the water jet there were no signs of ice in the pool tray. Presumably water displaced the liquid hydrogen so rapidly that there was no time for it to freeze. The tests showed an enhancement of the rate of vaporization of LH_2, which in case of ignition could result in severe consequences.

3.2.2.6 Ignition of condensed phase during releases of LH_2

Ignition of spills of LH_2 could produce strong overpressure as witnessed during HSL experiments in 2010. In the test, as the cloud was ignited, it burnt back to source creating a jet fire and then a secondary explosion appeared to emanate from the liquid/solid pool location. The highly energetic event occurred in a test with wind speed 2 m/s and could not be replicated in further attempts with similar wind conditions. Possible reasons of such a phenomenon could be the following:

- Solid oxygen was built-up within the condensate due to the relative differences in O_2 and N_2 melting/boiling points and then a large enough ignition source was able to ignite the mixture or;
- The condensate in whatever form underwent some sort of rapid phase transition (RPT) generating pressure through expansion. This liberated gas may then have ignited.

In order to understand the hazard surrounding the condensed phase generation, it is necessary to know what the composition of the condensate is and under what conditions it might form. It is possible that enrichment of oxygen only occurs at high wind speed conditions. HSE carried out an analytical and modeling study of the condensation and

freezing of air when mixed into a liquid hydrogen jet – focusing on the potential for oxygen enrichment. The results showed that moderate levels of oxygen enrichment can occur during the condensation of air. However, the conditions and chemical composition of solids formed from releases of LH_2 may depend significantly on wind conditions and release geometry. Mixtures of LH_2 with solidified air enriched to over 50% oxygen mole/mole are prone to rapid DDT if ignited. This is the most likely explanation for the observed secondary explosion in HSL test in 2010. It is believed that condensed phase reaction between solid air and LH_2 was as well the cause for an explosion occurred in experiment carried out by KIT on a different surface materials and different discharge conditions.

Within the frame of PRESLHY project (PRESLHY D4.2, 2021), Ulster University investigated numerically the potential of a 1×1 m^2 LH_2 pool to condense oxygen in air with wind velocity 3 m/s by modeling the multiphase flow through the mixture model and a RANS approach.

Highly energetic events imputed to ignition of LH_2/solid oxygen were reported in [ADL 1960]. [Rico 1970] investigated ignition of LH_2/solid oxygen mixture by injecting oxygen in LH_2 dewars. Experiments recorded detonation velocities of 5000 m/s and 8250 m/s for equivalence ratios equal to 3.5 and 4.5, respectively. These results were confirmed by theoretical predictions.

3.3 Combustion

3.3.1 Thermodynamics and Kinetics of Combustion

The laminar flame speed is one of the most important fundamental properties of combustion phenomena. It is an integral measure of chemical reactivity for combustible mixture. According to thermal theory of laminar flame by Zeldovich – Frank-Kamenetskii, the pressure-temperature dependence of laminar flame velocity can be expressed as follows:

$$Su(T,p) = Su_0 \left(\frac{T}{T_0}\right)^{\alpha} \left(\frac{p}{p_0}\right)^{\beta}$$

where Su_0 – laminar flame speed at standard temperature T_0 and pressure p_0, m/s; α and β – empirical exponents.

Since the laminar flame propagation is controlled by the diffusion of species between reactants and reaction zone, the temperature exponent α is about 1.5, the same as for the ratio of diffusion or thermo-diffusion coefficients

$$D(T)/D(T_0) \sim (T/T_0)^{3/2}$$

Empirical data on α and β exponents at elevated pressures and temperatures are given in [Malet 2005]. Using a spherical bomb and the pressure records, Bavoil [1997] studied the influence of cold initial temperature on the laminar flame speed of H_2-air mixtures in the range from 100 to 300 K for different equivalence ratios (Fig. 3-42). Empirical values of α exponent were found for different equivalence ratios to calculate the laminar flame speed at low temperature conditions. Data processing of experimental data for cryogenic temperatures gives the parameters of the above laminar flame speed equation in Table 3-1 [Bavoil 1997].

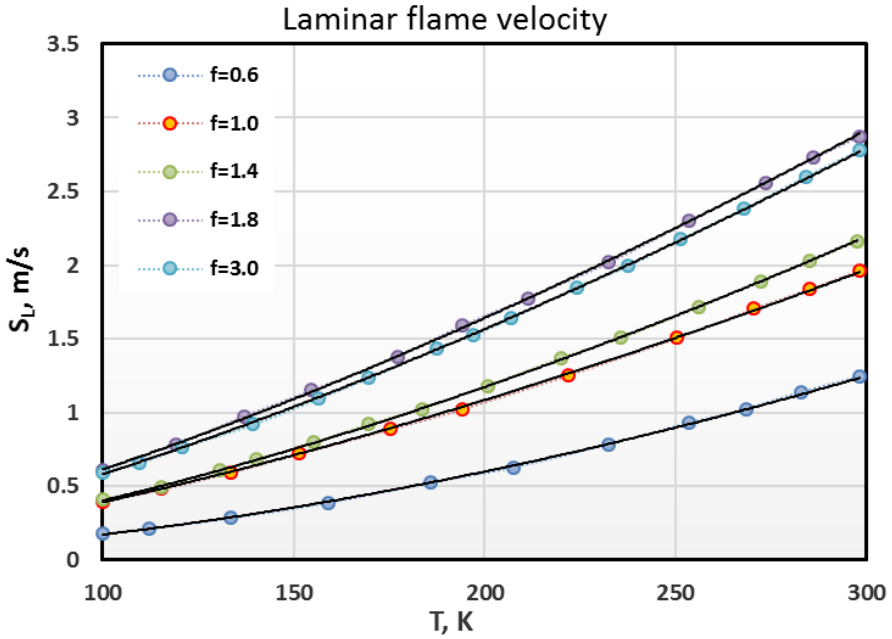

Figure 3-42. Laminar flame velocity as function of temperature for different hydrogen-air compositions [Bavoil 1997].

Table 3-1. Laminar flame velocities for different mixtures [Bavoil 1997].

Equivalence ratio	S_{u0} (m/s)	α
0.6	1.29	1.95
1.0	1.95	1.46
1.4	3.06	1.53
1.8	3.32	1.40
3.0	2.10	1.55

The laminar flame velocity at different initial conditions can also be directly calculated using the Cantera code [Goodwin 2009] with detailed chemistry (Lutz scheme [Lutz 1988] in this particular case). Figure 3-43 demonstrates the behavior of laminar flame velocity at low temperatures. The capability of the code was limited by 200 K. Then, the dependence was extrapolated to 80 K. Figure 3-43 shows an overprediction of theoretical calculations compared to experimental data: S_u = 0.50 m/s against 0.4 m/s (100K). Extrapolation calculations to 80K gives the value S_u = 0.36 m/s. Since the comparison of experimental and calculated data at ambient temperature 293 K gives the same trend S_u = 2.57 m/s (Cantera) and S_u = 1.95 m/s (experiments), then the accuracy of calculations is acceptable for further analysis.

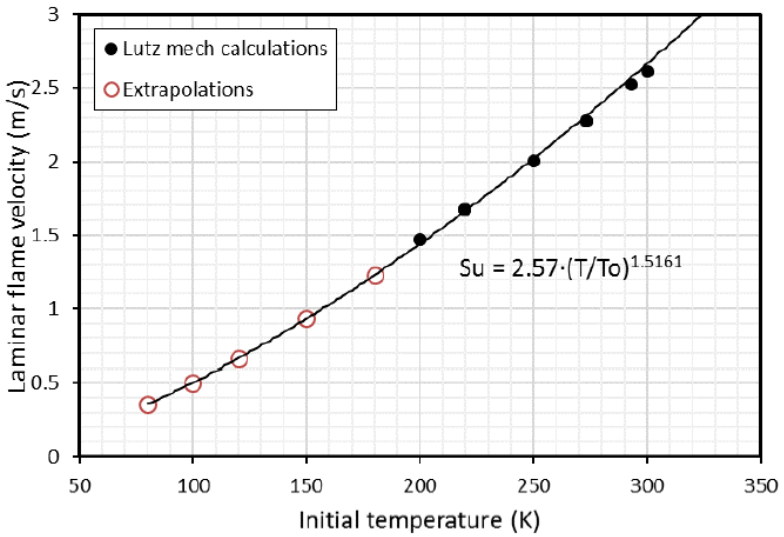

Figure 3-43. Calculated laminar flame velocity as function of temperature for stoichiometric hydrogen-air mixture (Cantera code with Lutz mechanism).

Expansion ratio is the ratio of the density of the fresh gases to the density of the burnt gases. This is also an important parameter for explosion modeling because it represents the piston effect of the flame due to the thermal expansion of combustion products. This may result in the formation of turbulent flow and advancing shock waves in front of the flame. Since the visible flame velocity S_f and flow velocity U_f ahead the flame are proportional to the expansion ratio, the expansion ratio is of great importance for combustion processes and flame acceleration and DDT:

$$S_f = \sigma \times S_u$$

$$U_f = (\sigma - 1) \times S_u$$

Theoretical calculations with STANJAN code [Reynolds 1986] show that expansion ratio increases almost inversely proportional to the temperature. For stoichiometric hydrogen-air mixture, it increases from 7 to 20 with initial temperature decrease from 300 K to 100 K (Fig. 3-44). Taking into account the real gas equation of state (according to the NIST data base) at cryogenic initial temperatures the expansion ratio changes not so much in comparison with the ideal gas equation of state.

Since the visible flame velocity S_f is the product of the expansion ratio (σ) and laminar flame velocity (S_u), the effect of cryogenic temperature on visible flame velocity S_f and flow velocity ahead the flame U_f will be not so significant because reduced chemical reactivity is compensated by higher density and larger expansion ratio at cryogenic temperature.

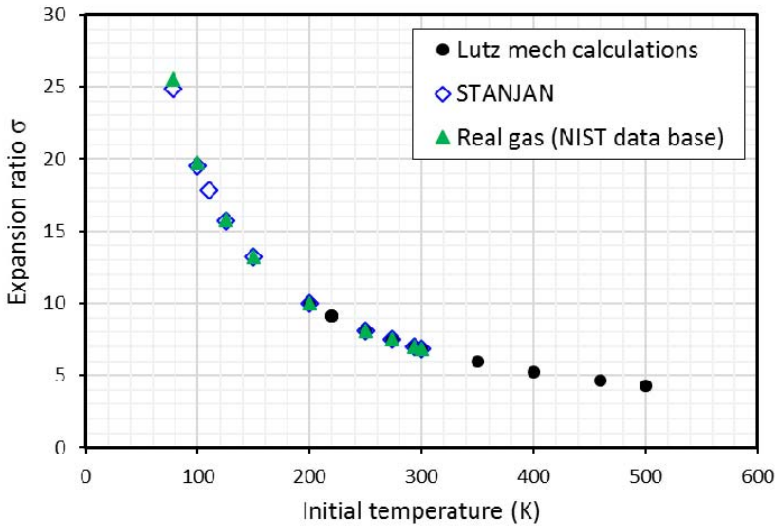

Figure 3-44. Calculated expansion ratio vs. temperature for stoichiometric hydrogen-air mixture (Cantera [Goodwin 2009] with Lutz mechanism [Lutz 1988]).

Adiabatic combustion temperature is also an important characteristic of combustion process. It is a measure of combustion energy. Since specific energy of combustion remains almost the same independent of the density, theoretical adiabatic combustion temperature calculated using Cantera code also remains practically constant in a wide range of temperatures (Fig. 3-45). For instance, four times changing of initial temperature from 300 K to 78 K leads to adiabatic combustion temperature changing less than 5%, from 2383 K to 2263 K, respectively.

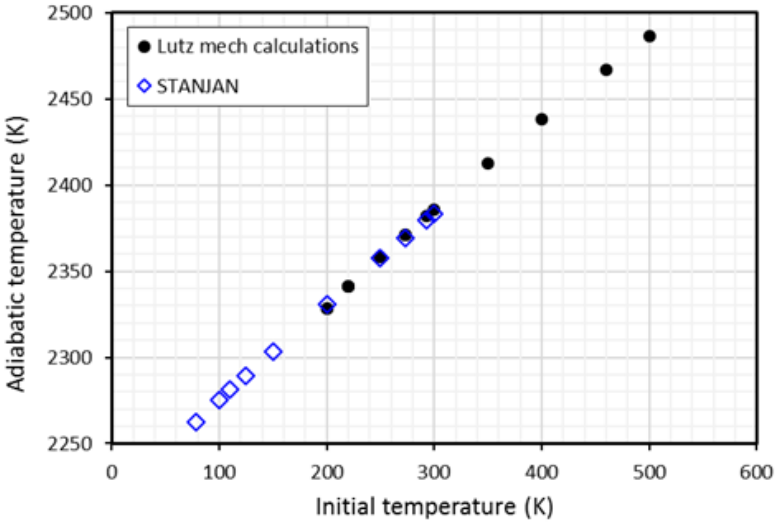

Figure 3-45. Calculated adiabatic combustion temperature as function of temperature for stoichiometric hydrogen-air mixture (by STANJAN and Cantera).

Together with laminar flame velocity, the maximum combustion pressure is also an integral characteristic of combustion process and strength of the explosion. The maximum pressure can theoretically be calculated using thermodynamic STANJAN code [Reynolds 1986]. Adiabatic combustion pressure, P_{icc}, associates with the maximum combustion pressure in a constant volume chamber and also it is roughly equal to characteristic pressure under sonic flame propagation in a channel geometry. In case of detonation, the

maximum combustion pressure is equal to the so-called Chapman-Jouguet pressure which also can be calculated by STANJAN code. Figure 3-46 shows a comparison of maximum combustion pressure for detonation and sonic deflagration at cryogenic temperature of 100 K with that at ambient conditions.

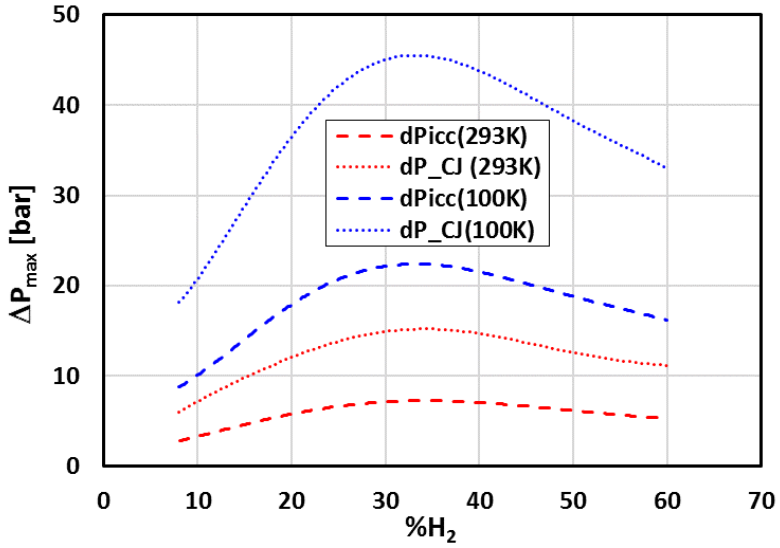

Figure 3-46. Calculated maximum combustion pressure as function of temperature for different hydrogen-air mixtures (STANJAN).

It follows that even sonic deflagration at cryogenic temperature produces the pressure 3 times higher than that at ambient initial temperature and exceeds in 1.5 times the detonation pressure at the ambient initial temperature. This means that cryogenic hydrogen combustion is much more dangerous than detonation at ambient temperature. The maximum combustion pressures at cryogenic temperature P(T) can be calculated from the reference data at ambient conditions P(T0) times the temperature factor:

$$P_{icc}(T) = P_{icc}(T_0)\cdot\left(\frac{T_0}{T}\right)$$

$$P_{CJ}(T) = P_{CJ}(T_0)\cdot\left(\frac{T_0}{T}\right)$$

where $P_{icc}(T)$ and $P_{CJ}(T)$ are the adiabatic combustion pressure and Chapman-Jouguet detonation pressure for a certain hydrogen concentration. The accuracy of such correlation is about 2% for P_{icc} and less than 1% for P_{CJ}.

Based on gas dynamic relationship and considering the flame as a piston propagation with the flame speed, there is a dependence of dynamic pressure against the flow velocity:

$$\frac{P_2}{P_1} = \frac{2\gamma}{\gamma+1}M^2 - \frac{\gamma-1}{\gamma+1}$$

where P_2 – dynamic combustion pressure in our case; P_1 – initial pressure 0.1 MPa; γ – adiabatic coefficient of gas composition; M = v/c – Mach number as a ratio of flow (flame) velocity v = U_f over the speed of sound in reactants c = c_r. Figure 3-47 shows a comparison of dynamic pressure at cryogenic temperature T = 100 K and ambient temperature for the same stoichiometric hydrogen-air mixture. It shows that dynamic pressure at cryogenic temperature is 2–3 times higher than that at ambient temperature for

the same flow velocity. The reasons are almost two times lower speed of sound and larger adiabatic coefficient at cryogenic temperature. Theoretically, the overpressure of about 0.26 MPa corresponds to the flow speed with the speed of sound c_r = 238 m/s (M = 1) in stoichiometric hydrogen-oxygen mixture at cryogenic temperature T = 100 K. This is the main reason to prevent fast sonic deflagration for safety applications to keep flame velocity not higher than the speed of sound.

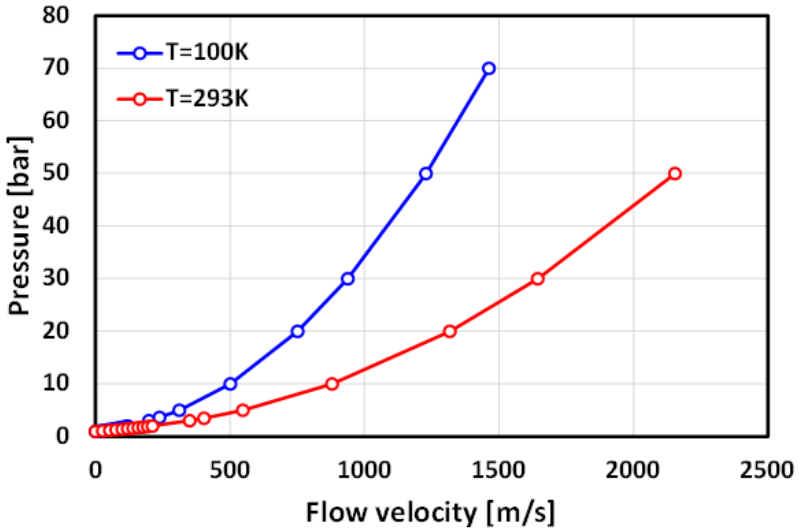

Figure 3-47. Theoretical dynamic pressure as a function of flow (flame) velocity calculated for stoichiometric hydrogen-air at two different temperatures.

3.3.2 Cryogenic Jet Fires

3.3.2.1 Thermal Loads

Several experimental studies were performed on thermal hazards from cryogenic hydrogen jet fires. In [Friedrich 2012] ignited hydrogen releases with absolute pressures up to 3.5 MPa and temperature in the range 34–65 K were analyzed. Radiation level up to 10 kW/m^2 was recorded at 0.75 m from the jet fire. According to published harm criteria [Lachance 2011], a person standing at this distance would suffer second-degree burns if exposed for 20 s to the jet fire. Sandia National Laboratories (SNL) measured the radiative heat flux from cryogenic jet fires with release temperatures down to 37 K and pressures up to 0.6 MPa, abs [Panda 2017]. Experiments showed that for a same mass flow rate, the decrease of release temperature led to an increase of radiative heat flux. The flame length was seen to correlate well with the square root of the Reynolds number.

Thermal radiation from hydrogen flames is significantly lower than that of hydrocarbons, where the radiative properties are dominated by continuum radiation from solid soot particles. In hydrogen jet flames gas the only steam band radiation is the dominant emitting part, resulting in much less heat radiation. This is an important safety advantage of GH_2 flames compared to hydrocarbon jet flames. The results obtained in [Breitung 2009, Friedrich 2012] for the radiant fraction as a function of flame residence time are compared in Fig. 3-46 with other known experimental data [Turns 1991, Schefer 2006]. The flame residence time τ is defined in [Turns 1991] as an average time for burned gas needed to pass through the jet flame region. In general the residence time τ is proportional to the visible flame length L_f.

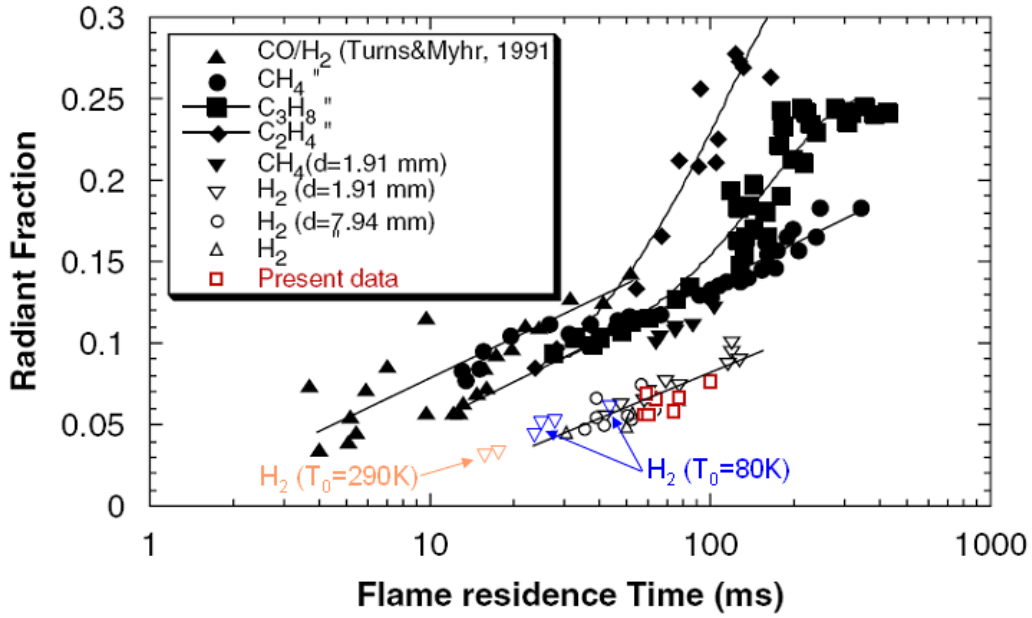

Figure 3-48. Comparison of radiant fractions obtained in [Breitung 2009] with other known data [Turns 1991, Schefer 2006]: black solid points – hydrocarbons [Turns 1991]; black open points – hydrogen [Schefer 2006]; colored empty points – hydrogen at different temperatures (orange – 290 K; blue – 80 K; red – 30-40 K.

The conclusions follow from the analysis of Fig. 3-48. The radiant fractions obtained in [Breitung 2009] agrees very well with earlier results of [Schefer 2006] for hydrogen jet flames at ambient reservoir temperatures 290–300 K. This confirms the proper heat flux measurements of [Breitung 2009, Friedrich 2012]. The radiant fraction increases from 0.03 to 0.06 with the visible flame length increase ($\tau \sim L_{vis}$) in accordance with release temperature decrease from 290 K to 80 K and then to 40 K.

Authors in [Saffers 2013] proposed a dimensionless correlation to determine flame length of both expanded and under-expanded hydrogen jet fires. The correlation was validated against jet fires with pressures in the range of 1–90 MPa and temperatures in the range of 187–300 K. Validation range of the correlation was further expanded in [Cirrone 2019a] to release temperature and pressure included in the ranges 46–295 K and 0.2–0.6 MPa, abs, respectively.

A cryogenic hydrogen jet fire behavior, including scaling and radiation properties was recently investigated within PRESLHY project with the DISCHA facility (see chapter 3.3.2.2). For the volume of 2.87 ℓ, the released hydrogen inventory was changed from 4.4 to 138 g H_2 with an initial pressure from 0.5 to 20 MPa at LN_2 temperature of about 80 K. The facility had varied nozzles (1–4 mm id) and was equipped with background imaging system (BOS) combined with a high speed camera, fast pressure sensors and thermocouples. With known mass flow rate and hydrogen distribution profile as a function of initial pressure and temperature, hydrogen ignition phenomena and further flame development were investigated with respect to maximum combustion pressure, temperature and heat flux radiation for model validation and hazard distance evaluation.

A side view thermo-vision FLIR camera (15 fps) allowed monitoring the temperature and thermal radiation of the jet fire. A sequence of frames with temperature distribution was

obtained by thermo-vision camera (15 fps) (Fig. 3-49). For ambient conditions of 285 K, the local maximum combustion temperature has changed from 1100 to 540 K corresponding to maximum heat flux of 85 kW/m^2. At the same time, the average integral heat flux of whole surface was about 6.5 kW/m^2. At cryogenic temperature release of 80 K, the maximum temperature has changed from 1330 to 710 K corresponding to a maximum heat flux of 177 kW/m^2 in the center of jet fire. The average integral heat flux of the whole surface is about 11 kW/m^2. The reason of such difference is four times larger hydrogen inventory and also 2.5 times higher mass flow rate at cryogenic temperature leading to 1.3 times higher temperature, 2 times higher heat flux of flame radiation, 1.5 times larger flame length and 1.4 times longer release time.

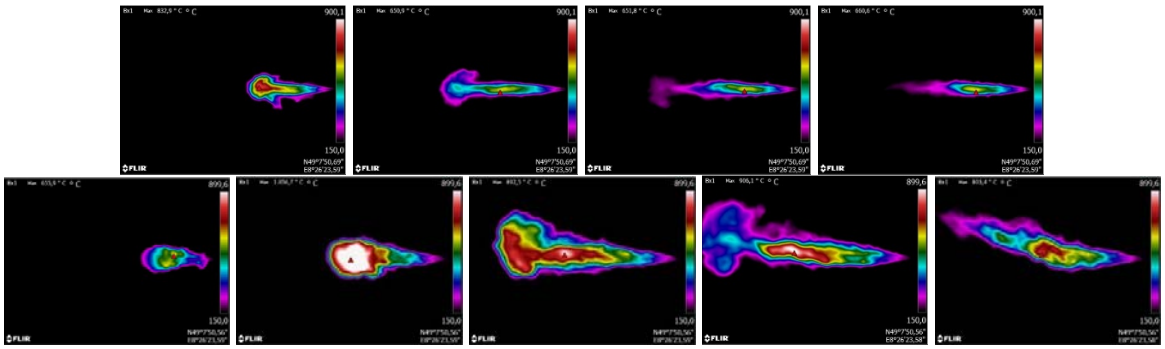

Figure 3-49. Temperature distribution within the jet fire structure. Jet fire radiation for 2-mm nozzle and 10 MPa of initial pressure at T=285 K (upper) and T=80 K (lower).

It was shown that all experimental data for maximum jet fire radiation at x/L_f = 0.6 at different temperatures are collapsed in one line against dimensionless distance r/L_f from the jet axis. All the data for maximum jet fire radiation at the plain x/L_f = 0.6 are well correlated as a hyperbolic function against a radial distance from the jet axis (r/L_f) [Breitung 2009]:

$$q_{\max} = 0.74\left(r/L_f\right)^{-1.59}\ kW/m^2$$

where L_f is the visible length of jet fire. Then, a damage diagram of human's skin by jet fire radiation was created (Fig. 3-50).

Figure 3-50 shows the critical exposure time for jet fire radiation to reach a certain damage degree at dimensionless safety distance measured in flame lengths. For instance, for jet fire length L_f = 2.1 m corresponding to cryogenic hydrogen release through a 4-mm nozzle with 4.4 g/s release rate at 80 K of temperature, the critical exposure time t = 40 s to reach a pain limit at the distance from the jet axis r = 1.05 m. For a distance r = L_f , the pain limit will not be achieved even within 2 minutes. At the same moment, at the flame surface (r = 0.2 m), the critical exposure time for a pain limit is t = 1 s.

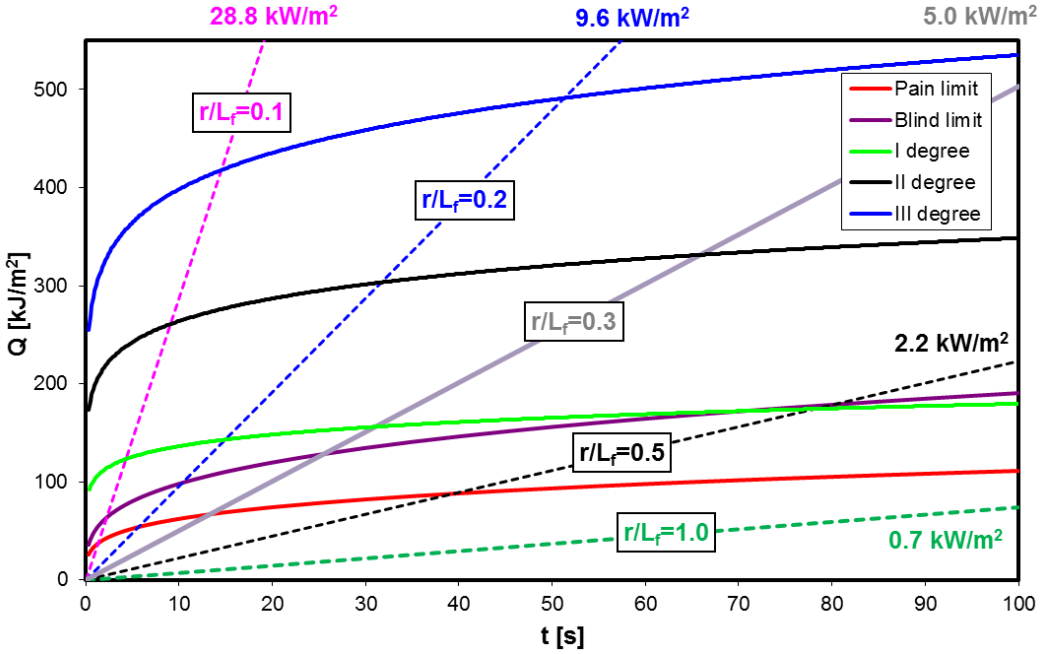

Figure 3-50. Maximum exposure time for different degree of skin damage by thermal radiation of cryogenic hydrogen jet fire calculated for KIT experimental data.

Since the jet fire length increases at cryogenic temperatures due to the density factor, the safety distance also increases with initial temperature decrease. Figure 3-51 shows that safety distance for skin pain limit under heat radiation of ignited high pressure hydrogen release is a factor 8 higher at initial temperature 33 K compared to ambient temperature 290 K. The figure also shows that the safety distance is proportional to nozzle diameter.

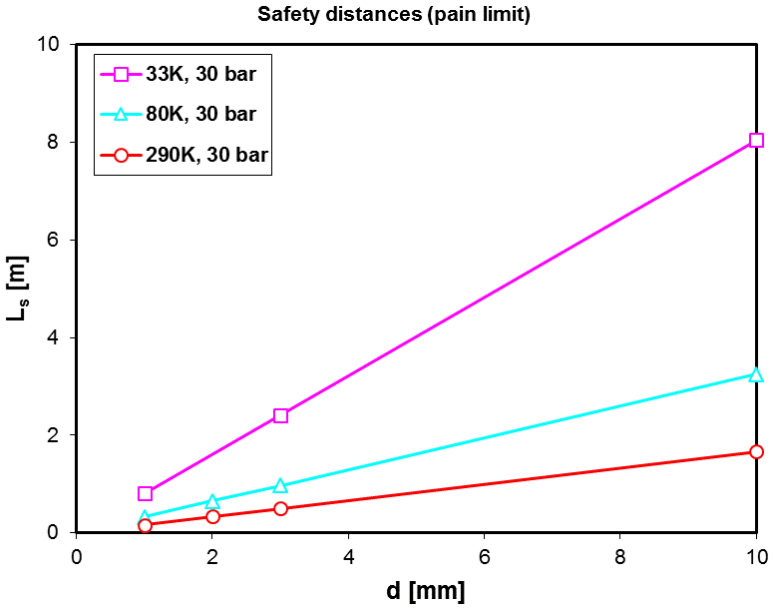

Figure 3-51. Safety distance for pain limit under jet fire radiation at different initial temperatures.

A selection of experiments by SNL [Panda 2017] was used to validate a computational fluid dynamics (CFD) model to simulate flame length and radiative heat flux for cryogenic hydrogen jet fires with pressure up to 0.5 MPa, abs, and temperature in the range of 48–82 K [Cirrone 2019c]. The thermal dose for such jet fires was assessed

in [Cirrone 2019b]. It was concluded that for all tests, at 0.5 m from the flame axis people should stand less than 30 s to not incur in first degree burns.

Within the frame of PRESLHY project (PRESLHY D5.2, 2021), Ulster University extended the CFD model validation to horizontal cryogenic hydrogen jet fires with pressures up to 2 MPa by comparison with experiments performed in [Breitung 2009]. The numerical results provided insights into the thermal hazards from horizontal jet fires and associated distances to "no-harm" levels for people. It was observed that the buoyancy of combustion products has a positive effect on the reduction of the "no harm" distance defined by temperature along the release direction. This decreased from $x = 3.5 \times L_f$ for vertical jet fires to $x = 2.2 \times L_f$ for horizontal jet fires (L_f being the flame length). Thermal radiation led to longer "no-harm" distances in the direction of the jet ($x = (3.0–3.2) \times L_f$) compared to a hazard distance defined by temperature. Ulster University developed a reduced tool to evaluate the radiative heat flux in the surrounding of hydrogen jet fires from vertical and horizontal releases of hydrogen at ambient and cryogenic temperature (PRESLHY D6.5, 2021). The reduced tool is based on the weighted multi-source flame radiation model developed by [Hankinson 2012] and further expanded by [Ekoto 2014] for application to large scale flames. The radiative heat flux prediction depends on the evaluation of the radiant fraction X, which is the ratio of the energy effectively emitted by the flame as radiation and the chemical energy associated to the fuel stream, based on the following correlation [Molina 2007]:

$$\chi = 0.08916 \cdot log_{10}\left(t_f \cdot \alpha_f \cdot T_{ad}^4\right) - 1.2172$$

Ulster University adapted the model to include evaluation of flame length and width through the dimensionless correlation validated against cryogenic releases in [Cirrone 2019a] and expanded the validation range to hydrogen jet fires with pressure in the range 0.2–90 MPa and temperatures in the range 48–315 K.

3.3.2.2 Pressure Loads from Delayed Ignition

Significant deflagration pressures may be created in case of a delay between the beginning of the release and ignition of flammable mixture in the highly turbulent hydrogen jet. Experiments on delayed ignition of releases at ambient temperature and 40 MPa spouting pressure generated an overpressure up to 20 kPa at 4 m distance [Takeno 2007]. Several experimental studies on ambient hydrogen releases demonstrated the dependency of blast wave overpressure on release conditions, i.e. pressure and orifice diameter, and ignition parameters, i.e. delay time and location [Grune 2013, Royle 2010a].

The study by [Friedrich 2012] presents experiments on delayed ignition of hydrogen releases with pressure up to 3.5 MPa, release temperatures in range 34–65 K and nozzle diameters of 0.5–1.0 mm. Results showed that the maximum ignition distance was found for location corresponding to 7% by vol hydrogen in air. The maximum flashback distance was found for H_2 = 9% by vol, which is slightly lower than the distance for ambient temperature releases corresponding to 11%. During the tests, measured sound levels were recorded below 120 dB(A).

Pro-Science and KIT DisCha Experimental Campaign (2020)

Pro-Science and Karlsruhe Institute of Technology performed approximately 300 tests to characterize the thermal and pressure hazards from delayed ignition of hydrogen releases at ambient and cryogenic temperatures within the frame of PRESLHY project. The DisCha experimental setup (Fig. 3-52) included five cameras for investigating jet fires using a BOS technique and one infrared camera for temperature/heat flux measurements. The maximum pressure load for hydrogen release from a 4 mm diameter was reached with an ignition delay of approximately 80 ms.

Figure 3-52. Test site location (left); DisCha experimental setup (right).

Maximum overpressure was found to be up to 3 times higher for the cryogenic releases at 80 K compared to releases at ambient temperature. About 100 tests were performed on cryogenic hydrogen releases at 80 K from three nozzle diameters (d = 1, 2, 4 mm) at four initial pressures in the range of 0.5-20 MPa. Pressure load measurements after delayed ignition are shown in Fig. 3-53 for the example of a release at 80 K and d = 4 mm.

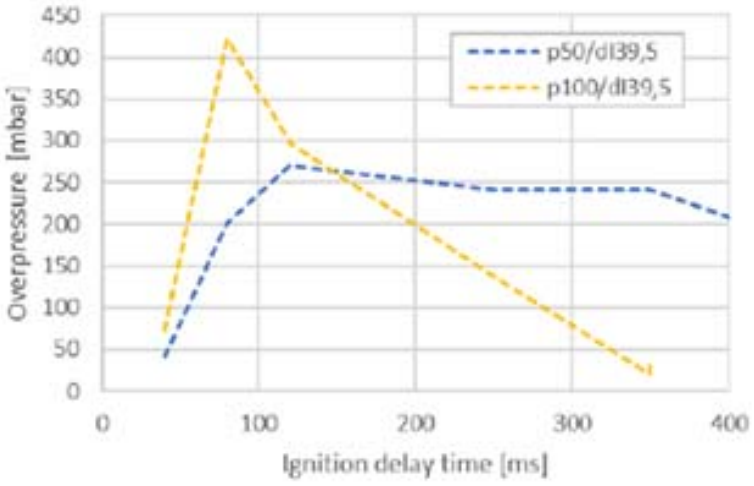

Figure 3-53. Pressure load following the delayed ignition of a cryogenic hydrogen release at 80 K and d = 4 mm (right).

In one experimental series, the ignition distance was varied from 0.4 to 2 m to investigate its effect on the produced pressure load for an ignition delay of 120 ms. A strong explosion with formation of a spherical shock wave might occur just after ignition (Fig. 3-54, left). Then, a stationary jet fire was formed (Fig. 3-54, right). The

overpressure of 0.4 bar corresponds to a visible shock wave velocity of 390 m/s measured by high speed BOS imaging. According to [Grune 2013], such high pressure could only be achieved in the case of a short ignition time delay after release opening (25–120 ms) and a distance from the nozzle (0.2–1.5 m). At such conditions, an envelope of proper hydrogen-air mixtures of sufficiently large volume was formed. For a stationary unburned hydrogen jet release, for a longer time delay, there are no conditions for strong explosion under external ignition.

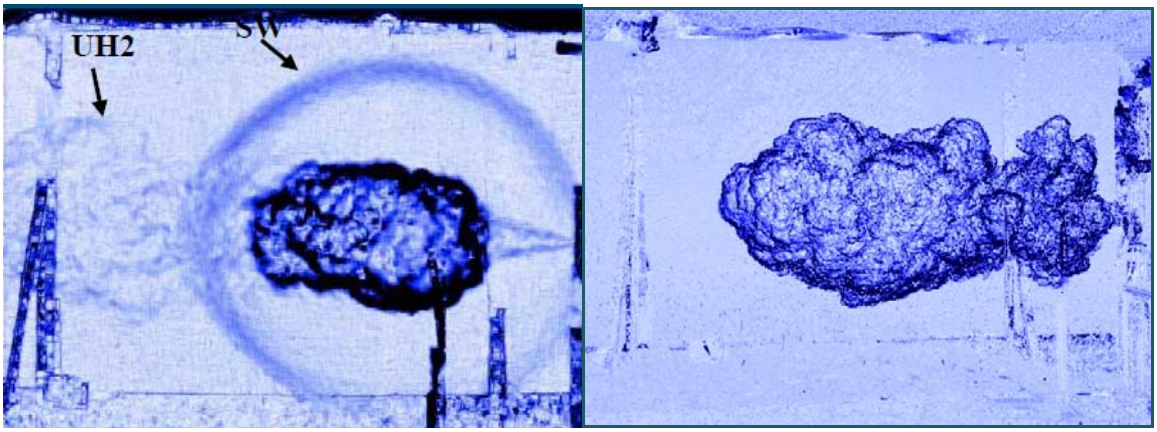

Figure 3-54. Shock wave formation (left) and a stationary jet fire (right) developed under ignition of 4-mm nozzle and 20 MPa pressure: SW – shock wave; UH2 – unignited hydrogen.

Within the frame of PRESLHY project, an engineering correlation was developed by partner UU to predict the maximum overpressure that could be produced by a hydrogen jet for a given storage pressure and release diameter (PRESLHY D6.5, 2021). The similitude analysis was applied to build a correlation. The dimensionless overpressure generated by delayed ignition of hydrogen jets at an arbitrary location, $\Delta P_{exp}/P_o$, is correlated to the dimensionless parameter composed of the product of the ratio of the dimensionless storage pressure, P_s/P_o, and the square of ratio of release diameter to the distance between the center of the fast burning mixture in the jet (25–35% by volume) and the target location, $(d/R_w)^2$.

3.3.2.3 Pressure Peaking Phenomenon

The pressure peaking phenomenon (PPP) can be produced by hydrogen releases in confined spaces with limited ventilation. This is characterized by transient pressure dynamics with a distinctive peak exceeding the steady state pressure. The magnitude of the peak pressure depends mainly on hydrogen release rate, ventilation rate, and enclosure volume. A first theoretical description of the phenomenon was given in [Brennan 2010] for unignited hydrogen releases. The authors found that the produced peak pressure in an enclosure could be significantly higher than thresholds for preventing destruction of civil structures (10–20 kPa). In case of ignited releases, a pressure peak is even more pronounced than for unignited releases [Makarov 2018]. Numerous experimental, analytical, and numerical works have been performed on PPP originated by releases of ambient temperature hydrogen [Brennan 2013, Brennan 2018, Makarov 2018, Lach 2020, Lach 2021, Hussein 2018, Brennan 2019]. In the frame of PRESLHY project, the PPP for cryogenic hydrogen ignited releases in a garage-like scenario was investigated by partner Ulster University through numerical modeling (PRESLHY D5.2, 2021).

The storage temperature, T_S, was varied from 277 K to an intermediate temperature of 200 K and to cryogenic temperature of 100 K. Storage pressure (11.78 MPa) and release nozzle (4 mm) were maintained constant. For a same discharge coefficient, the decrease of temperature caused an increase of released hydrogen from 11.37 g/s for T_S = 277 K, to 14.11 g/s for T_S = 200 K, and 23.16 g/s for T_S = 100K. As a consequence, pressure peak increased from 20.86 kPa for T_S = 277 K to 26.95 kPa for T_S = 200 K. The peak pressure almost doubled (42.82 kPa) for T_S = 100 K and hydrogen mass flow rate equal to 23.16 g/s. To a higher peak pressure corresponded a more pronounced underpressure (-5.36 kPa).

Simulations conducted maintaining a constant mass flow rate of 11.37 g/s showed a slight decrease of peak pressure in the enclosure when storage temperature was decreased. This varied from 20.95 kPa for T_S = 277 K to 20.51 kPa for T_S = 200 K, and to 19.96 kPa for T_S = 100 K. This result is expected as a decrease of the hydrogen temperature mixing with air leads to a decrease of temperature in combustion.

3.3.2.4 Modeling of Cryogenic Jet Fires

The ignition of the released cryogenic jets will lead to either jet fires or deflagrations in the event of delayed release. The latter in particular relates to ignition locations further up from the release nozzle as discussion in the previous section of the experimental analysis. There are various computational fluid dynamics (CFD) tools which can be used to model the combustion processes following ignition. However, the available literature in the open domain related to modeling has so far mainly been directed to the ignited releases of hydrogen gas jets at environmental temperatures. An example is illustrated here about the CFD simulations recently conducted by Warwick FIRE using three-dimensional (3-D) large-scale large eddy (LES) simulations techniques. The numerical simulations were conducted for the experimental conditions similar to those used in the KIT tests for hydrogen gas release at cryogenic temperatures.

The numerical simulations were conducted within the frame of open source CFD code OpenFOAM using rhoReactingFOAM, which is a compressible reacting flow solver. One-equation eddy-viscosity subgrid scale (SGS) model [Yoshizawa 1993] is used for the SGS stress tensor. The combustion is treated by the Eddy Dissipation Concept (EDC) model [Parente 2016] with detailed hydrogen-air chemistry [Ó Conaire 2004]. According to the experiment measurement of hydrogen combustion in PRESLHY, the total pressure is 20 MPa and total temperature is 80 K for the hydrogen reservoir. The notional nozzle approach [Keenan 2017] is used to bypass the under-expanded near field region and provide the velocity and temperature conditions for the hydrogen jet after expanding to the ambient pressure at a notional nozzle diameter. In the experiments, the release was a dynamic blow down process with continuous decrease of the reservoir pressure. The simulation of this process has been developed by NCSRD. In the quoted simulations here, the measured temperature, pressure velocity and calculated notional nozzle diameter were used to provide the transient inlet boundary conditions through the so-called timeVaryingMappedFixedValue method in OpenFOAM.

Figure 3-54 illustrates the initial development of hydrogen jet. Following fast penetration from time 1 ms to 3 ms, the jet tip propagates more slowly due to shearing and momentum exchange with the surrounding ambient air.

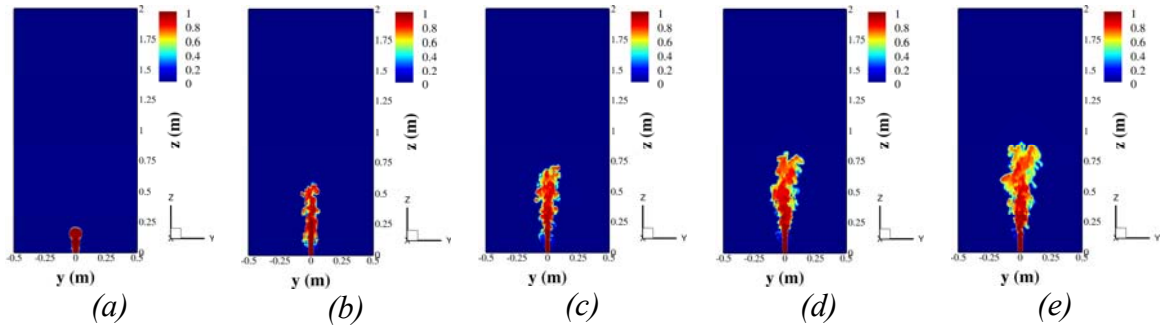

Figure 3-54. Instantaneous distributions of hydrogen mole fraction of hydrogen jet from time 1 ms to 9 ms shown in time intervals of 2 ms.

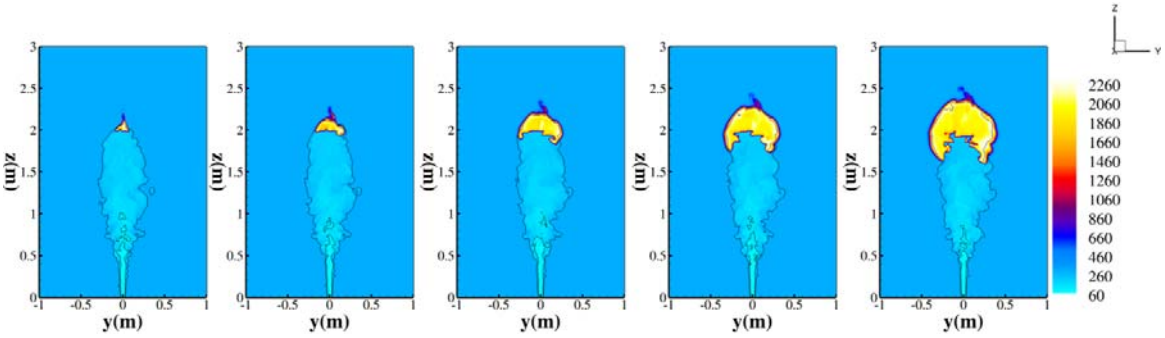

Figure 3-55. Instantaneous distributions of temperature (K) at y-z plane. Black iso-lines refer to the hydrogen explosion limit with the hydrogen mole fraction (0.04, 0.756).

Figure 3-55 shows the instantaneous distributions of temperature of the ignited hydrogen jet. The ignition source with temperature of 2000 K is set at the streamwise location z = 2.0 m from the time 0 s. It is found that the initial flame kernel propagates quickly around the jet tip to envelop the jet within the explosion limit of hydrogen.

Using the same modeling approach, numerical simulations are also being conducted for the delayed release scenarios which resulted in deflagrations. The results will be provided in a later release of the handbook.

3.3.3 Liquid Pool Burning

3.3.3.1 Phenomenology

Regarding open burning pools of flammable liquids, the essential parameters are the burning rate and the temperature or heat flux distribution. For a burning gas cloud above a ground pool or tank, heat transport from the burning cloud to the pool is given by conduction, convection, and radiation enhancing the vaporization rate and the pool regression rate, respectively. The fire of a burning vapor cloud may also be able to travel back to the spill point and continue to burn as a pool fire. Hazards associated with pool fires are strongly depending on pool size and shape, burning rate, flame geometry, and heat radiation.

Two regimes for the regression rate have been identified depending on the pool dimension [Zabetakis 1967]. For small diameters (D < 0.2 m), heat transport by conduction is dominant, and the regression rate decreases with increasing radius (Fig. 3-56).

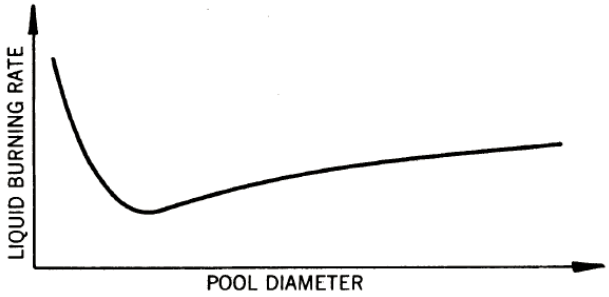

Figure 3-56. Qualitative liquid burning rate dependence on pool diameter [Zabetakis 1967].

Liquid hydrogen pool fires were observed to be dynamic and non-homogeneous with a highly intermittent pulsing structure of the flame. This cyclic changing of flame height is mainly due to the turbulent mixing of air and subsequent combustion and has an influence on the flame temperature. The height of the flame indicates the radiation hazard imposed by the fire, since it directly relates to the heat transfer from the flame into the surroundings. Usually the flame height is defined as the height at which flame is present at least 50% of the time.

Effects of wind on the flame length are complex. For smaller pools, enhanced ventilation may improve air entrainment and thus allows for a more efficient combustion. Wind tilts the flame expanding the flame base area and also changing the distribution of radiant heat flux distribution. This influence may even enhance the regression rate. For larger pools, measurements indicate enhanced burning rates. There is, however, a slight decrease for very large pools (D > 5–10 m) which could be explained by having several separate burning cells rather than one big pool fire [Babrauskas 1983, Rew 1995].

Another observation from LNG pool fires is that burning rates and flame heights of pools on water are by a factor of 2 higher than those of pools on solid ground [Luketa-Hanlin 2006]. This is explained by the higher heat transfer from the water into the pool due to the rapid interaction with the water and fragmentation of the pool increasing the heat transfer area. This effect tends to produce smaller pool diameters, but taller flames. The total radiation area is reduced, since a larger fraction of the vapor produced may escape unburnt from the plume.

3.3.3.2 Experimental Work

Bureau of Mines (1960)

As part of a research program on liquid hydrogen conducted by the Bureau of Mines, U.S. DOI, during the period January 1958 to December 1959, burning rates on LH_2 pools were measured and compared with those of other liquid fuels to examine the feedback by radiation heat onto the pool [Zabetakis 1960]. After a short phase of “burning-in”, the temperature at the liquid surface reaches the boiling point and the burning proceeds in a steady state. For LH_2, the burning-in phase is extremely short, as the dominant heat source, which is the ground, keeps the liquid’s temperature at the boiling point. Figure 3-57 shows a comparison of the burning rates at steady state between liquid hydrogen and liquid natural gas, which were measured in a 150 mm diameter dewar.

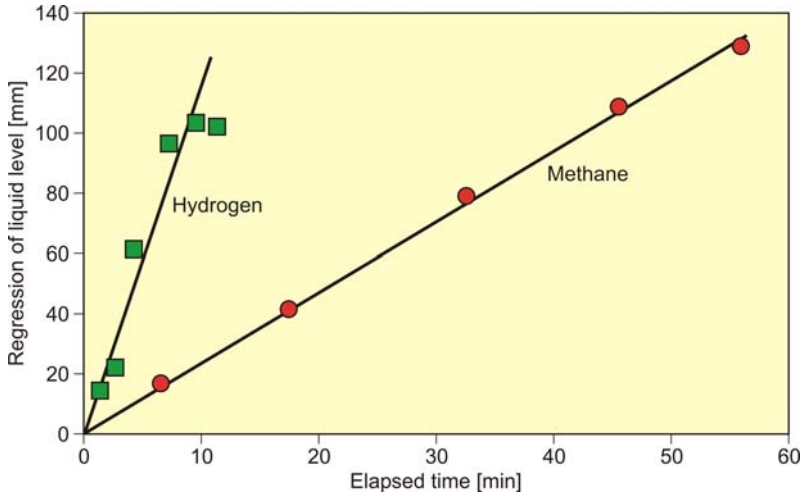

Figure 3-57. Steady-state burning rate comparison between LH_2 and LCH_4 [Zabetakis 1960].

For the LH_2 spill and ignition tests, with quantities of 54-90 ℓ given onto a steel plate or loose gravel, the overpressures were measured at a distance of ~50 m. The results shown in Fig. 3-58 as a function of the ignition time after spillage are given in decibel, dB, (scale on the left-hand ordinate) and in Pa (right-hand ordinate). The blast pressures produced were relatively small and were depending on the time delay for ignition [Zabetakis 1960]. They were found to increase with delay time, until after more than 5–6 s of delay, they were decreasing again as soon as the H_2 concentration in the rising and diffusing vapor clouds became smaller.

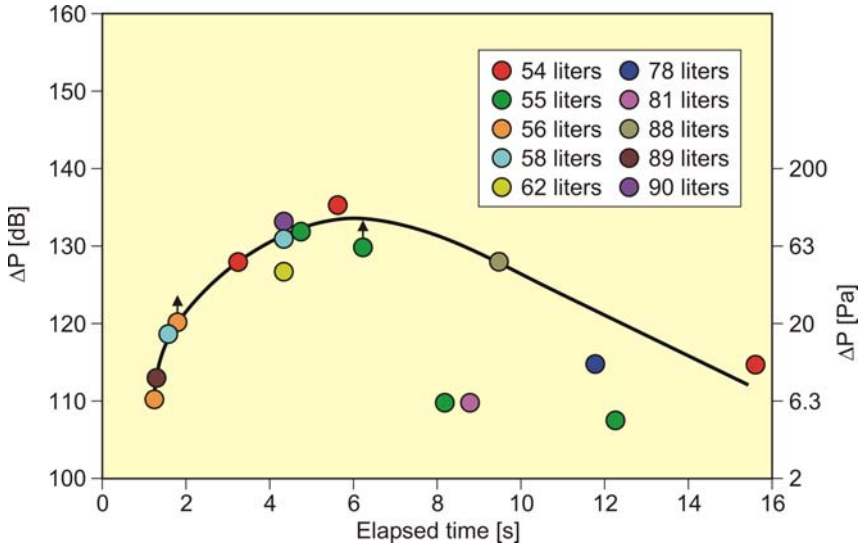

Figure 3-58. Overpressures measured at 49 m distance after ignition of vapor cloud above LH_2 pools vs. time of ignition after spillage [Zabetakis 1960].

Health and Safety Laboratory

Fourteen ignition tests were performed in total (Fig. 3-59), of which four were non-ignitions. The reason for the non-ignitions is not clear; it may be that the gas cloud was under or over-rich in hydrogen at the point that the igniters were fired due to differing dispersion and wind effects, or a quenching effect was created by the water vapor created by the cold hydrogen cloud.

Figure 3-59. Ignition of the LH_2 vapor cloud during low wind conditions (no secondary explosion).

During the test program the ignition delay was varied between ~60 and ~320 s. The longer tests allowed for a larger build-up of flammable cloud and also reproduced the liquid/ solid pooling phenomena first seen during unignited releases of LH_2 [Hall 2014]. The extent of the flammable cloud appeared to be congruent with the visible extent of the water vapor cloud created by the very cold hydrogen cloud when IR footage was compared with visible footage. The flame speeds were measured for each test from the high-speed video and found to develop from 25 m/s up to 50 m/s with increasing release duration.

On one occasion, as the cloud was ignited, it burnt back to source creating a jet fire and then a secondary explosion appeared to emanate from the liquid/solid pool location. The separate phases of the burning cloud are highlighted in the radiometer plot from the test, shown in Fig. 3-60. The first peak on the plot represents the initial deflagration of the cloud back to the release point or "burn-back"; the second, larger peak represents the secondary explosion and the longer radiative phase after represents the resulting jet fire. The varying plot levels correspond to the six radiometers located at increasing distances from the release point.

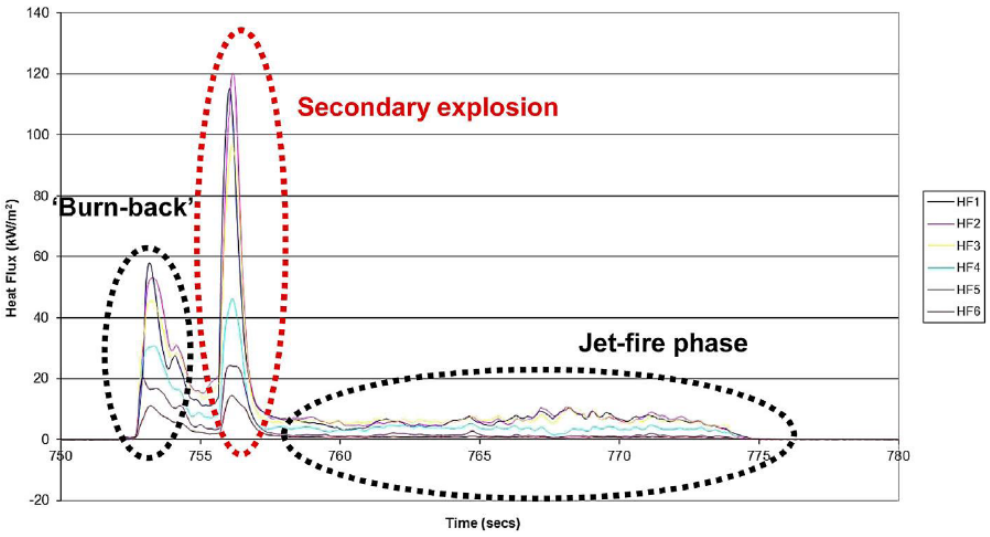

Figure 3-60. Radiometer readings from ignited release exhibiting a secondary explosion.

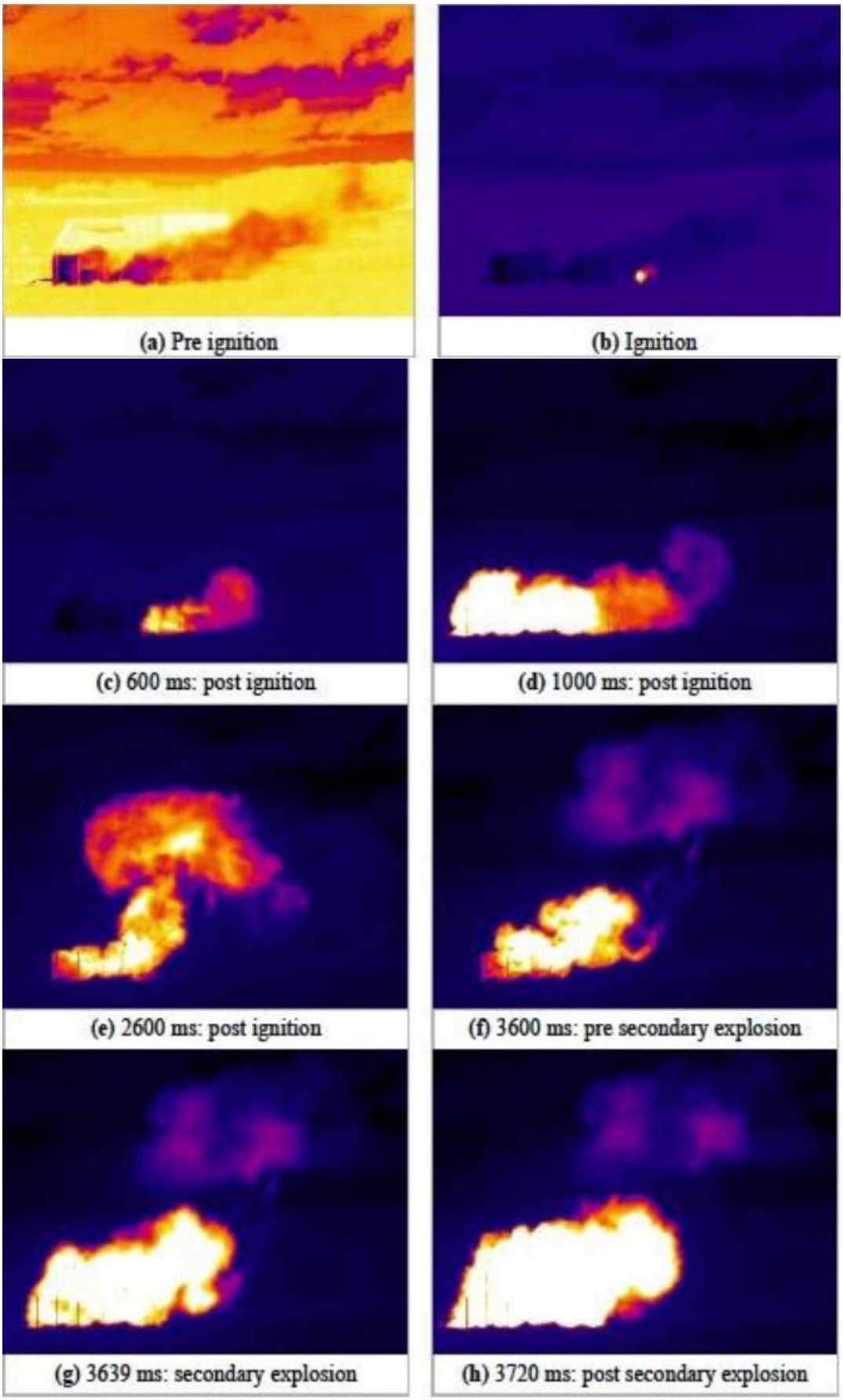

Figure 3-61. IR video stills of Test 6 including secondary explosion.

In Test 6, ignition occurred from igniter no. 3 and propagated back through the horizontal cloud towards the release point. The flame front accelerated up to speeds of 50 m/s and began to lift upwards once momentum was lost. A jet of flame continued to burn from the release point after the vapor cloud had been consumed as in the previous test. However, approximately 3.6 s after the initial cloud ignition, a secondary explosion occurred emanating from the liquid/solid pool location (Fig. 3-61, images f–h). This secondary explosion created an 8 m diameter hemispherical fireball around the solid/liquid pool location and created a noise level audible from over a mile away. Following the secondary explosion seen in Test 6, further tests were performed to try to replicate this phenomenon. However, the meteorological conditions during other tests were different from Test 6 and no secondary explosion could be replicated.

The experimental evidence of the past 50 years or so [Cassut 1960, ADL 1960, Zabetakis 1960, Zabetakis 1961, Witcofski 1984, Urano 1986, Verfondern 1997] illustrates that even very large spills of LH_2 do not create lasting hazardous situations that are typical to hydrocarbons spills. The thermal load generated by an LH_2 pool fire is about 3–3.5 times lower than that of equal-size hydrocarbon pools.

There is no propensity to detonation either in the open environment. The most hazardous phenomenon develops when solidified air is becoming enriched with oxygen and then gets into contact with a burning (otherwise relatively mildly) hydrogen plume or jet. From this perspective, a secondary explosion induced by solid oxygen-enriched air (as was registered by HSL in their test 6) appears to be a more hazardous event than a BLEVE (considering a LH_2 spill and a BLEVE occur on an equal size tanker).

A BLEVE that would result in a tank failure and instantaneous spill of all LH_2 inventory, will, of course, freeze surrounding air. But, since the amount of LH_2 will be dominant (vs a spill that develops gradually), this solid air will not have time to get enriched with oxygen and, since it is heavier than LH_2, it will be covered by the vaporizing liquid. We know from the NASA and AD Little experiments that whether the liquid is ignited or not, it does not affect LH_2 pool evaporation or its regression rate. As was shown by Urano [Urano 1986], the only real accelerant is the contact with solid air enriched with oxygen. But since under BLEVE condition it is covered by the liquid hydrogen, it is not involved in the combustion until most of the liquid has vaporized and risen to the atmosphere. Hence, solidified air would only affect a relatively small quantity of hydrogen and since it is not oxygen-enriched, an “explosion” (which would be a fast deflagration) is unlikely as was shown by the HSL experiments.

The unignited HSL test performed at 86 cm above ground demonstrated that it does not result in solidification of air. It is possible that some sort of air “rain” or droplets might be present in the jet. However, due to moisture content in the air that condenses together with air in the cold hydrogen plume, the potential for oxygen enriched air is significantly reduced, if not completely eliminated. In this case, a secondary explosion would not be possible. However, because the hydrogen plume is high enough above the ground and thus free from friction, it may travel farther than the vaporizing cloud from the LH_2 pool. Hence, this scenario presents a new condition worth analyzing separately.

Finally, the recent analysis of unignited experiments by HSL has shown that the gas-liquid slurry coming out of release orifice is a two-phase fluid even before it reaches the orifice. Calculations suggested that the gaseous component at the exit is 96% by volume and 31% by mass, respectively. This indicates that analyzing (cold) hydrogen gas leaks is as relevant as analyzing liquid leaks.

3.3.4 Deflagration of Cold Hydrogen-Air Mixtures

Within the flammability limits, three flame propagation regimes can be distinguished for gaseous mixtures:

- slow subsonic deflagrations ($v < c_r$ - flame velocity v is less than the speed of sound in reactants cr);
- fast supersonic flame ($c_r < v < c_p$ - flame velocity is less than the speed of sound in products c_p, but more than the speed of sound in reactants);
- detonation ($v = D_{CJ}$ Chapman-Jouguet velocity).

All possible regimes and characteristic pressure profiles are shown in Fig. 3-62 for hydrogen-air mixtures at initial pressure of 0.1 MPa. It was suggested in [Dorofeev 2000 and Dorofeev 2001], that critical expansion rate σ* and 7 λ - criteria can be used as potentials for strong flame acceleration and detonation onset, respectively. Mixtures with the expansion rate σ above the critical value σ* can effectively accelerate to the speed of sound and then detonate, if the detonation criteria $L > 7\lambda$ is satisfied (L is the characteristic size of the combustible domain; λ is the detonation cell size). The mixtures with $\sigma < \sigma^*$ cannot accelerate to the speed of sound and only subsonic combustion regimes may occur. Characteristic combustion pressure depends on flame propagation velocity and can be changed from 0.1–0.2 MPa for slow combustion, to 0.6–0.8 MPa for sonic deflagration and 2–4 MPa for detonation at initial pressure 0.1 MPa (Fig. 3-62).

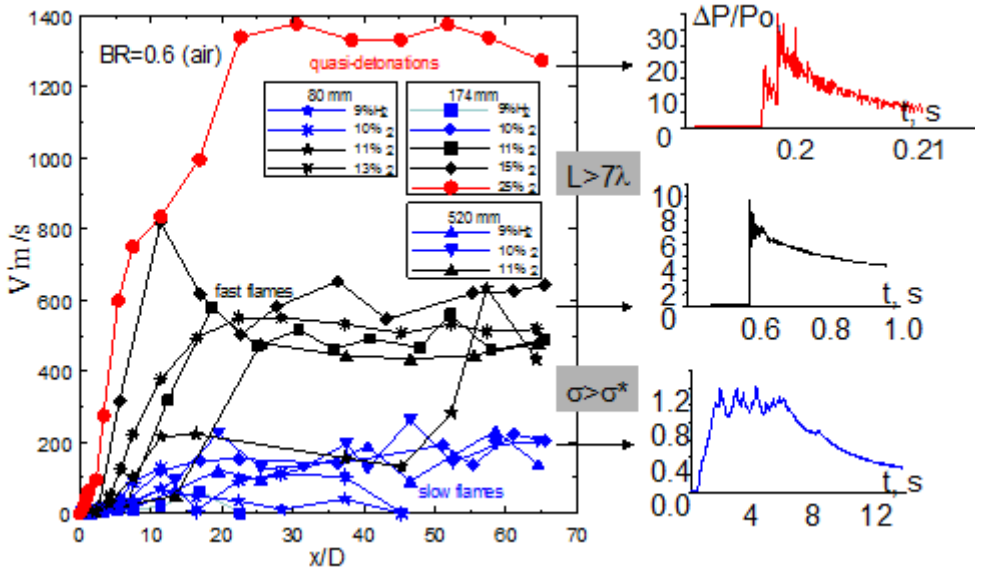

Figure 3-62. Combustion regimes for different hydrogen-air mixtures (P = 0.1 MPa, T = 293K): right pictures correspond to pressure signals for different regimes [Dorofeev 2000, Dorofeev 2001].

The critical expansion ratio σ* is a function of dimensionless integral scale as Peclet number $Pe = L_T/\delta$ (L_T – turbulent length scale, δ – laminar flame thickness) and Zeldovich number β ($\beta = E_a(T_b-T_u)/T_b^2$). The critical Peclet number $Pe > 100$ was experimentally found to be required for the strong flame acceleration and to exclude a local flame extinction due to heat losses. The Peclet number lower than 40 may even

result in local extinction. The critical expansion ratio σ* decreases with initial temperature T_u increase and overall energy activation E_a decrease. Since adiabatic combustion temperature T_b is almost independent of the initial temperature T_u, the critical expansion ratio is only a function of the energy activation and temperature [Dorofeev 2001]:

$$\sigma^* = 9.0 \cdot 10^{-6} x^3 - 0.0019 x^2 + 0.1807 x + .2314$$

where $x = E_a/RT_u$. Assuming a constant activation energy E_a = 7500 K for hydrogen-air mixtures in wide range of temperatures and concentrations, an extrapolation to cryogenic temperatures gives the values of the critical expansion ratio σ* = 6.9 at T = 100 K, which roughly corresponds to 7–8% H_2 in air. The assumption about the constant activation energy in wide range of temperatures and concentrations is very strong and may lead to over-conservative results by shifting the critical concentration to leaner hydrogen-air mixtures that requires stronger measures to the hydrogen safety.

Figure 3-63 shows an extrapolation of critical expansion ratio to cryogenic temperatures without an effect of the energy activation. Far extrapolation to low temperatures gives the values of critical expansion ratio σ* and critical hydrogen concentration leading to an effective flame acceleration to the speed of sound at different initial temperatures: σ* = 8.5 (9.6% H_2) at 100 K.

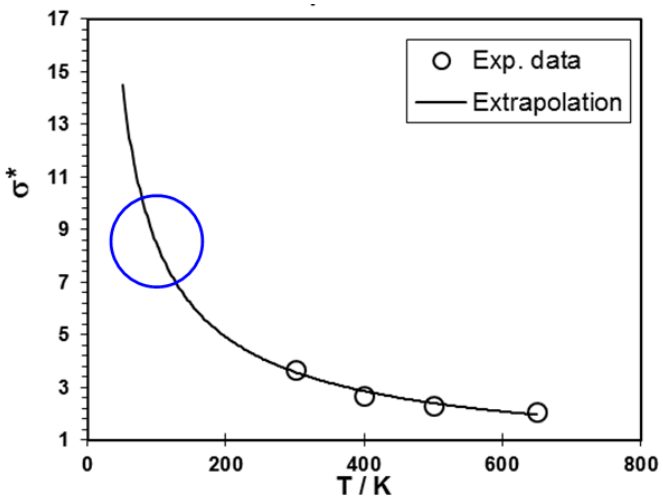

Figure 3-63. Critical expansion ratio σ versus initial temperature T_u for hydrogen-air mixtures.*
The critical points at elevated temperatures are taken from [Dorofeev 2001].

Such far extrapolation to cryogenic temperatures may lead to erroneous prediction of the critical expansion ratio for safety assessment and thus strongly needs experimental validation.

Karlsruhe Institute of Technology (2019)

A series of more than 100 experiments with hydrogen-air mixtures (8–60% H_2) at cryogenic temperatures 80–130 K have been performed in a shock tube in the frame of the PRESLHY project. The facility consists of a stainless steel tube 5 m long with an outer diameter of 73 mm and an inner diameter D = 54 mm. The tube might be equipped with three different blockage ratios BR = 0, 0.3, 0.6 (where $BR = 1 - d^2/D^2$). To provide the cryogenic temperature, the tube was exposed in a metal basin filled with liquid

nitrogen LN_2 at 77 K (Fig. 3-64). A basin made of stainless steel was insulated with Styrofoam to keep the temperature constant along the tube with an accuracy ± (2–3) K.

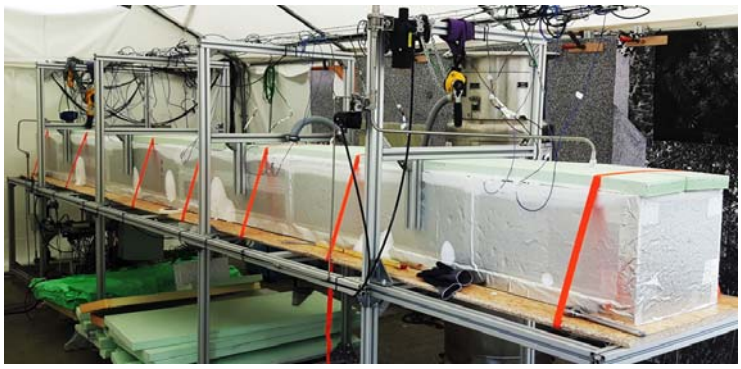

Figure 3-64. Cryo-shock tube inside a bath of LN_2 with supporting aluminum frame.

Pressure sensors and InGaAs-photodiodes along the tube have been mounted with a step of about 0.5 m to monitor the flame and shock propagation velocity of the process. The experiments at ambient pressure and temperature were conducted as the reference data for cryogenic experiments. A critical expansion ratio for an effective flame acceleration to the speed of sound was experimentally found at cryogenic temperatures.

Figure 3-65 distinguishes the critical expansion ratio σ* = 12.5 for hydrogen-air mixtures at cryogenic temperature 100 K. It corresponds to hydrogen concentrations above 16% H_2 at which the characteristic flame velocity is above the speed of sound in reactants c_r (blue dotted line in Figure 3-65, right) and characteristic combustion pressure is above the adiabatic combustion pressure ΔP_{icc} (red dotted line in Figure 3-65, left). Similar to reference warm tests, for high reactive mixtures, the velocity establishes at the level of the speed of sound in combustion products c_p typical to chocked flames in congested areas when the detonation transition is suppressed due too small orifice diameter, less than the detonation size. The same flame acceleration threshold σ* = 12.5 was found for BR = 0.6 with the difference that in this case the critical detonation cell size is three times smaller.

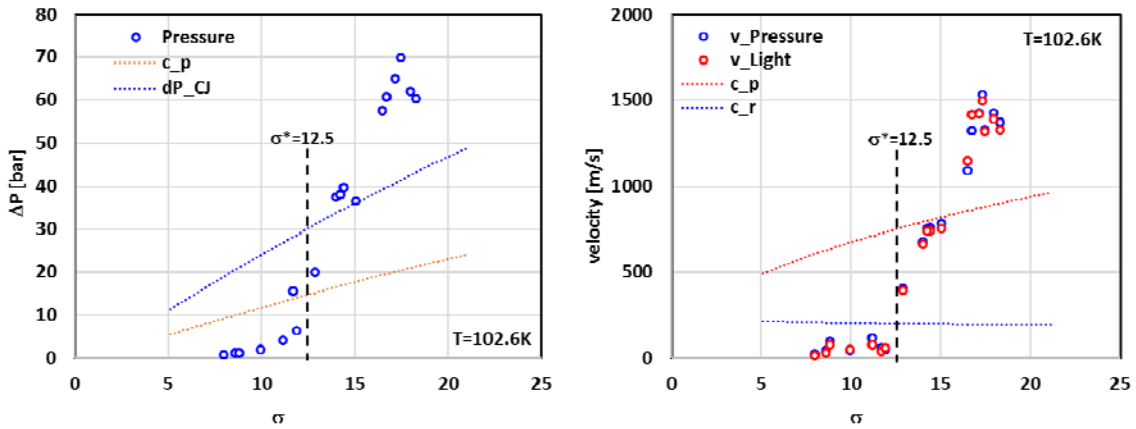

Figure 3-65. Experimental characteristic pressure (left) and flame velocity (right) as function of expansion ratio in obstructed tube (BR=0.3) at cryogenic temperature (T=102.6 K): black dashed line is a cut-off line at σ=12.5.*

All experimental data at cryogenic temperatures 90–130 K performed within PRESLHY combustion campaign were summarized in Figure 3-66 with an extension to elevated temperature T = 650 K from the paper [Dorofeev 2000], so that it covers the temperature range from cryogenic temperature T = 90 K to elevated temperature T = 650 K. Open

points show current experimental data on expansion ratios at different temperatures. With a good accuracy the border line between slow (M < 1) and fast sonic deflagration (M > 1) can be approximated by exponential dependence on initial temperature T[K]:

$$\sigma^* = 2200 \cdot T^{-1.12}$$

or in terms of critical hydrogen concentration:

$$[H_2]^* = 4.817 \times 10^{-5} \cdot T^2 - 0.044 \cdot T + 19.96$$

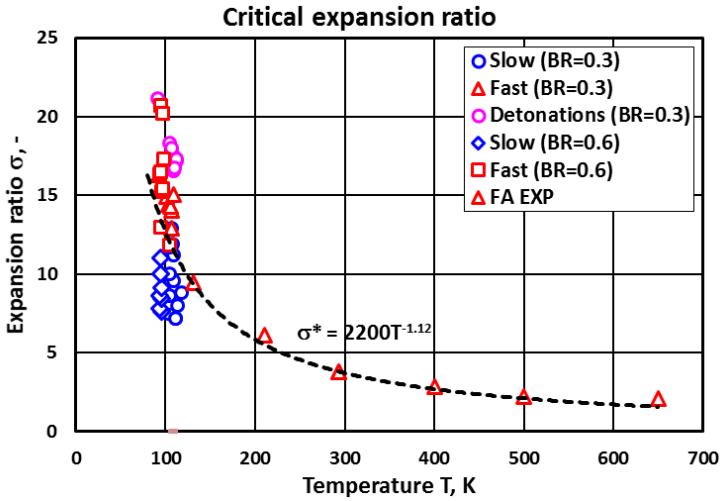

Figure 3-66. Critical expansion ratio as function of initial temperature based on experiments in obstructed tubes (BR=0.3–0.6): black dashed line is the border between slow and fast flames.

The cut-off line for fast and slow deflagration described by experimental approximation is very close to hyperbolic dependence on initial temperature. It can be transformed in a simplified form

$$\sigma^*(T) = \sigma^*(T_0) \cdot \left(\frac{T_0}{T} \right)$$

where $\sigma^*(T_0) = 3.75$ at ambient temperature $T_0 = 293$ K. Then, for T = 100 K, we get more conservative value of $\sigma^*(T) = 11.0$ instead of $\sigma^*(T) = 12.6$ according to exact experimental approximation. It gives more conservative value of critical hydrogen concentration with valuable accuracy compared to the experiments.

Health and Safety Executive (2010)

HSE carried out an extensive experimental campaign to assess the effect of congestion or confinement on an ignited hydrogen cloud stemming from a release of LH_2, potentially leading to deflagration to detonation transition (DDT). Experimental measurements included overpressure, heat flux, and noise levels. A total of 23 ignited trials were conducted on LH_2 releases from a tanker with pressure of 1 or 5 barg and through nozzle diameters equal to 6 mm, 12 mm and 25.4 mm.

The congestion and confinement was created by a configurable steel structure placed directly in the path of the release. Results showed that the increase in volumetric

congestion increases the measured overpressures in releases with the same initial conditions. In case of densely congested area with a volume blockage ratio and volume larger than 4% and 15 m^3, respectively, it could be reasonable to assume that a high level explosion or DDT may occur. The results also showed that an increasing hydrogen inventory, either through an increased release pressure or larger nozzle, can result in a larger event upon ignition. It was observed that the ambient conditions, in particular the wind speed and direction, were a significant factor in the outcome of each ignition (Fig. 3-67).

Figure 3-67. Pictures showing sudden gust immediately prior to ignition for test with release P=1barg, d=12mm, and wind velocity=2m/s.

3.3.5 Detonation of Cold Hydrogen-Air Mixtures

The interaction between flame of cold hydrogen/air mixtures and obstacles such as pipe racks, vaporizers, etc. may lead to flame accelerations and to deflagration to detonation transitions (DDT). There is yet a lack of knowledge regarding flame acceleration and DDT at cryogenic temperatures.

The detonation may only occur if the flame is able to reach the speed of sound. For an obstruct channel, the characteristic geometrical size of the system, L, should be larger than 7 detonation sizes, λ, i.e. the critical condition $L > 7\times\lambda$ should be satisfied (see previous Fig. 3-62).

There is a lack of experimental data on detonation cell size at cryogenic and reduced (lower than normal) temperatures in mixtures containing H_2. To the author knowledge, only one study is available in literature which presents data on detonation cell size for H_2-O_2 mixtures at 123 K and different initial pressures [Zitoun 1995], see Table 3-2.

Table 3-2. Detonation cell sizes for stoichiometric H_2-O_2 mixtures at reduced temperatures.

Temperature T (K)	Pressure p (bar)	Detonation cell width, λ (mm)
123	0.4918	1.4819
123	0.6953	0.9901
123	0.9827	0.6889

Experimental data on hydrogen air mixtures with temperature range 278–373 K and Φ = 0.5 showed that, in this temperature range, detonation cell size increases with the decrease of temperature [Tieszen 1987]. These experimental results were well reproduced by the code CELL_H2 [Gavrikov 2000] to assess the detonation cell (Fig. 3-68). However, the code has an applicability limit to 200 K and at this temperature limit the code significantly underestimates extrapolations based on experimental data by [Zitoun 1995] (Fig. 3-69).

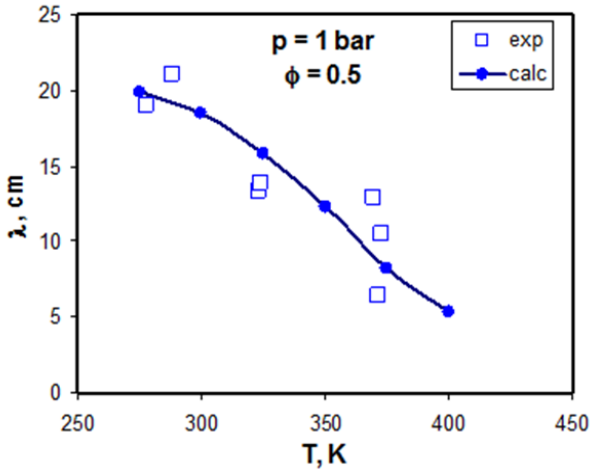

Figure 3-68. Comparison of calculated and experimental detonation cell size data for H_2-air mixtures at different temperatures (p = 0.1 MPa).

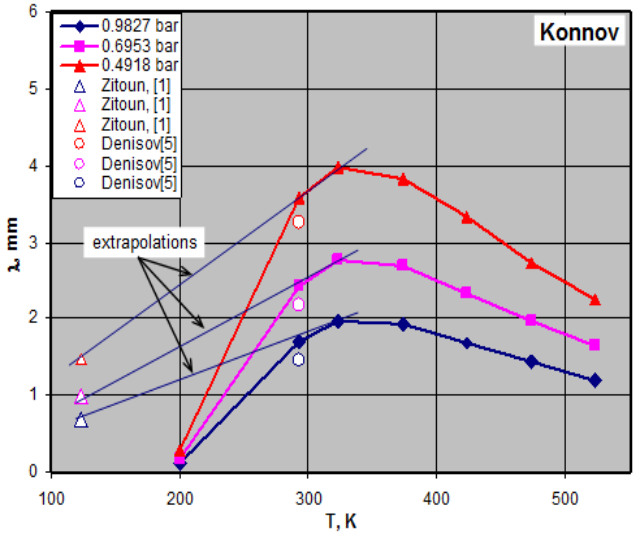

Figure 3-69. Comparison of calculated and experimental detonation cell size data for H_2-O_2 mixtures at different temperatures and pressures.

The confidence of the proposed extrapolation and CELL_H2 code at cryogenic temperatures is very low. With the lack of experimental data on detonation cell sizes for hydrogen-air mixtures at cryogenic temperatures, the PRESLHY project is dedicated to close this knowledge gap with additional experiments on detonation cell size evaluation.

Arthur D. Little (1960)

In a number of open LH_2 spill tests conducted, the vaporized gases were ignited by spark or flame sources. Instrumentation was provided to measure overpressures in the event of a detonation. In no case, however, a detonation or even the tendency towards a detonation was observed. Also at the presence of solidified air in the liquid hydrogen (by adding liquid air into the LH_2 vessel), the risk was only small that the explosions obtained result in a detonation. Detonations could only be achieved under the conditions of the presence of pure oxygen or at least air with a considerable oxygen enrichment the existence of stable spherical detonation waves in experiments, or by the employment of shock-wave initiators [Cassut 1960].

Karlsruhe Institute of Technology (2019)

The same facility shown in Fig. 3-64 was used for cryogenic detonation. Within the previous series of PRESLHY experiments on flame propagation regimes for cryogenic hydrogen-air mixtures in a shock tube, the border line between ‘detonation’ and ‘no detonation’ regimes was distinguished. Figure 3-70 shows an example of so-called distance-time diagram for DDT process of cryogenic hydrogen-air mixture in a smooth tube without obstructions. The blue line corresponds to the flame trajectory versus time in ms. It is seen that the flame initially accelerates until the DDT point (a star) at 2.5 m from the ignition. Afterwards, a straight line with a constant slope corresponds to detonation velocity of D = 2200 m/s which is quite close to theoretical Chapman-Jouguet detonation velocity D_{CJ} = 2144 m/s. Similar pictures were taken for all tube geometries with blockage ratios BR = 0, 0.3, 0.6.

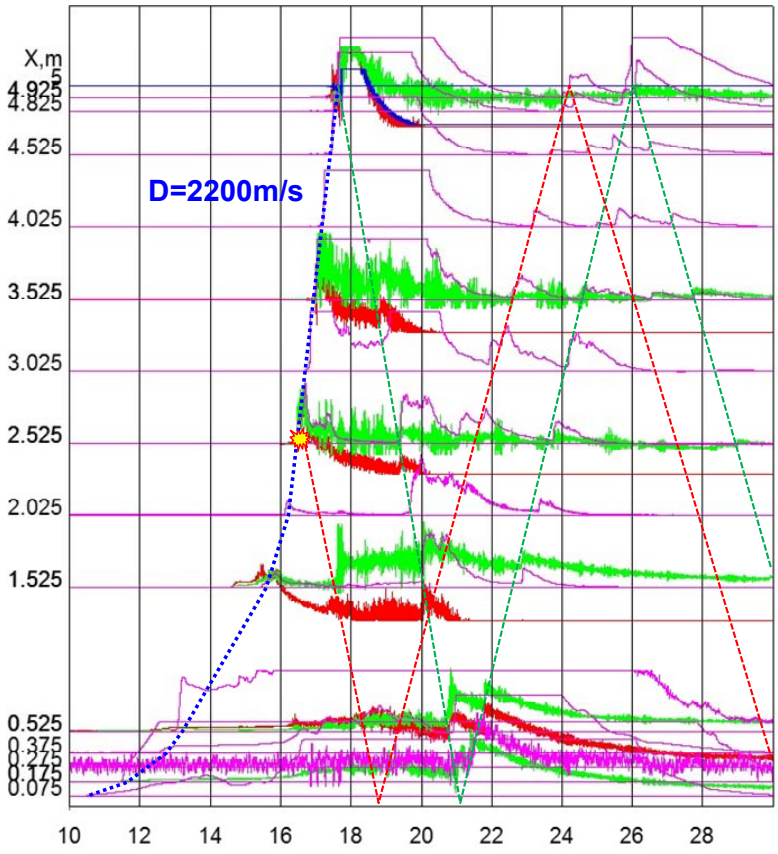

Figure 3-70. Distance-time diagram for detonation transition in 45% H_2 (T=106 K): flame trajectory (blue dotted line); shock wave trajectory (red and green dashed lines); light signal (pink solid line); pressure signal (red and green solid lines); the star is DDT point.

The detonation cell sizes in current project have not been directly measured using sooted plates. LN_2 surrounded the shock tube does not allow to open the flanges to install the sooted plates. The detonation cell sizes were derived on the base of existing detonability criteria for smooth and obstructed channels:

$d > \lambda/\pi$ for detonation propagation in a smooth tube (BR = 0)

$X_D < 500 \cdot \lambda$ for run-up-distance XD in a smooth tube (BR = 0)

$d > \lambda$ for detonation propagation in an obstructed tube (BR = 0.3)

$d > 3 \cdot \lambda$ for detonation propagation in an obstructed tube (BR = 0.6)

All the criteria for detonation onset are based on experimental papers [Teodorczyk 1988, Dorofeev 2000, Kuznetsov 2000, 2005] and have been checked at ambient temperature with known detonation cell sizes. Then the criteria were applied to cryogenic temperatures for detonation cell size evaluation (Fig. 3-71). The data are shown as a comparison of detonation cell sizes at cryogenic and ambient temperatures. There is some difference in detonation cell sizes at cryogenic and ambient temperature but much less than expected in our predictions (see Fig. 3-68). For rich mixtures, the detonation cell sizes at cryogenic temperature are even smaller than at ambient conditions. The data for detonation cell sizes at 100 K can be approximated as a polynomial dependence against hydrogen concentration [% H_2]:

$$\lambda = 0.0006724[H_2]^4 - 0.1039[H_2]^3 + 6.0786[H_2]^2 - 159.74[H_2] + 1603.3$$

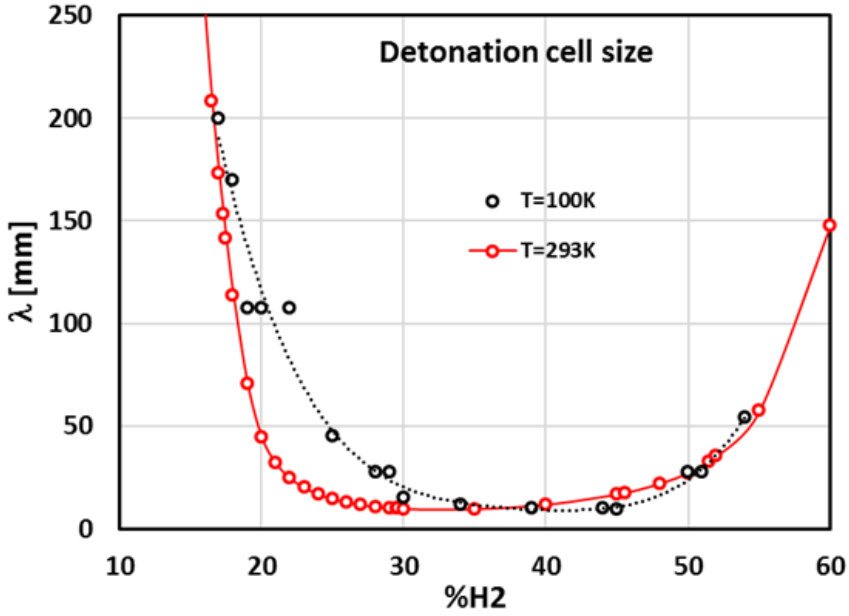

Figure 3-71. Experimental detonation cell size at cryogenic temperature T=100 K in comparison with the data at ambient temperature T=293 K.

With known detonation cell sizes the detonability of hydrogen-air mixture at cryogenic temperature of about 100 K can be assessed for a channel or multi-room geometry using known criteria as given in above equations. The main peculiarity of cryogenic combustion with respect to the safety assessment was that the maximum combustion pressure was several times higher compared to that at ambient temperature. For instance, it was shown that the maximum combustion pressure at the temperature T = 100 K is about 2 times higher than at ambient temperature (Fig. 3-72). It is of practical interest that the dependence of maximum combustion pressure vs. characteristic flame velocity is linear. Other peculiarities of cryogenic combustion compared to that at ambient conditions were that the run-up distance to detonation was almost two times shorter for the same hydrogen concentration and also a very quick flame acceleration to the speed of sound in a smooth channel with the following flame propagation until end of the tube with the speed of sound in combustion products (Fig. 3-73). This means that the explosivity and a danger of cryogenic mixtures with the same hydrogen concentration is much stronger than that at ambient temperature.

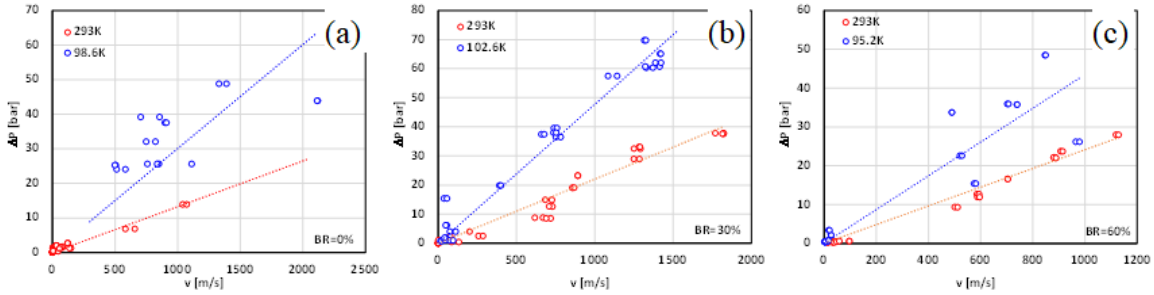

Figure 3-72. Maximum combustion pressure as function of characteristic flame velocity in obstructed and smooth tube: (a) BR=0; (b) BR=0.3; (c) BR=0.6.

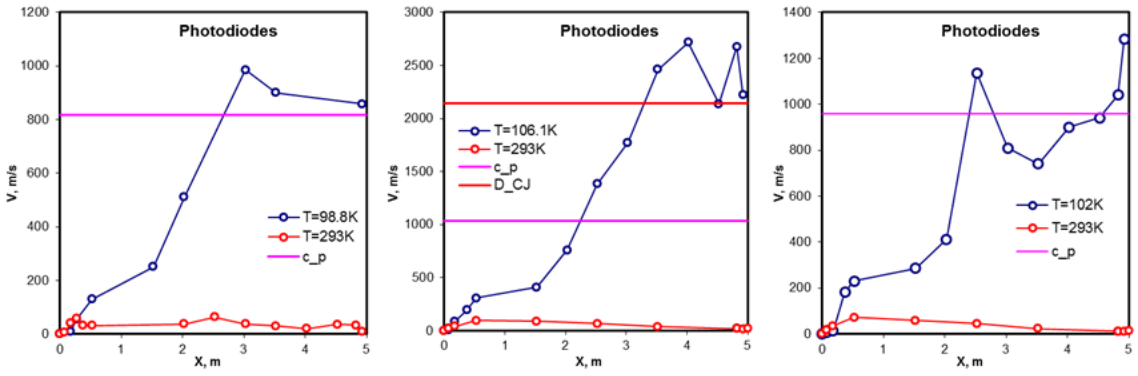

Figure 3-73. Comparison of flame velocity in smooth tube (BR=0) at cryogenic and ambient temperatures: c_p is the speed of sound in combustion products; D_CJ is the detonation velocity: 20% H_2-air (left); 45% H_2-air (center), 50% H_2-air (right).

3.3.6 BLEVE

Boiling Liquid Expanding Vapor Explosion (BLEVE) is a physical explosion associated with the catastrophic failure of a pressure vessel containing a liquefied gas at temperature above its boiling point at atmospheric pressure. The originating blast wave, fireball and tank projectiles can pose a serious risk to people or facilities in the accident surroundings. Many experimental and analytical studies on BLEVEs are available for substances, such as butane, propane, LNG, etc., e.g. [Hardee 1973]. Fewer studies have been conducted on eventuality and consequences of an LH_2 BLEVE. A study [Zabetakis 1960] attempted to define a correlation to evaluate the flame volume produced by the ignition of the hydrogen-air mixture created from spillages of liquid hydrogen in the range 2.8 ℓ –89 ℓ. The flame volume was found to be proportional to the liquid hydrogen volume (ℓ) by a coefficient of 750. The authors published a correlation to define the height and width of a fireball as function of the mass m_{LH2} of liquid hydrogen:

$$H_{max} = W_{max} = 8.056 \sqrt{m_{LH_2}}$$

An updated correlation for fireball size based on work by [Zabetakis 1960] to best-fit experiments and calculate hazard distances for the scenario of liquid hydrogen storage tank rupture in a fire in the open atmosphere was suggested [Makarov 2021]. Analytical and theoretical models were proposed in [Ustolin 2020a, Ustolin 2020b] to assess the consequences from BLEVE in terms of pressure and thermal hazards.

A series of experiments was conducted in 1996 investigating the potential hazards from rupture of LH_2 tanks [Pehr 1996]. Experimental tests employed a single wall tank with a volume of 120 ℓ. Totally ten tests were performed. Hydrogen mass was included in the range of 1.8–5.4 kg. Maximum pressure in the tank was 1.13 MPa. Tanks were ruptured by using a cutting charge along the tank circumference. Duration of the charge was about 2 ms and was deemed to not significantly contribute to the explosion. The patterns of the blast wave pressure dynamics varied from test to test depending on how the following different contributions verified in rapid succession or aggregately:

- Explosion of the cutting charge;
- Spontaneous vaporization of the liquid fraction after tank rupture and sudden expansion of gaseous hydrogen in the tank;

- Acceleration of flames and expansion of combustion products from the burning hydrogen/air mixtures.

A maximum overpressure of approximately 50 kPa was measured at 3 m distance from the tank. The maximum fireball diameter was between 6 and 15 m depending on the tank pressure. The maximum height achieved by the fireball varied between 16 and 20 m above the ground prior to extinction, which happened after about 4 s.

4 Safety Measures and Engineering Solutions

Hydrogen transportation and distribution pose specific issues in terms of safety. The issues are strongly related to the chemical and physical properties of hydrogen: its ability to embrittle materials, its ease in escaping from containment, its wide flammability range, and the limited amount of energy needed to ignite it, all represent barriers to safe use. At the same time, its extremely low density is a guarantee that the gas will likely ascend instead of forming dense dangerous clouds as other hazardous gases do.

A major problem when producing and handling liquid hydrogen is the potential contamination of the hydrogen with air or other impurities which will, with the exception of helium, freeze and might block then pipes, filters or armatures.

On the exterior of poorly insulated containers or pipes the cryogenic temperatures may condense air with serious enrichment of oxygen. Liquefied or frozen solid oxygen promotes ignition and oxidizes easily materials which are usually non flammable.

The extreme low temperatures require careful selection of materials. Conventional carbon steels will suffer from a transition to nil ductility (NDTT). Aluminum or stainless steels are typically suitable structural materials for cryogenic hydrogen and welded connections are preferred to screwed connections. If, however, cryogenic hydrogen is leaking, it might lead also to condensation of air and to hazardous oxygen enrichment. The leaking cryogenic hydrogen is as heavy as ambient air. This suppresses buoyancy effects and promotes dispersion of flammable mixtures on ground level.

Countermeasures are careful purity control of the feed hydrogen and purging the cold boxes with helium. Leaks may be detected by temperature drop and visually identified via the fog formed from condensation of ambient humidity.

Safety considerations are related to the separation of the LH_2 containing facilities from roads, buildings, or runways, the ventilation for enclosed areas, the preclusion of air ingress, automated system shutdowns, confinement and control of large-scale spills, or the use of non-sparking electric devices. Particularly numerous LH_2 refueling processes increase the possibility of a potential accumulation of impurities, solid N_2 or O_2, which enhance the risk of fuel system component damage and explosion. Conventional warm-up in order to vaporize impurities is not practicable for frequently used tanks.

Both kinds of analyses generally start from the definition of an event tree that allows selecting and concentrating on more representative and risky combinations. The possible initiating events are those that might affect natural gas pipelines (e.g. external events, impacts, mechanical or service failures, etc.). The good buoyancy of hydrogen has been taken into account by analysts in order to be accurate in forecasting the behavior of a gas leakage in the atmosphere and wind direction and speed are here particularly influent. The very wide flammability range does not work in favor of safety but the buoyancy decreases the possibility of cloud formations at low heights (where human receptors are closer). In the event that large clouds are produced, these can be lately ignited and cause explosions. Another possibility is the formation of jet fires due to leakages in pipelines under pressure with an ignition that is not too much delayed. The safety distance for receptors, both humans and buildings, depends on many factors. A good reference for evaluating this distance was presented by Jo and Ahn (2006), and it is proportional to the square root of the steady state pressure in the pipeline and to the diameter of the pipeline.

As in the usual practice of risk prevention, artificial barriers may be inserted to decrease the safety distances from the possible release point to the receptor. In the case of hydrogen, barriers have been studied and proposed for application and vary in size, height, and inclination. For example, NFPA 55 [NFPA 2005] proposes a 60° inclined barrier to protect from jet fires originating from storages. In Royle and Willoughby (2011) these barriers have been tested against vertical ones and showed mixed response, being more suitable to protect the leakage area against overpressure and heat flux but less efficient to protect the area behind the barrier from the heat flux. A vertical barrier proved more efficient at protecting receptors behind it.

It should be noted that within the PRESLHY project an entire deliverable D6.2 “Guidelines for safe design and operation of LH_2 infrastructure” will be dedicated to the aspects of LH_2 safety.

5 Accident Statistics

5.1 Statistics

An evaluation of reports and statistics of accidents with hydrogen in industrial facilities in the period 1965–1977 covers a total of 409 accidents investigated with 78.5% related to gaseous H_2, 20.8% related to liquid H_2, and 0.7% related to hydrides [Zalosh 1978]. Major findings were that accidents were main ly caused by leakage or insufficient purging or venting, and that most releases eventually led to ignition. Also spontaneous ignition was observed from jets escaping from a burst disk or a safety valve. In partially obstructed areas, most explosions resulted in a fast deflagration or even detonation. The average damage per accident was independent of the state of the H_2.

Many different situations are conceivable which can give rise to the emission of a flammable substance and which have great influence on the evolution of a vapor cloud. Depending on the thermodynamic conditions of the fluid, it can be released as a liquid or a gas or a two-phase mixture. The component, from which the substance is released, may be a tank, a pump, a valve, pipe work or other equipment. The orifice, through which it is leaking, can vary over different shapes and sizes. The leaking fluid can flow into different geometries.

NASA statistics on 96 accidents during hydrogen operations revealed that ignition occurred in all cases with release into confined spaces, and in 60% of the cases with release into the open atmosphere. Improper system purging was the cause in 25% of the mishaps. Some cases were due to air entrainment into LH_2 systems. Hydrogen leaks were discovered to be mainly due to personnel not following prescribed procedures [Ordin 1974]. Considering accidents during transportation, in 71% of the inadvertent H_2 release cases recorded, no ignition was observed, a trend that is also confirmed by NASA experience [Schödel 1978].

A description of the evaluation of 287 occurrences, of which 86 were with cryogenic H_2, is given in [Kreiser 1994]. Main conclusions from this analysis were

- There is a high probability of an explosion of accidentally released gaseous hydrogen (96%), whereas only about half of the occurrences with cyrogenic H_2 were leading to an ignition (Fig. 5-1).
- The perception of an LH_2 occurrence as an accident with its good visibility (condensation of moisture in the air) appears to be much stronger than with gaseous H_2 (hardly visible and rapidly diffusing away).
- The tendency of (partial) confinement to favor the formation of flammable H_2-air mixtures, flame acceleration, and overpressures is obvious for accidents with gaseous H_2, but can also be recognized for LH_2 (although the statistical basis is less strong).
- In most cases, hot surfaces or open fire represent the ignition source (21% for gaseous H_2, 10% for liquid H_2);
- With regard to injuries of humans: from 201 accidents with gaseous H_2, there were 56 with a total of 199 injuries corresponding to a ratio of ~1 injury per accident; from the 86 accidents with liquid H_2, there were 8 with person damage and a total of 10 injuries corresponding to a ratio of ~ 0.12 injuries per accident.

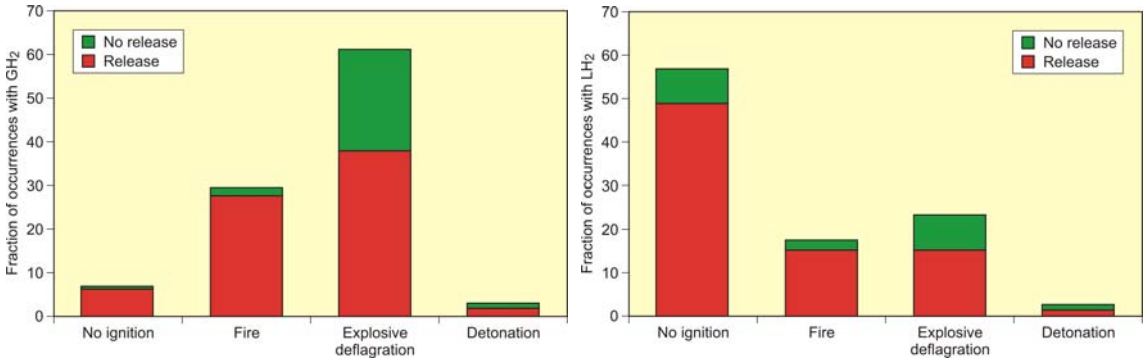

Figure 5-1. Statistics of investigated accidents with gaseous H_2 (top) and cryogenic H_2 (bottom) [Kreiser 1994].

Main safety goal of cryogenic storage tanks is the prevention of damage to the inner container. Mitigation measures to reduce the risk of a tank loss are

- Properly designed pressure relief;
- Minimum pipework and ancillary equipment;
- Backup instrumentation.
- Water spray system;
- Availability of sufficient quantity of water/foam;
- Prevention of overfilling;
- Generous spacing between tanks;

Major sources of hazards for cryogenic tanks are rapid mechanical changes of the system such as pipe ruptures. They may cause blast waves and high exit velocities or catalytic effects at the fracture location; they also may result in a jet fire or an unconfined vapor cloud explosion (UVCE). Also thermal changes such as rapid cooling of connecting elements or heat ingress (loss of isolation vacuum) may lead to mechanical loads on the system and significantly enhanced vaporization rates of the cryogen. At elevated temperatures and pressures, hydrogen attacks mild steels severely, causing decarburization and embrittlement. This is a serious concern in any situation involving storage or transfer of hydrogen gas under pressure. Proper material selection, e.g. special alloy steels, and technology is required to prevent embrittlement.

If the pressure in an LH_2 tank is kept constant, i.e. the vapor boil-off being removed, the temperature also remains constant (auto-refrigeration). If the boil-off is not removed, both temperature and pressure will rise. Thermal expansion of the cryogen also results in a pressure increase. Thermal expansion coefficients are higher for cryogens with lower boiling point. Therefore overfilling must be avoided.

Another hazardous situation is given, if air penetrates the system leading to the formation of condensation products of liquid/solid air or ice with the risk of plugging pipes or valves.

If there is heat input in a confined volume of a cryogen, the pressure will rise. The container will eventually rupture, if no or not sufficient gas can be vented from the system. Therefore a safe and reliable relief system must be provided. At closed valve, the heat input from the outside initiates a thermal stratification, which makes the pressurization process somewhat faster than in the case of thermal equilibrium. However,

the relative heat transfer into the tank is lower, the larger the tank and the better the surface-to-volume ratio and the insulation. The speed of pressurization also depends on the boiling temperature of the cryogen. The lower the boiling point, the stronger is the driving force for heat input.

Undesired events are caused by either human error or component failure or external impact. They can occur during steady-state operation or during the loading/unloading process such as leakage or rupture of the pressure vessel, leakage or rupture of transfer lines, overfilling, vessel failure due to impact from outside, or BLEVE. According to the type of event and according to the state of the fluid, it may exhibit a different physical release behavior, if accidentally released:

- Volatile liquid at ambient conditions showing slow evaporation;
- Flashing liquefied gas under pressure showing immediate large flash-off and slower evaporation of any residue; considered as the most serious case;
- Semi-refrigerated liquefied gas under pressure and at low temperature showing initial flash-off and violent evaporation;
- Refrigerated liquefied gas at low temperature and atmospheric pressure showing initial flash-off and relatively slow evaporation;
- Gas under pressure showing large physical energy release.

Fire protection of storage serves the purpose to minimize hazards to personnel and loss as well as prevent a spreading of initial fire. For atmospheric storage, stationary or mobile water or foam spray systems are employed. In refrigerated storage, it has to be considered that heating and vaporization is much more rapid. Initial protection is given by fire proof insulation to obtain a fire resistance of at least two hours.

Once a fire is established, subsequent failures can occur; for example, pipework fails within approx. 15 minutes, if exposed to fire. The scale of fire/explosion on a storage tank can be very large. Fires can occur in the vapor phase of the tank or outside, when an escaping vapor cloud ignites. Causes for fires are often given due to malfunctions in the operation procedure such as overfilling, failure of instrumentation, or operator error.

If an LH_2 pool fire is extinguished, the remaining pool still continues to vaporize, where the developing vapor cloud could easily re-ignite. For hydrogen on fire, best practice is therefore to cut off or isolate the source and allow the fire to burn, until the hydrogen is consumed [NASA 1997a].

Regarding road transportation incidents, of the 18 incidents identified, 5 (28%) occurred in transit and 13 (72%) during loading/offloading. The causes of the incidents were classified as follows:

Design/Construction failure/inadequate Hazard Assessment	0 (0%)
Equipment failure	6 (33%)
Incorrect operation / procedural deficiency/poor maintenance	8 (44%)
Impact or Road Traffic Accidents RTA	3 (17%)
Contamination	0 (0%)
Natural causes/Terrorism	1 (5%)
Escalation	0 (0%)

All the incidents attributed to "Incorrect operation/Procedural deficiency" arose during unloading operations. For example, due to overpressurizing the head space, or operating valves incorrectly or too quickly. Deviating from procedures relating to transfer hoses was also noted and using an impromptu procedure accounted for one incident. The consequences of these incidents were varied leading to gas venting, sometimes liquid release, fire, gas entering a building, and explosion. Equipment failure included unexpected burst disc failure, loss of vacuum or a loose flange connection. Of the five cases during transit, two related to Road Traffic Accidents (RTA) and the other three concerned venting due to burst disc failure and/or loss of vacuum. In one of the RTAs, the tanker overturned and landed in a ditch. Subsequently, the safety discs functioned and the liquid load was dumped. In the event of blockage of the relief, this incident could have resulted in more serious consequences. Overall, the consequences which arose were:

No release	2 (11%)
Accumulation/Dispersion	12 (67%)
Fire	4 (22%)
Explosion	1 (5%)
BLEVE	0 (0%)

(Note: multiple consequences can arise).

Injury to personnel occurred in 3 (17%) cases, 2 of which were cold burns. This rate of injury is greater than that noted for incidents concerning storage and liquefaction (see below) and probably reflects the required proximity of personnel during tanker operations. Property/equipment damage occurred in 7 (39%) of cases.

Of the 39 incidents identified in the realm of liquefaction and storage, the locations of the incidents were:

Liquefier/Purifier	2 (5%)
Vent system and pipework	11 (28%)
Storage vessels including fittings, valves and reliefs	14 (36%)
Valves/Components/Fittings	6 (15%)
Pumps/Compressors/Vaporizers	6 (15%)
Transfer lines/ pipelines	5 (13%)

Incidents concerning storage vessels had a tendency to be either minor in nature, that is, a small leak from a fitting or valve packing or a major incident. It was also noted that out of six major incidents involving storage vessels, three occurred during decommissioning/ commissioning (warm-up/cool-down). Further two less serious incidents also occurred when the vessel was not in service. There were several incidents relating to venting systems where unexpected ignition had occurred resulting in fire or explosion in vent system pipework or in the vicinity of the vent stack outlet. The causes of the incidents were classified as:

Design/Construction failure/Inadequate Hazard Assessment	12 (31%)
Equipment failure	8 (21%)
Incorrect operation/procedural deficiency/poor maintenance	18 (46%)
Impact or RTA	0 (0%)
Contamination	1 (3%)
Natural causes/Terrorism	5 (13%)
Escalation	2 (5%)

(Note: multiple causes in some cases).

The incidents attributed to poor design included four where the wrong material had been used. Two cases related to storage systems, which were over-sized and, after a prolonged period of storage, this led to failure of a burst disc and a leak from a gland nut. Two other cases were interesting in that it was inadequate hazard assessment (perhaps due to insufficient knowledge at the time), which led to an unforeseen explosion in the vicinity of a vent stack. It had been assumed that the hydrogen would disperse quickly, but due to prolonged venting of cold gas in calm conditions an accumulation formed around the vent stack, which then ignited. Incorrect operation, procedural deficiency or poor maintenance was the most common cause, as it was for the transportation incidents. Of these 18 incidents, seven were attributed to inadequate purging, leading to the formation of a flammable mixture. In terms of equipment failure, this typically related to leaking seals, valve packings or O rings. In four incidents cold weather and/or still conditions contributed to the cause of an incident and in one case lightning was believed to have ignited a vent stack. Overall, the consequences, which arose from the incidents, were:

No release	5 (13%);
Accumulation or Dispersion	14 (36%);
Fire	9 (23%);
Explosion	13 (33%);
BLEVE	1 (3%).

Injury occurred in 3 (8%) of incidents and non-trivial damage in 23 (59%) of cases. Note: apparently there was one case of attempted terrorism, but since there was no specific description, it did not result in significant damage, if any.

Based on the reported evidence, it is clear that despite occasional rupture disk failures and operator errors leading to occasional gas venting and fires, the overall safety record of LH_2 delivery, transfer and storage is very impressive. There were no recorded fatalities and only relatively minor injuries reported. Property damage was either none or not significant. Ironically, most hazardous situations were created by the erroneous / inappropriate actions of the first responders / fire fighters due to lack of knowledge of and training on LH_2.

Events like BLEVE and fireballs, typical for cryogenic hydrocarbons such as primarily LPG (propane and butane) and to the lesser extent LNG, appear to be not very typical for liquid hydrogen and mostly come from the academic / research assessments. Many assessments, for example, consider that all content of a ruptured tank will ignite simultaneously thus producing an enormous size fireball. In reality, such phenomena are not possible: even after a tank rupture, most of the hydrogen is still in liquid form, the produced gas is very cold and concentrated and, thus, cannot all ignite at once. In this case, a relatively small flash fire is a much more realistic scenario.

A reality of modern society is that even given the best technologies and engineering available, no energy system can be made 100% safe no matter how concerted the effort. Considering the wide-spread dependence of today's economies on various forms of energy and their associated systems, it is no surprise that accidents and other failures occur worldwide on a regular basis. This incident illustrates both the need for exercising caution and also how the characteristics of hydrogen may have helped minimize the severity of the event.

What incidents underscore is the need for rigorous training on hydrogen properties and behavior, not only for the operators of fueling equipment but also for emergency responders and the general public. The physical and chemical characteristics of hydrogen

are different from those of fossil fuels and must be communicated, understood, and accounted for in hydrogen handling and use if the transition to a hydrogen-fueled economy is to be accomplished in the safest manner possible.

5.2 Examples of Accidents Involving LH_2

During the first approximate 50 years of handling liquid hydrogen in small (lab-scale) quantities only, numerous inadvertent explosions occurred, fortunately not disastrous due to the small amounts. With increasing quantities handled and the need for larger storage devices, experimenters aware of its hazards used testing facilities which were equipped with safety devices. Initial difficulties in handling LH_2 were often caused by leakages from lines due to insufficient tightness of plumbing connections. Some incidents occurred in liquefaction plants resulting from the accumulation of solid air.

5.2.1 Burst Disk Failure

In 2008, a 9000-gallon (~34 m^3) cryogenic liquid hydrogen storage vessel, installed outdoors at a manufacturing plant, over-pressurized and released hydrogen into the atmosphere through a safety relief device (burst disk). When the burst disk released pressure, gaseous hydrogen escaping from the vessel's vent stack rose about 5–6 m into the air, but there was no fire. A technician found the tank pressure at zero and the burst disk blown. He switched the three-way diverter valve to the other safety relief device and replaced the burst disk when the line defrosted.

Cause of the over-pressure was the fact that the cryogenic LH_2 storage vessel had experienced a long period of non-use and gradually heated up despite its vacuum-jacket. The normal storage pressure for this vessel was 1.03 MPa. There were no injuries or damage reported from this incident.

About seven months later, the same incident occurred again, when back pressure against the burst disk caused premature failure. No outside emergency response was involved here, as once again the pressure relief system worked as designed. Following this incident, some modifications were made to the hydrogen piping to eliminate all back pressure on the burst disk.

5.2.2 LH_2 Tank BLEVE

In a large liquid hydrogen tank, a burst disk blew and exhausted cold gaseous hydrogen through the vent stack. To stabilize the tank, the remaining hydrogen was removed from the tank except for a small volume in the heel of the tank. Firefighters responding to the hydrogen release sprayed water on the tank and vent stack. Since the vent stack was open, some water entered and froze, plugging the stack and sealing off the only hydrogen pressure-relief exit path. With the tank warming up, it became over-pressurized, and ruptured. Vent stack design and the emergency response actions did not allow the vent stack to function. The lessons learned were (1) never use water to be sprayed on the vent stack of an LH_2 vessel, and (2) install backup pressure relief vent stack in case the main vent stack fails.

5.2.3 Incident during LH_2 Transfer

In the course of a liquid hydrogen transfer at a Ballard facility in Burnaby, BC, in 2004, a plume of hydrogen gas escaped from the offloading valve of a Praxair LH_2 delivery truck. The plume ignited resulting in a flash and concussion to set off the building's seismic event detectors. A small amount of hydrogen gas continued to escape from the trailer tank and burn until the critical valve was manually shut off almost eight hours later.

The actual cause of this incident appears to have been primarily driver error. A number of steps required as part of the standard safety procedure were either incorrectly applied or omitted altogether. The problem started when the driver of the truck was preparing to complete the second of two deliveries at the facility. The manual valve was apparently left in open position following the first unloading. The driver next failed to perform the required procedure of seven purges intended to eliminate contaminants and water from the piping before connecting the hose for the second unloading. He then opened the pneumatic valve before connecting the hose, which, due to the open manual valve, resulted in a direct release of liquid hydrogen into the ambient air. This liquid immediately vaporized into a hydrogen cloud and quickly ignited, presumably caused by static electricity. The flow was eventually stopped when a specialist closed the manual valve with a special tool. The driver escaped with only minor injuries similar to those from sunburn, also the truck received only minor damage.

5.2.4 Liquefaction and Storage Incidents

Two incidents were attributed to an escalation event. In both cases, an improper method of fire fighting was used:

- In one case, firefighters were attending a fire on a vessel relief vent. Although the vessel had been part drained, some LH_2 remained in the tank. The firefighters directed water at the fire on the relief and water entered the vent and froze, blocking it. The residual LH_2 warmed up, vaporised and due to the blocked relief, a BLEVE occurred.
- In the second case, again, a fire was present on a vessel relief. Firefighters attempted to protect an adjacent vessel by spraying it with liquid nitrogen, but the cold temperatures caused cracking of the outer skin of the vessel and loss of the vacuum. This caused a rapid increase in temperature and pressure. Subsequent failure of the rupture disc on this second vessel resulted in an additional fire, as the contents of this vessel boiled off. Although it did not occur in this case, the potential for a BLEVE is obvious.

5.2.5 Ignition while Venting

In a test for a rocket nozzle in 1964, the Los Alamos National Laboratory at Jackass Flat has conducted an intentional venting of 1000 kg of hydrogen at 23 MPa within 30 s, when unintentionally a spontaneous ignition occurred after 26 s. The burning gas cloud of approx. 9 m diameter and 45 m height contained about 9 kg of H_2. The flame speed reached about 35 m/s, the overpressure an estimated 3.5 kPa at buildings in a distance of about 60 m.

5.2.6 Space Shuttle Accident

The catastrophic accident of the Challenger Space Shuttle in 1986 shortly after launching was said by NASA officials to have been caused by the failure of an O-ring rubber seal in one of the two solid rocket boosters due to erosion by hot gases. A steady flame developed which was directed towards the surface of the External Tank containing the LH_2 and LOX tanks. The flame eventually breached the tank resulting in an explosive combustion of the hydrogen and oxygen. This official NASA theory was questioned in another study assuming so-called "phantom" fires which resulted from undetected LH_2 leakages (< 1.4 kg/s) from the External Tank and their early ignition at low altitude by plumes from the adjacent rocket booster causing a quick deterioration of the tank structure [NASA 1997b, Chirivella 1997].

5.2.7 Tank Truck Overturn

In a tank truck accident near Columbus, Ohio, the truck overturned and the cryo-tank lost its vacuum. The vaporizing hydrogen was vented, but did not ignite, and therefore no significant damage was observed [Ringland 1994].

5.2.8 Catastrophic Failure of Storage Tank

An explosion of a 9000 gal (34 m^3) LH_2 storage tank took place, when – due to repair work on the vent stack – the vessel was purged with N_2 gas to boil away the LH_2. Pressure inside the vacuum jacket increased despite opening the vacuum valve eventually leading to a catastrophic tank rupture where one end of the tank blew off [Lodhi 1989].

6 Regulations, Codes and Standards

Liquid hydrogen production, storage, transportation and distribution for multiple applications in the industries and transport sectors will become a major part in a hydrogen-assisted energy economy. However, there does currently exist a lack of comprehensive experience with buildup and operation of an LH_2-based infrastructure in a public environment. Even after the start of the penetration of hydrogen in worldwide energy mixes, some regulations are still missing or not fully applied at national level.

The technological development has to be sustained by a parallel development of codes and standards to assure safe use and to allow manufacturers to play in a regulated field that couples the protection of the customer and the competition on the market.

At an international level, ISO Technical Committee 197 is in charge of developing standards related to hydrogen applications. The standards are available for some specific applications (such as those related to onboard systems, fuel tanks and refueling systems for vehicles) and for the production part of the chain (electrolysis and steam methane reformers are already covered), but standards for refueling stations as part of the distribution chain and pipelines are still under development at the time of writing.

It is connected with the need to investigate LH_2-specific accident scenarios.

LH_2-based installations are to be framed by a set of commonly accepted regulations, codes and standards:

- Science-based and validated tools, which are required for hydrogen safety engineering, and risk-informed, performance-based, LH_2-specific, international standards
- Specific knowledge, specific international standards, safety strategies in existing installations
- Support of international standards developing Organisations SDOs, in particular ISO/IEC and CEN/CENELEC, in either updating existing standards or developing new international performance based and risk informed standards.

Any liquid hydrogen storage and handling facility requires significant clearances for placement of a LH_2 storage tank and a vaporizer and associated auxiliary equipment as well as for LH_2 tanker transfer and potential spill area (Fig. 6-1).

Also the adaptation of natural gas regulations on distribution networks was accompanied by field tests developed to understand the safety distances to be imposed between hydrogen installations and the nearest buildings. The need for this accurate evaluation is particularly relevant in the case of hydrogen because the vector is new in application and tough restrictions (such as important barriers or excessive safety distances) may reduce the possibility for the wider public to accept it [Royle 2010a].

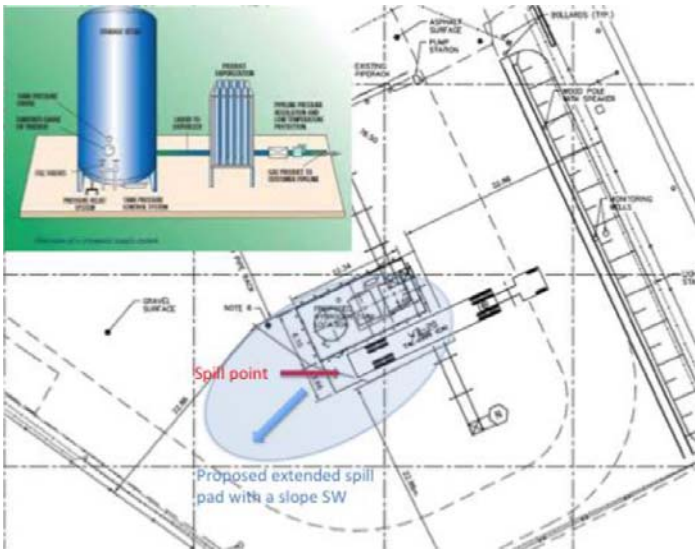

Figure 6-1. Example of LH_2 equipment placement.

6.1 NFPA Standards

National Fire Protection Association or NFPA publishes two very relevant standards, NFPA 55 Compressed Gases and Cryogenic Fluids Code (latest published is 2013 edition) [CGA 2014] and NFPA 2 Hydrogen Technologies Code (latest published is 2016 edition) [EIGA 2002].

With respect to liquid hydrogen both standards' requirements are virtually identical and most of NFPA 2 LH_2 related clauses come from NFPA 55. The nuances between the two relate to the coverage: NFPA 55 covers bulk storage, while NFPA 2 covers both bulk and non-bulk storage applications. Also, NFPA 2 covers hydrogen fueling facilities, while NFPA 55 does not.

6.1.1 Separation Distance

Both latest editions of NFPA 55 and NFPA 2 provide identical separation distances for liquid hydrogen which give rise to some important questions:

- LH_2 storage capacities are ranging from 0.15 to 284 m3 (orders of magnitude difference in capacity), whereas the maximum separation distances differ only by the factor of 3. Some separation distances even remain the same and seem to be independent of the quantity stored.
- Maximum separation distances are 30.5 m (100 ft). Note: 100 ft was mentioned in A.D. Little (1960) videos as the worst case separation from the effects of premixed combustion / deflagration tests.
- Fire resistance rating of 3 h for unsprinklered buildings or structures is required to significantly reduce the separation distances (by 5 to 15 times).

6.1.2 Hazardous (Electrical) Areas Classification Requirements

Both standards show identical electrical areas classification requirements for bulk LH_2 storage facilities. Note that in North American classification, Division 1 corresponds to Zone 1 and Division 2 corresponds to Zone 2 in IEC / ATEX classification.

It is interesting that despite being unanimous on LH_2 electrical classification, the NFPA standards differ in setting requirements for bulk gaseous hydrogen facilities. Apparently, the difference is due to higher attention to venting arrangements of gaseous hydrogen, but not for liquid. The logic of this approach is not immediately plausible.

Comparing electrical classifications for bulk LH_2 and GH_2 systems, the distance requirements for LH_2 are larger (7.6 m vs 4.6 m) than for GH_2 facilities. The reason is likely based on the assumption that warm hydrogen has a higher buoyancy than cold hydrogen and thus less likely to spread in horizontal direction than cold hydrogen upon exiting from the vent stack.

In addition to bulk hydrogen storage systems, NFPA 2:2016 also provides electrical classification requirements for both LH_2 and GH_2 fueling facilities. They are similar to those for bulk systems: classified areas for LH_2 fueling facilities are with 7.6 m bigger than those for GH_2 fueling facilities with 4.6 m.

6.1.3 Hydrogen Vent Stack Requirements

Both NFPA standards refer to CGA G-5.5 for vent stack design and termination requirements. It should be noted that this standard is referred to by a number of other standards including ISO/TS 19880-1:2017 for hydrogen fueling stations.

CGA G-5.5 standard will be reviewed in detail in the next section 6.2.

6.1.4 LH2 Spill Mitigation and Control

Both NFPA standards state “Diking shall not be used to contain an LH_2 spill”.

Proposed changes to NFPA 2:2019 includes the following clause:

- Diking or berms shall be used when necessary to direct the spill away from an additional hazard.
- The site design for liquid hydrogen storage shall prevent pooling of the leak, but may use berms or dikes to redirect a spill away from storm sewers, building access points or other hazards and to direct the release to an appropriate area.

This indicates that site planning for LH_2 transfer and storage facilities need to allocate space for a spill area that will not lead to pooling.

6.2 CGA G-5.5 Hydrogen Vent Systems

In 2014 CGA published an updated (3rd edition) G-5.5 standard for hydrogen vent stack systems [CGA 2014]. It specifically highlights now vents stack designs which are recommended for hydrogen use and those which are not. It also gives an example of the recommended miter cut for a T-venting shown in Fig. 6-2.

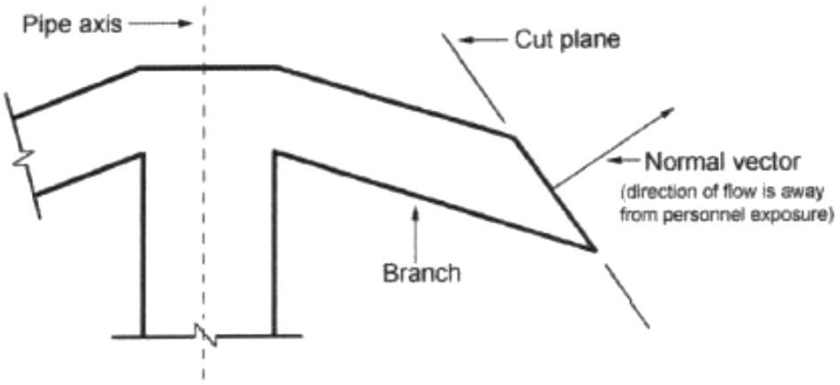

Figure 6-2. Example of an acceptable miter cut [CGA 2014].

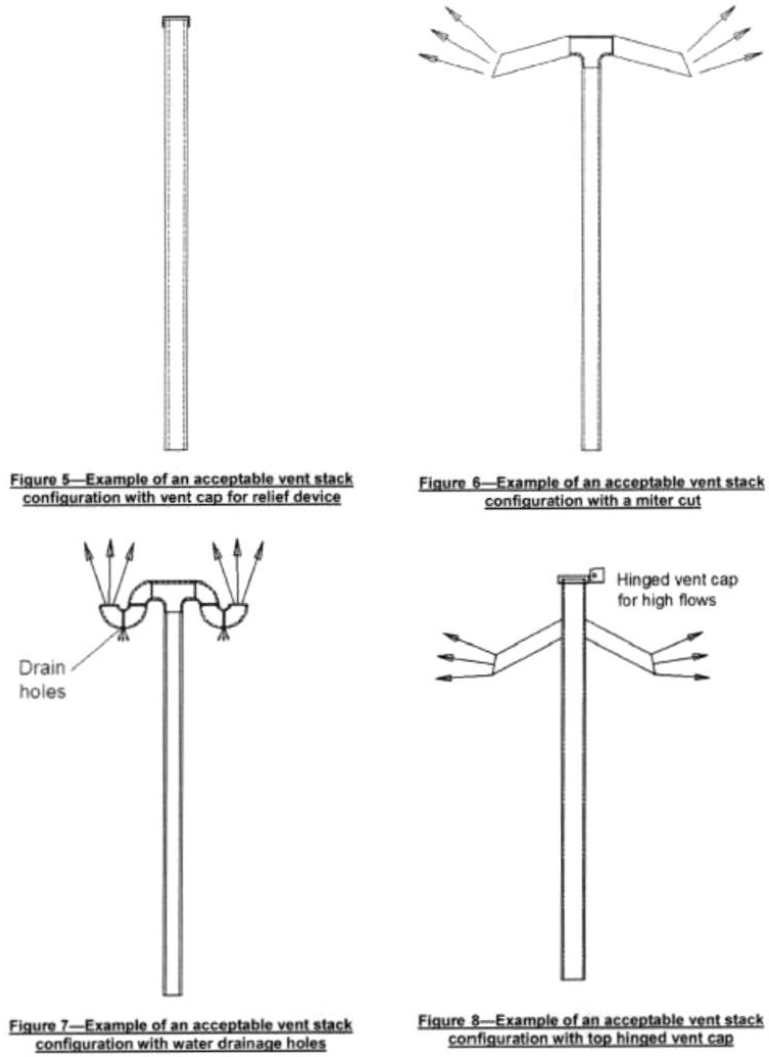

Figure 6-3. Examples of acceptable vent stack configurations [CGA 2014].

Referring to the above miter cut and to examples of recommended stack designs shown in Fig. 6-3, the standard states that "the miter cuts on the ends of the vent cap are designed to direct the resultant discharge vector with some vertical component as the gas is discharged. The vent exit shall not downwards since it can direct flow to an area of potential personnel exposure".

This statement, however, may only partially be true. If the exit velocity is close to sonic, the flow of hydrogen will be initially directed downwards. If the velocity is low, the flow will be horizontal and then rise.

The rationale provided by the standard is that "they either direct the hydrogen downward or create an unbalanced thrust that could cause deflection or damage to the vent stack during high velocity discharges."

The standard provides the following guidance regarding thermal radiation and impingement aspects: "Vent stacks shall be located to prevent impingement exposure and lessen the effects of high temperature and thermal radiation exposure from the escaping plume to the supply system, personnel and adjacent structures."

Regarding the discharge of cold hydrogen specifically, CGA G-5-5:2014 requires that:

- Exist of vent stacks for cold hydrogen gas releases should be at a height that is sufficient to avoid vapour clouds.
- Cold hydrogen vents need to be higher than warm hydrogen vents because the exiting gas can be at a higher density than the ambient air and could cause the hydrogen to accumulate.

6.3 EIGA Code of Practice for Liquid Hydrogen

EIGA's (European Industrial Gas Association) Code of Practice "Safety in Storage. Handling and Distribution of Liquid Hydrogen" was published in 2002 [EIGA 2002].

6.3.1 Safety Distance

EIGA-recommended minimum safety distances for liquid hydrogen are listed in Table 6-1 [EIGA 2002].

Items of particular interest in Table 6-1 are:

- Only 90 min fire rating requirements for fire break walls without mentioning the sprinkler requirements (vs 3 hrs in NFPA 2 & 55);
- Separation from Places of public assembly is similar to and a bit lower than in NFPA standards (23 m); however, the largest separation is required for Public establishments that are not considered by NFPA 2 & 55.

Also, EIGA document establishes blanket requirements for all LH_2 storage facilities regardless of size (vs NFPA standards that have 3 size categories).

Table 6-1. Recommended minimum safety distances for Liquid Hydrogen storage.

Items	Distance (m)
90 min fire resistive walls	2.5
Technical and unoccupied buildings	10
Occupied buildings	20
Air compressor intakes, air conditioning	20
Any combustible liquids	10
Any combustible solids	10
Other LH_2 fixed storage	1.5
Other LH_2 tanker	3
Liquid oxygen storage	6
Flammable gas storage	8
Open flame, smoking, welding	10
Place of public assembly	20
Public establishments	60
Railroads, roads, property boundaries	10
Overhead power lines	10

6.3.2 Hazardous (Electrical) Areas Classification Requirements

There are no specific requirements for electrical classification except for the reference to national regulations, standards and codes of practice.

6.3.3 Hydrogen Vent Stack Requirements

EIGA document gives specific instruction on the height of the vent stack:

“The height of the vent stack outlet should be either 7 metres above ground level or 3 metres above the top of the tank whichever is the greater for protection of the operating personnel and equipment.”

It also makes a specific guidance in regards to vapor clouds:

“When siting an installation, due consideration shall be given to the possibility of the movement of vapour clouds, originating from spillage or venting; in addition wind direction and the topography shall be taken into account.”

6.3.4 LH2 Spill Mitigation and Control

EIGA document prescribes avoidance of pooling similar to NFPA standards:

"Dykes, diversion curbs or grading shall be used to ensure that liquid leakage from adjacent combustible liquid or liquid oxygen storages installed at a higher level than the liquid hydrogen storage, is discouraged from accumulating within 15 metres of the liquid hydrogen storage.

The slope of the ground shall be such as to provide normal surface water drainage."

6.4 Dutch PGS 35 Guidelines

PGS 35 Guidelines "Hydrogen: installations for delivery of hydrogen to road vehicles" was published in April 2015 under Hazardous Substances Publication Series 35, version 1.0 [PGS 2015].

PGS team 35 included representatives from the government and the business community such as representatives from the authorities (the Association of Interprovincial Authorities (IPO), the Association of Dutch Municipalities (VNG), the Social Affairs and Employment Inspectorate (Inspectorate SZW), the Dutch Fire Service, the business community (VNO-NCW and MKB Nederland) and employees.

The relevance and value of this document is underscored by the paragraph below cited from the "reason for this Publication":

"In the past, the Dutch Code of Practice NPR 8099:2010 on Hydrogen fuelling stations – Guide for safe application of installations for delivery of hydrogen to vehicles and boats with respect to fire, workplace and environment was available for the construction of hydrogen delivery installations in the Netherlands. This Code of Practice comprised a lot of knowledge relevant to the construction of a hydrogen delivery installation. A tour of safety specialists revealed that they preferred a PGS publication due to the uniformity of regulations that are important in the context of granting licenses and due to the footing and transparency they provide as regards granting licenses for the construction of a hydrogen delivery installation. As regards the necessary physical space, a PGS gives internal safety distances that shall be observed. Thus, a

PGS offers a guideline of regulations, requirements and safety distances, enabling licensing procedures for hydrogen delivery installations to be performed in a uniform manner."

6.4.1 Safety Distance

PGS 35 document differentiates between internal and external safety distances:

The internal safety distances to be complied with shall be determined using radiation calculations.

In order to determine the internal distances, it is important to know whether the Major Accidents (Risks) Decree (Brzo) [NLD 1999] applies to the establishment. This decree identifies 5 tonnes as a minimum "qualifying quantity" for hydrogen. It also states that "Dangerous substances present at an establishment only in quantities equal to or less than 2% of the relevant qualifying quantity shall be ignored for the purposes of calculating the

total quantity present if their location within an establishment is such that it cannot act as an initiator of a major accident elsewhere on the site." This essentially means that any hydrogen quantities up to 100 kg (2% of 5000 kg) may not be taken into account for internal safety distances.

A quantitative risk analysis (QRA) shall be carried out in order to determine the external safety distances.

6.4.2 Hazardous (Electrical) Areas Classification Requirements

There are no specific requirements for electrical classification except for the reference to NEN-EN-IEC 60079-14 (in ATEX zones) for electrical devices.

There is, however, an interesting note with regard to hydrogen detection around the points of dispensing (Note: NEN-EN-IEC 60079-10-1 describes the locations where the probability of a gas leak is the greatest):

- At least two gas detectors shall be present, one of which is near the dispenser and one is in the dispenser.
- At 10% LEL, an automatic preliminary warning shall be sent to the manager of the installation.
- At 20% LEL, the emergency shutdown circuit (ESD facility) shall be activated.

A detector inside the dispenser is certainly required and is an established industry practice. A detector near the dispenser, however, will not serve any useful purpose.

6.4.3 Hydrogen Vent Stack Requirements

PGS35 document gives specific instruction on the design of the vent stack for LH_2:

The outlet of liquid hydrogen shall be designed in such a way that:

- the heat radiation from a flare from the central vent stack onto neighbouring objects has been taken into account;
- this source is at least 3 m above ground level;
- the heat radiation at ground level is lower than 3 kW/m^2 within the establishment limit and lower than 1 kW/m^2 outside the establishment limit in order to protect people;
- the heat radiation intensity from a flare from the central vent stack on the gaseous hydrogen storage unit is less then 10 kW/m^2;
- the heat radiation intensity from the flare on the liquid hydrogen storage unit is less than 35 kW/m^2;
- the material of the flare can withstand the high temperatures at the exhaust (and for liquid hydrogen it can also withstand low temperatures at the intake).

Comparing EIGA and PGS35 requirements the difference in approach is obvious: while EIGA requirements are fully prescriptive, PGS35 is half-performance based in view of the expected thermal radiation. Yet, PGS35 seems to be overly conservative in prescribing thermal radiation at 2/3 of generally accepted safe radiation threshold of 1.6 kW/m2 and "pain threshold" of 4.7 kW/m2 respectively.

6.4.4 LH_2 Spill Mitigation and Control

PGS35 document does not provide any specific requirements for potential LH_2 spill control. However, it provides a detailed checklist for transfer of liquid hydrogen from a delivery tanker to the ground storage vessel.

6.5 Other Standards for Liquid Hydrogen

This section provides brief description of the scope or content of other existing LH_2 standards and relevant documents.

6.5.1 ISO 13984: 1999

ISO 13984: 1999 Liquid hydrogen – Land vehicle fueling system interface [ISO 1999] was prepared for liquid hydrogen fueled vehicles and for this reason is not relevant in today's market environment orientated on compressed gas vehicle storage systems.

Its scope includes the following:

- "This International Standard specifies the characteristics of liquid hydrogen refueling and dispensing systems on land vehicles of all types in order to reduce the risk of fire and explosion during the refueling procedure and thus to provide a reasonable level of protection from loss of life and property.
- This International Standard is applicable to the design and installation of liquid hydrogen (LH_2) fuelling and dispensing systems. It describes the system intended for the dispensing of liquid hydrogen to a vehicle, including that portion of the system that handles cold gaseous hydrogen coming from the vehicle tank, that is, the system located between the land vehicle and the storage tank."

6.5.2 ISO 13985: 2006

ISO 13985: 2006 Liquid hydrogen – Land vehicle fuel tanks [ISO 2006] was prepared for liquid hydrogen fueled vehicles and for this reason, as the standard above, is not relevant in today's market environment orientated on compressed gas vehicle storage systems.

Its scope includes the following:

- "This International Standard specifies the construction requirements for refillable fuel tanks for liquid hydrogen used in land vehicles as well as the testing methods required to ensure that a reasonable level of protection from loss of life and property resulting from fire and explosion is provided.

- This International Standard is applicable to fuel tanks intended to be permanently attached to land vehicles."

6.5.3 HSL Position Paper

HSL Position paper on hazards of liquid hydrogen [HSL 2010] was published in 2010 per request from the UK Health and Safety Executive "to identify and address issues relating to bulk liquid hydrogen transport and storage and update/develop guidance for such facilities."

"This position paper, the first part of the project, assesses the features of the transport and storage aspects of the refuelling stations that are now being constructed in the UK, compares them to existing guidance, highlights gaps in the regulatory regime and identifies outstanding safety issues. The findings, together with the results of experiments to improve our understanding of the behaviour of liquid hydrogen, will inform the development of the guidance for refuelling facilities."

This position paper in a very concise form addresses various issues related to liquid hydrogen. Clearly, this paper played a significant role at the time of publication since it was the precursor of the non-ignited and ignited tests performed at HSL in the following years and referred to earlier in this report.

6.5.4 US-DOE Publications

Two very useful and relevant reports coming from the US DOE National Labs need to be mentioned here. Both documents briefly described below will be referred to in Section 9 for proposed case studies.

6.5.4.1 Hydrogen Technologies Safety Guide

Hydrogen Technologies Safety Guide was developed and published by National Renewable Energy Lab (NREL) in January 2015 [Rivkin 2015]. Similar to HSL Position paper mentioned above, it discusses hydrogen hazards as well as in great detail relevant codes and standards, but with US focus.

Its particular value for PRESLHY project is the Permit Example where a layout of a typical hydrogen station is presented, including both compressed and liquid hydrogen storage, with the required separation distances as prescribed by NFPA 2.

6.5.4.2 Safety, Codes and Standards for Hydrogen Installations

The report Safety, Codes and Standards for Hydrogen Installations: Hydrogen Fueling System Footprint Metric Development was developed and published Sandia National Labs (Sandia) in April 2014 [Harris 2014].

The significant value of this report is the demonstration how footprint metrics can effectively demonstrate the impact on installation code requirements on the land footprint required for placement of a hydrogen station. The abstract of the report states:

“The development, implementation, and advancement of meaningful codes and standards is critical to enable the effective deployment of clean and efficient fuel cell and hydrogen solutions in the energy technology marketplace. Metrics pertaining to the development and implementation of safety knowledge, codes, and standards are important to communicate progress and inform future R&D investments. This document describes the development and benchmarking of a metric specific to the development of hydrogen specific codes relevant for hydrogen refueling stations: “number of fueling stations that can readily accept hydrogen.

The report includes very useful exercise of overlaying separation distances requirements from NFPA 2 over existing (real world) sites selected for hydrogen station placement. Some of the material from this report will be used in the next Section.

7 References

ADL. Final report on an investigation of hazards associated with the storage and handling of liquid hydrogen. Report C-61092, Arthur D. Little Inc., Cambridge, MA (1960).

Airbus, Airbus reveals new zero-emission concept aircraft. (2020). Available at https://www.airbus.com/newsroom/press-releases/en/2020/09/airbus-reveals-new-zeroemission-concept-aircraft.html

Asadnia, Large-scale liquid hydrogen production methods and approaches: A review. Applied Energy 212 (2018) 57–83.

Astbury G.R., Hawksworth S.J., Spontaneous ignition of hydrogen leaks: A review of postulated mechanisms. 1st Int Conf Hydrogen Safety (ICHS-1), Pisa (2005).

Babrauskas V., Estimating large pool fire burning rates. Fire Technology, 19 (1983) 251-261.

Bavoil E., Etude expérimentale de l'influence de la diminution de la température initiale (jusqu'à 100K) sur les déflagrations des mélanges H_2-air, PhD thesis, University of Orleans, France (1997).

Bazhenova T., Bragin M., Golub V.,Ivanov M., Self-ignition of a fuel gas upon pulsed efflux into an oxidative medium. Technical Physics Letters 32(3) (2006) 269–271.

Bell I.H., Wronski J., Quoilin S., Lemort V., Pure and pseudo-pure fluid thermophysical property evaluation and the open-source thermophysical property library CoolProp. Industrial & Engineering Chemistry Research 53(6) (2014) 2498–2508.

Birch A.D., Brown D.R., Dodson M.G., Swaffield F., The structure and concentration decay of high pressure jets of natural gas. Combustion Science and Technology 36(5) (1984) 249–261.

Bragin M.V., Makarov D.V., Molkov V.V., Pressure limit of hydrogen spontaneous ignition in a T-shaped channel. Int J Hydrogen Energy 38(19) (2013) 8039–8052.

Brandeis J., Ermak D.L., Numerical simulation of liquefied fuel spills: I. Instantaneous release into a confined area. Int J Numerical Methods in Fluids, 3 (1983) 333–345, and II. Instantaneous and continuous LNG spills on an unconfined water surface. Int J Numerical Methods in Fluids, 3 (1983) 347–361.

Breitung W. and Redlinger R. A model for structural response to hydrogen combustion loads in severe accidents. Nuclear Technology 111 (1995) 420–425.

Breitung W., et al., Experimental and theoretical investigations of sonic hydrogen discharge and jet flames from small breaks. Final Report for project ICEFUEL, Karlsruhe Institute of Technology (2009).

Brennan S., Makarov D., Molkov V., Dynamics of flammable hydrogen-air mixture formation in an enclosure with a single vent. Sixth International Seminar on Fire and Explosion Hazards, Leeds (2010).

Brennan S., Molkov V., Safety assessment of unignited hydrogen discharge from onboard storage in garages with low levels of natural ventilation. Int J Hydrogen Energy 38(19) (2013) 8159–8166.

Brennan S., Molkov V., Pressure peaking phenomenon for indoor hydrogen releases. Int J Hydrogen Energy 43(39) (2018) 18530–18541.

Brennan S., Hussein H.G., Makarov D., Shentsov V., Molkov V., Pressure effects of an ignited release from onboard storage in a garage with a single vent. Int J Hydrogen Energy 44(17) (2019) 8927–8934.

Brentari E.G., Smith R.V., Nucleate and film pool boiling design correlations for O_2, N_2, H_2, and He. International Advances in Cryogenic Engineering, paper T-1, Plenum Press, New York (1965).

Calcote H.F., Gregory C.A., Barnett C.M., Gilmer R.B., Spark ignition. Effect of molecular structure. Industrial & Engineering Chemistry 44(11) (1952) 2656–2662.

Carslaw H.S., Jaeger J.C., Conduction of heat in solids. Clarendon Press, Oxford (1959).

Cassut L.H., et al., A study of the hazards in the storage and handling of liquid hydrogen. Advances in Cryogenic Engineering 5 (1960) 55–61.

CGA G-5.5 Hydrogen vent systems. Third edition, Compressed Gas Association, McLean, VA (2014).

Chen C., Rodi W., Vertical turbulent buoyant jets - A review of experimental data. Pergamon Press, Oxford (1980).

Chirivella J.E., Witcofski R.D., Experimental results from fast 1500-Gallon LH_2 spills. AIChE Symp Ser 82(251) (1986) 120–40.

Chirivella J.E., Analysis of the “phantom” fires on the Space Shuttle external tank base and the nature of the Space Shuttle “phantom” fires: LH_2 Leaks. In: JANNAF 34th Combustion Systems Hazards Subcommittee and Airbreathing Propulsion Subcommittee Joint Meetings, Palm Beach (1997).

Chitose K., et al., Activities on hydrogen safety for the WE-NET Project - Experiment and simulation of the hydrogen dispersion, Presentation at the 14th World Hydrogen Energy Conf (WHEC14), Montreal (2002).

Cirrone D., Makarov D., Molkov V., Cryogenic hydrogen jets: Flammable envelope size and hazard distances for jet fire. Proc. 8th Int Conf on Hydrogen Safety (ICHS2019), Adelaide, Australia (2019a) paper 191.

Cirrone D., Makarov D., Molkov V., Near field thermal dose of cryogenic hydrogen jet fires. Proc 9th Int Seminar on Fire and Explosion Hazards (ISFEH9), St. Petersburg, Russia (2019b) 1360–1366.

Cirrone D., Makarov D., Molkov V., Thermal radiation from cryogenic hydrogen jet fires. Int J Hydrogen Energy 44(17) (2019c) 8874–8885.

CRRCGC, T85 Type Liquefied Hydrogen Tank Car. (2016). Available at https://www.crrcgc.cc/xaen/g11117/s21282/t271695.aspx

Dadashzadeh M., Makarov D., Kashkarov S., Molkov V., Non-adiabatic under-expanded jet theory for blowdown and fire resistance rating of hydrogen. Proc. 8th Int Conf on Hydrogen Safety (ICHS-8), Adelaide, Australia (2019).

DASA. CRYOPLANE – Deutsch-Russisches Gemeinschaftsprojekt zum Einsatz kryogener Treibstoffe in der zivilen Luftfahrt – Realisierbarkeitsstudie 1990/91/92. Report, Deutsche Aerospace Airbus GmbH, Hamburg (1992).

Dawson V.P., Bowles M.D., Taming liquid hydrogen: The Centaur upper stage rocket 1958-2002. The NASA History Series, Report NASA SP-2004-4230. National Aeronautics and Space Administration, Washington DC (2004).

Decker L., Latest global trend in liquid hydrogen production. Presentation at the HYPER Closing Seminar, Brussels (2019a).

Decker L., Liquid hydrogen distribution technology. Presentation at the HYPER Closing Seminar, Brussels (2019b).

Dienhart B. Ausbreitung und Verdampfung von flüssigem Wasserstoff auf Wasser und festem Untergrund. Report Jül-3155, Research Center Jülich (1995).

Dorofeev S.B., Sidorov V.P., Kuznetsov M.S., Matsukov I.D., Alekseev V.I., Effect of scale on the onset of detonations. Shock Waves 10 (2000) 137–149.

Dorofeev S.B., Kuznetsov M.S., Alekseev V.I., Efimenko A.A., Breitung W., Evaluation of limits for effective flame acceleration in hydrogen mixtures. J Loss Prevention in the Process Industries 14(6) (2001) 583–589.

Edeskuty F.J., Stewart W.F., Safety in the handling of cryogenic fluids. The International Cryogenics Monograph Series, Plenum Press, New York (1996).

Eichert H., et al. Gefährdungspotential bei einem verstärkten Wasserstoffeinsatz. Study for the Büro für Technikfolgenabschätzung des Deutschen Bundestags, Deutsches Zentrum für Luft- und Raumfahrt (DLR), Stuttgart (1992).

EIGA, Code of Practice “Safety in storage, handling and distribution of liquid hydrogen”. Doc 06/02/E, European Industrial Gases Association, Brussels (2002).

Ekoto I.W., et al., Updated jet flame radiation modeling with buoyancy corrections. Int J Hydrogen Energy 39(35) (2014) 20570–20577.

ESS. The ESS Project Volume III Update. European Spallation Source Technical Report, Status 27.05.04. (2004). Available at http://neutron.neutron-eu.net/n_documentation/ n_reports/n_ess_reports_ and_ more/106 (2004).

FCB, Fuel Cells Bulletin 2016(12) 14–15.

Friedrich A., et al., Ignition and heat radiation of cryogenic hydrogen jets. Int J Hydrogen Energy 37(22) (2012) 17589–17598.

Funke T., Development of large scale hydrogen liquefaction. Presentation at the Hydrogen Liquefaction & Storage Symp, Perth (2019).

Gavrikov A.I., Efimenko A.A., Dorofeev S.B., A model for detonation cell size prediction from chemical kinetics. Combustion and Flame 120(1-2) (2000) 19–33.

Giacomazzi G., Gretz G., Euro-Quebec Hydro-Hydrogen Project (EQHHPP): A challenge to cryogenic technology. Cryogenics 33 (1993) 767–771.

Golub V.V., et al., Shock-induced ignition of hydrogen gas during accidental or technical opening of high-pressure tanks”, J Loss Prevention in the Process Industries 20(4–6) (2007) 439–446.

Golub V.V., et al., Mechanisms of high-pressure hydrogen gas self-ignition in tubes. J Loss Prevention in the Process Industries 21(2) (2008) 185–198.

Golub V., Volodin V., Baklanov D., Golovastov S., Lenkevich D., Experimental investigation of hydrogen ignition at the discharge into channel filled with air. Physics of

Extreme States of Matter (2010) 110–113.

Goodwin D., Malaya N., Moffat H., Speth R., Cantera code (2009).

Grune J., Sempert K., Kuznetsov M., Jordan T., Experimental study of ignited unsteady hydrogen releases from a high pressure reservoir. Int J Hydrogen Energy 39(11) (2013) 6176–6183.

Haidn O.J., et al. Improved combustion efficiency of a H_2/O_2 steam generator for spinning reserve application. Proc 11th World Hydrogen Energy Conference (WHEC-11), Stuttgart (1996).

Hall J.E., Hooker P., Willoughby D. Ignited releases of liquid hydrogen: Safety considerations of thermal and overpressure effects. Int J Hydrogen Energy 39 (2014) 20547–20553.

Hardee H.C., Lee D.O., Thermal hazard from propane fireballs. Transportation Planning and Technology 2 (1973) 121–128.

Harris A.P., Dedrick D.E., LaFleur C., San Marchi, C., Safety, codes and standards for hydrogen installations: Hydrogen fueling system footprint metric development. Report SAND2014-3416, Sandia National Laboratory, Albuquerque, NM (2014).

Hecht E.S., Panda P.P., Mixing and warming of cryogenic hydrogen releases. Int J Hydrogen Energy 44(17) (2019) 8960–8970.

Hooker P., et al., Experimental releases of liquid hydrogen. Hazards XXIII (2012).

HSL, Position paper “Hazards of liquid hydrogen”, Health and Safety Laboratory, Buxton (2010).

Hu X.Y., Wang Q., Adams N.A., An adaptive central-upwind weighted essentially non-oscillatory scheme. J Computational Physics 229(23) (2010) 8952–8965.

Hudders R.S., Dorf C.J., Holcombe A.H., Railway tank car for transcontinental shipment of liquefied hydrogen. In: Timmerhaus K.D. (ed), Advances in Cryogenic Engineering 8 (1963) 461–466.

Hussein H.G., Brennan S., Shentsov V., Makarov D., Molkov V., Numerical validation of pressure peaking from an ignited hydrogen release in a laboratory-scale enclosure and application to a garage scenario. Int J Hydrogen Energy 43(37) (2018) 17954–17968.

ISO 13984: 1999 Liquid hydrogen – Land vehicle fueling system interface. International Organization for Standardization, Geneva (1999).

ISO 13985: 2006 Liquid hydrogen – Land vehicle fuel tanks. International Organization for Standardization, Geneva (2006).

Jäkel C., et al., Validation of a 2D multiphase multicomponent CFD model for accidental liquid and gaseous release. Proc. 7th Int Conf on Hydrogen Safety (ICHS2017), Hamburg (2017).

Jin T., et al., CFD modeling and analysis of the influence factors of liquid hydrogen spills in open environment. Int J Hydrogen Energy 42 (2017) 732–739.

Karlsson E., Catalytic ortho- to parahydrogen conversion in liquid hydrogen. (2017). Available at https://www.semanticscholar.org/paper/Catalytic-ortho-to-parahydrogen-conversion-in-Karlsson/d90cd059e742fe7ea68bb86130ce6b770ec496d1

Kennan J.J., Makarov D.V., Molkov V.V., Modelling and simulation of high-pressure

hydrogen jets using notional nozzle theory and open source code OpenFOAM. Int J Hydrogen Energy 42(11) (2017) 7447–7456.

KHI, World's first liquefied hydrogen carrier SUISO FRONTIER launches building an international hydrogen energy supply chain aimed at carbon-free society (2019). Available at https://global.kawasaki.com/en/corp/newsroom/news/detail/?f=20191211_3487

KHI, Kawasaki completes installation of liquefied hydrogen storage tank for marine transport applications on world's first liquefied hydrogen carrier. (2020a). Available at https://global.kawasaki.com/en/corp/newsroom/news/detail/?f=20200309_3090

KHI, Kawasaki completes world's first liquefied hydrogen receiving terminal Kobe LH_2 terminal (Hytouch Kobe). (2020b). Available at https://global.kawasaki.com/en/corp/newsroom/news/detail/?f=20201203_2378

Klier J., et al, A new cryogenic high-pressure H_2 test area: First results. Proc 12th IIR Int Conf, Dresden (2012).

Kobayashi H., et al., Experiment of cryo-compressed (90-MPa) hydrogen leakage diffusion. Int J Hydrogen Energy 43(37) (2018) 17928–17937.

Kondo S., Takahashi A., Tokuhashi K., Calculation of minimum ignition energy of premixed gases. J Hazardous Materials 103(1–2) (2003) 11–23.

Kreiser A.M, et al. Analyse von Störfällen mit Wasserstoff in bisherigen Anwendungsbereichen mit besonderer Berücksichtigung von LH_2. Report IKE 2-116, Institut für Kernenergetik und Energiesysteme der Universität Stuttgart (1994).

Krieg D., Konzept und Kosten eines Pipelinesystems zur Versorgung des deutschen Straßenverkehrs mit Wasserstoff. Series Energy&Environment Vol 144, Research Center Jülich (2012).

Kusterer H., Scherf H., HYDROSS Einsatz von Wasserstoff zur Sofortreservebereitstellung. Proc Status Seminar Wasserstoff als Energieträger, Würzburg, Projektträger Biologie, Energie, Okologie, Research Center Jülich (1995) 95–128.

Kuznetsov M.S., Alekseev V.I., Dorofeev S.B., Comparison of critical conditions for DDT in regular and irregular cellular detonation systems. Shock Waves 10 (2000) 217-224.

Kuznetsov M., Alekseev V., Matsukov I., Dorofeev S., DDT in a smooth tube filled with a hydrogen-oxygen mixture. Shock Waves 14 (2005) 205–215.

Kuznetsov M., Czerniak M., Grune J., Jordan T., Effect of temperature on laminar flame velocity for hydrogen-air mixtures at reduced pressures. Proc. 5th Int Conf Hydrogen Safety (ICHS-5), Brussels (2013), paper 231.

Lach A.W., Gaathaug A.V., Vaagsaether K., Pressure peaking phenomena: Unignited hydrogen releases in confined spaces – Large-scale experiments. Int J Hydrogen Energy 45(56) (2020) 32702–32712.

Lach A.W., Gaathaug A.V., Large scale experiments and model validation of Pressure Peaking Phenomena-ignited hydrogen releases. Int J Hydrogen Energy 46(11) (2021) 8317– 8328.

Lachance J., Tchouvelev A., Engebo A., Development of uniform harm criteria for use in quantitative risk analysis of the hydrogen infrastructure. Int J Hydrogen Energy 36(3)

(2011) 2381–2388.

Law C.K., Combustion physics, Cambridge University Press (2006).

Leachman J.W., Jacobsen R.T., Penoncello S.G., Lemmon E.W., Fundamental equations of state for parahydrogen, normal hydrogen, and orthohydrogen. J Physical and Chemical Reference Data 38 (2009) 721.

Lewis B., Elbe G. von., Combustion, flames and explosions of gases. Zeitschrift f Physikalische Chemie 36 (1961), Academic Press, New York. Available at https://doi.org/10.1524/zpch.1963.36.3_4.136.

Lind C.D., What causes unconfined vapor cloud explosions. Loss Prevention, 9 (1975) 101–105.

Lodhi M.A.K., Mires R.W., How safe is the storage of liquid hydrogen? Int J Hydrogen Energy 14(1) (1989) 35–43.

Luketa-Hanlin A., A review of large-scale LNG spills: Experiments and modeling. J Hazardous Materials 132(2–3) (2006) 119–140.

Lutz A.E., A numerical study of thermal ignition. Sandia Report SAND88-8228 (1988).

Maas U., Warnatz J., Ignition processes in hydrogen-oxygen mixtures. Combustion and Flame 74(1) (1988) 53–69.

Makarov D., Shentsov V., Kuznetsov M., Molkov V., Pressure peaking phenomenon: Model validation against unignited release and jet fire experiments. Int J Hydrogen Energy 43(19) (2018) 9454–9469.

Makarov D., Shentsov V., Kuznetsov M., Molkov V., Hydrogen tank rupture in fire in the open atmosphere: Hazard distance defined by fireball. Hydrogen 2(1) (2021) 134–146.

Malet F. Numerical and experimental study of premixed turbulent hydrogen flame propagation in lean and wet atmosphere. PhD thesis in French: Etude experimentale et numerique de la propagation de flammes premelangees turbulentes dans une atmosphere pauvre en hydrogene et humide, Orleans University (2005).

Malkov M.P., Industrial production of heavy water. Atomnaya Energiya, 7(2) (1958) 101-109.

Markowz G., Dylla A., Elliger T., icefuel® – An infrastructure system for cryogenic hydrogen storage, distribution and decentral use. Proc 18th World Hydrogen Energy Conference (WHEC-18), Essen, Report Energy & Environment, Vol. 78-1, Research Center Jülich (2010).

Martin-Valdepenas J.M., Jimenes M.A., Exploring MIE as a safety indicator parameter in practical applications. In EU-5th Framework Programme, EVG1-CT-2001-00042: Experimental and numerical study of reactive flows with relevance to industrial safety for explosion protection (2003).

Mei R.W., Klausner J., Project title: Chill down processes of hydrogen transport pipelines. Report NASA/CR-2006-214091, National Aeronautics and Space Administration, Washington DC (2006).

Merilo E.G., et al., Self-ignition of hydrogen releases through electrostatic discharge induced by entrained particulates. Int J Hydrogen Energy 37(22) (2012) 17561–17570.

Middha P., Ichard M., Arntzen B.J., Validation of CFD modelling of LH_2 spread and

evaporation against large-scale spill experiments. Int J Hydrogen Energy 36 (2011) 2620–2627.

Miller A., Heavy water: A manufacturers' guide for the hydrogen century. Canadian Nuclear Society Bulletin, 22(1) (2001) 1–14.

Molina A., Schefer R.W., Houf W.G., Radiative fraction and optical thickness in large-scale hydrogen-jet fires. Proc Combustion Institute 31(2) (2007) 2565–2572.

Molkov V., Makarov V., Bragin M.V., Physics and modelling of underexpanded jets and hydrogen dispersion in atmosphere. Physics of Extreme States of Matter (2009) 146–149.

Monakhov V.T., Methods for studying the flammability of substances. Amerind Publishing Co. (1986).

NASA, Safety standard for hydrogen and hydrogen systems: Guidelines for hydrogen system design, materials selection, operations, storage and transportation. ID: 19970033338, Technical Memorandum NASA-TM-112540 (1997a).

NASA. Report of the Presidential Commission on the Space Shuttle Challenger accident (1986). (1997b). Available at http://science.ksc.nasa.gov/shuttle/missions/51-l/docs/rogers-commission/table-of-contents.html

NFPA News. 9 (2005) 1–3.

NLD, Major Accidents (risks) Decree 1999. The Netherlands (1999).

NORLED, World's first ship driven by LH_2. Presentation at GCE Ocean Technology workshop, Floro, Norway (2019). Available at https://www.gceocean.no/media/2683/norled.pdf

Ó Conaire M., Curran H.J., Simmie J.M., Pitz W.J., Westbrook C.K., A comprehensive modeling study of hydrogen oxidation. Int J Chemical Kinetics 36(11) (2004) 603–622.

Ono R., Nifuku M., Fujiwara S., Horiguchi S., Oda T., Minimum ignition energy of hydrogen-air mixture: Effects of humidity and spark duration. J Electrostatics 65(2) (2007) 87–93.

Ordin P.M., Review of hydrogen accidents and incidents in NASA operations. Technical Memorandum NASA TM X-71565, Lewis Research Center, Cleveland, OH (1974).

Oyama S., Kamiya S., Harada E., Inoue K., Nishimura M., CO_2-free hydrogen supply chain project and risk assessment for the safety design. Proc. 5th Int Conf on Hydrogen Safety (ICHS-5), Hamburg (2013) paper 171.

Panda P.P., Hecht E.S., Ignition and flame characteristics of cryogenic hydrogen releases. Int J Hydrogen Energy 42(1) (2017) 775–785.

Parente A., Malik M.R., Contino F., Cuoci A., Dally B.B., Extension of the Eddy Dissipation Concept for turbulence/chemistry interactions to MILD combustion. Fuel 163 (2016) 98–111.

Pehr K., Aspects of safety and acceptance of LH_2 tank systems in passenger cars. Int J Hydrogen Energy 21(5) (1996) 387–395.

Peschka W. Liquid hydrogen: Fuel of the future. Springer-Verlag Wien New York (1992).

Petersen U., et al., Design and safety considerations for large-scale sea-borne hydrogen transport. Int J Hydrogen Energy 19 (1994) 597–604.

PGS 35 Guidelines “Hydrogen: installations for delivery of hydrogen to road vehicles”. Hazardous Substances Publication Series 35, version 1.0, Publicatiereeks Gevaarlijke Stoffen, Delft (2015).

Poling B.E., Prausnitz J.M., O'Connell J.P., The properties of gases and liquid. New York: McGraw-Hill (2001).

Pratt J.W., Klebanoff L.E., Feasibility of the SF-BREEZE: a Zero-Emission, Hydrogen Fuel Cell, High-Speed Passenger Ferry. Report SAND2016-9719, Sandia National Laboratory, Livermore CA (2016).

Proust C., Lacome J.-M., Jamois D., Perrette L., Processes of the formation of large unconfined clouds following a massive spillage of liquid hydrogen on the ground. Proc 2nd Int Conf Hydrogen Safety (ICHS2007), San Sebastian (2007).

Proust C., INERIS research performed within PRESLHY. Presentation at the 13th Int Symp Hazards, Prevention, and Mitigation of Industrial Explosions (ISHPMIE), Braunschweig (2020).

Ren Z., Wen J.X., Numerical characterization of under-expanded cryogenic hydrogen gas jets. AIP Advances 10(9) (2020) 095303.

Rew P.J., Hulbert W.G., Development of pool fire thermal radiation model. HSE Contractor Report WSA/RSU8000/018, UK (1995).

Reynolds W.C., The element potential method for chemical equilibrium analysis: implementation in the interactive program STANJAN. Stanford University (1986).

Rico H.Y., Etudes théorique et expérimentale de la détonation des mélanges d’hydrogène liquide et d’oxygène solide à 20 K. Thèse de doctorat de l’Université de Paris (1970).

Ringland J.T., Safety issues for hydrogen-powered vehicles. Report SAND94-8226, Sandia National Laboratory, Albuquerque (1994).

Rivkin C., Burgess R.,. Buttner W., Hydrogen technologies safety guide. Technical Report NREL/TP-5400-60948, National Renewable Energy Laboratory, US-DOE, Golden, CO (2015).

Royle M., Willoughby D., HSL Liquid hydrogen spills – Initial trials. Presentation at the expert meeting of IEA HIA Task 31, May 2010.

Royle M., Willoughby D.B., Consequences of catastrophic releases of ignited and unignited hydrogen jet releases. Int J Hydrogen Energy 36(3) (2010) 2688–2692.

Saffers J.B., Molkov V.V., Towards hydrogen safety engineering for reacting and non-reacting hydrogen releases. J Loss Prevention in the Process Industries 26(29 (2013) 344–350.

Schefer R.W., Houf W.G., Bourne B., Colton J., Spatial and radiative properties of an open-flame hydrogen plume Int J Hydrogen Energy 31 (2006) 1332–1340.

Schefer R.W., Houf W.G., Williams T.C., Bourne B., Colton J., Characterization of high-pressure, underexpanded hydrogen-jet flames. Int J Hydrogen Energy 32 (2007) 2081–2093.

Schmidtchen U., et al., Simulation of accidental spills of cryogenic hydrogen in a residential area. Cryogenics 34(Suppl 1) (1994) 401–404.

Schödel J.P., Hydrogen – A safety risk? Proc. CEC Seminar on Hydrogen as an Energy

Vector: Its Production, Use and Transportation, Report EUR 6085, Commission of the European Communities, Brussels (1978) 567–581.

Simoneau R., Hendricks R., Two-phase choked flow of cryogenic fluids in converging-diverging nozzles. NASA Tech. Rep. Pap. 1484 (1979).

Sittig M., Cryogenics research and applications. D. van Nostrand Company, Princeton (1963).

Sloop J.L., Liquid hydrogen as a propulsion fuel, 1945-1959. NASA History Office. Report NASA SP-4404. National Aeronautics and Space Administration, Washington DC (1978).

Soave G., Equilibrium constants from a modified Redlich-Kwong equation of state. Chemical Engineering Science 27(6) (1972) 1197–1203.

Takeno K., et al., Evaporation rates of liquid hydrogen and liquid oxygen spilled onto the ground. J Loss and Prevention in the Process Industries 7(5) (1994) 425–431.

Takeno K., et al., Dispersion and explosion field tests for 40 MPa pressurized hydrogen. Int J Hydrogen Energy 32 (2007) 2144–2153.

Takiguchi M., Furuhama S., Suzuki T., Tsujita M., Combustion improvement of liquid hydrogen fueled engine for medium-duty trucks. Proc. 4th Int Pacific Conf Automotive Engineering, Melbourne (1987).

Teodorczyk A., Lee J.H., Knystautas R., Propagation mechanism of quasi-detonations. 22nd Int Symp on Combustion. The Combustion Institute, Pittsburgh (1988) 1723–1731.

Tieszen S.R., Sherman M.P., Benedick W.B., Berman M., Detonability of H_2-air-diluent mixtures. Technical Report NUREG/CR-4905, SAND85-1263 (1987).

Travis J.R., Piccioni Koch D., Breitung W., A homogeneous non-equilibrium two-phase critical flow model. Int J Hydrogen Energy 37(22) (2012) 17373–17379.

Tupolev. Development of cryogenic fuel aircraft. (2008). Available at http://www.tupolev.ru/English/Show.asp? SectionID=82

Turner J., HySHIP: inside Europe's flagship hydrogen ship demonstrator project. (2020). Available at https://www.ship-technology.com/features/hydrogen-vessel/

Turns S.R., Myhr F.H., Oxides of nitrogen emissions from turbulent jet flames: Part I-Fuel effects and flame radiation. Combustion and Flame 87 (1991) 319–335.

Urano Y., et al. Hazards of burning liquefied hydrogen. Part 1: Flame of stable burning. Part 2: Flame of abnormal burning. National Chemical Laboratory for Industry 81 (1986) 143–157 (In Japanese).

Ustolin F., Paltrinieri N., Hydrogen fireball consequence analysis. Chemical Engineering Transactions 82 (2020a) 211–216.

Ustolin F., Paltrinieri N., Landucci G., An innovative and comprehensive approach for the consequence analysis of liquid hydrogen vessel explosions. J Loss Prevention in the Process Industries 68 (2020b) 104323.

Vander Arend P.C., et al., The liquefaction of hydrogen. In: Scott R.B., et al. (Eds.), Technology and uses of liquid hydrogen. Pergamon Press Ltd (1964) 38–105.

Venetsanos A.G., Bartzis J.G., CFD modeling of large-scale LH_2 spills in open environment. Int J Hydrogen Energy 32(13) (2007) 2171–2177.

Venetsanos A.G., Giannissi S.G., Release and dispersion modeling of cryogenic under-expanded hydrogen jets. Int J Hydrogen Energy 42(11) (2017) 7672–7682.

Venetsanos A.G., Homogeneous non-equilibrium two-phase choked flow modeling. Int J Hydrogen Energy 43(50) (2018) 22715–22726.

Venetsanos A.G., Giannissi S., Proust C., CFD Validation against large scale liquefied helium release. Proc. 8th Int Conf Hydrogen Safety, Adelaide, Australia (2019).

Verfondern K., Dienhart B., Experimental and theoretical investigation of liquid hydrogen pool spreading and vaporization. Int J Hydrogen Energy 22(7) (1997) 649–660.

Verfondern K., Dienhart B., Pool spreading and vaporization of liquid hydrogen. Int J Hydrogen Energy 32(13) (2007) 2106–2117.

Winters W.S., Houf W.G., Simulation of Small-Scale Releases from Liquid Hydrogen Storage Systems. Int J Hydrogen Energy 36(6) (2011) 3913–3921.

Witcofski R.D., Dispersion of flammable clouds resulting from large spills of liquid hydrogen. NASA Technical Memorandum 83131 (1981).

Witcofski R.D., Chirivella J.E., Experimental and analytical analyses of the mechanisms govering the dispersion of flammable clouds formed by liquid hydrogen spills. Int J Hydrogen Energy 9(5) (1984) 425–435.

Wolanski P., Wojcicki S., Investigation into the mechanism of diffusion ignition of a combustible gas flowing into oxidizing atmosphere. Proc 14th Int Symp Combustion, Pittsburgh (1973) 1217–1223.

Yamane K., et al., Some performance of engine and cooling system of LH_2 refrigerator van Musashi-9. Int J Hydrogen Energy 21(9) (1996) 807–811.

Yoshizawa A., Bridging between eddy-viscosity-type and second-order turbulence models through a two-scale turbulence theory. Physical Review E 48(1) (1993) 273.

Zabetakis M.G., Burgess D.S., Research on the hazards associated with the production and handling of liquid hydrogen. Report No. WADD TR 60-141, Wright Air Development Division, OH (1960).

Zabetakis M.G., et al., Explosion hazards of liquid hydrogen. Advances in Cryogenic Engineering 6 (1961) 185–194.

Zabetakis M.G., Safety with cryogenic fluids. Plenum Press, New York (1967).

Zalosh R.G., et al., Compilation and analysis of hydrogen accident reports. Final Technical Report COO-4442-4, Factory Mutual Research Corporation, Norwood, MA (1978).

Zitoun R., Desbordes D., Guerraud C., Deshaies B., Direct initiation of detonation in cryogenic gaseous H_2-O_2 mixtures. Shock Waves 4 (1995) 331–337.

Zittel W., Wurster R., Bölkow L., Hydrogen in the energy sector. TÜV SÜD Industrie Service GmbH (1996). Available at http://www.hyweb.de/Knowledge/w-i-energiew-eng.html}.(BibTeX)

Zuber N., Hydrodynamic aspects of boiling heat transfer. Report, US Atomic Energy Commission, Research Laboratory Los Angeles and Ramo-Wooldridge Corporation, University of California (1959).